Control Methods for Powered Prostheses to Improve Mobility and Stability in Persons with Lower Limb Amputation

By

Amanda Huff Shultz

Dissertation

Submitted to the Faculty of the

Graduate School of Vanderbilt University

in partial fulfillment of the requirements

for the degree of

DOCTOR OF PHILOSOPHY

in

Mechanical Engineering

August 31, 2017

Nashville, Tennessee

Approved:

Michael Goldfarb, Ph.D.

Karl Zelik, Ph.D.

Robert J. Webster III, Ph.D.

Robert Bodenheimer, Ph.D.

To Jeremy, my better half, who has supported and believed in me in every way throughout this process. He's the best.

ACKNOWLEDGMENTS

The work presented in this document describes my contributions to a project which saw years of development before I joined it. There are several people I would like to acknowledge, without whom I would not have been able to complete this work, the first of whom is my advisor, Dr. Michael Goldfarb, who has inspired and guided my work at the CIM and has allowed me to pursue the avenues of this research which were most interesting to me. I would also like to thank Drs. Zelik, Webster, and Bodenheimer for serving on my committee and for their respective input, whether in coursework or in completing my research and dissertation, which has been invaluable to me during my time at Vanderbilt.

I would like to recognize the funding sources which made my work possible, including the Eunice Kennedy Shriver National Institute of Child Health and Human Development of the National Institutes of Health under award number R01HD075493 and the discretionary funds from the H. Fort Flowers endowment.

I would next like to thank Professor Joel Lenoir of Western Kentucky University who first suggested that I consider applying to be a student in Dr. Goldfarb's Lab, as well as Dr. Ryan Farris for introducing me to the CIM and recommending me to Dr. Goldfarb. There are several other researchers who came before (and after) me who have have helped to shape my work and my graduate experience. Among these, I would also like to thank my fellow lower-limb prosthesis team members, particularly Dr. Brian Lawson, who welcomed me to the lab and who has been a mentor, sounding board, and friend throughout my time at Vanderbilt. I have learned a great deal from him, and without his guidance and all of the work he contributed to the project, I could have neither come up to speed with the project as quickly as I did nor achieved all that I am presenting in this document. I must also thank Dr. Erdem Erdemir for his help and cheerful presence, as well as Elissa Ledoux and Harrison Bartlett for their assistance and ideas during our times together at the CIM. I would also like to thank the amputee subjects who participated in my research, especially my most

recent subject who was extremely dedicated and dependable–rare qualities without which I could not have completed my research as I did. I would also be remiss if I did not thank the members of the CIM and BAT Lab who participated in my research as subjects and who provided a great deal of assistance with experimental setup and data processing techniques.

Needless to say, my contribution to the lower limb prosthesis project would have been impossible without both Jason Mitchell and Don Truex, who not only supplied the prototypes used in this work but also immeasurable advice and troubleshooting expertise. I would like to thank Don especially for the guidance he provided with regard to printed circuit board design for the generation 3 transtibial board layout I completed; I certainly could not have done so without it.

I would now like to thank the all of my fellow CIM members. I am very grateful for the environment I have enjoyed while at the CIM, which has been one filled not only with advice and discussion but also camaraderie. And, of course, I must thank Drs. Brian Lawson and Daniel Bennett from whom I am essentially copying this dissertation format. Both suggested in their Acknowledgements section that they be acknowledged for this, and I have responded accordingly.

I would finally like to thank my family. First, my parents, Darrel and Glenda, instilled in me from a young age the importance of education and hard work, and have helped me in countless ways to achieve my goals. My sister, Alyssa, among other things has been the one person I know outside of school who can relate to the challenges of research and graduate school, and I have been very grateful to be able to discuss and share with her parts of this experience. Finally, I want to thank my husband and best friend, Jeremy. He has been been with me throughout graduate school and has encouraged and supported me daily in whatever way I have needed. I absolutely could not have done this without him.

TABLE OF CONTENTS

LIST OF TABLES

Table Page

LIST OF FIGURES

CHAPTER 1

INTRODUCTION

The work reported herein summarizes my research at the Center for Intelligent Mechatronics, consisting primarily of development and evaluation of control strategies for powered lower limb prostheses. These control strategies have been developed with the intent to improve mobility and stability in the target population, with a focus on that for a powered ankle prosthesis for persons with unilateral below-knee amputation. The remainder of this chapter describes the scope of my work in terms of a brief description of the contents of the remaining chapters and then introduces its motivation with respect to the demographics of the target population and an overview of the needs my work addresses. Further, I have included a review of the current state of the art and related research efforts, and a section on the Vanderbilt powered lower limb prosthesis project, including a brief history as well a details about the prostheses and controller development methods which apply to the research described in the succeeding chapters.

The remaining chapters consist of manuscripts which are published or pending publication, as well as additional information for clarification and/or supplementation. This material exists in the form of an addendum to published (or pending) manuscripts. Chapter 2 contains the only published work in this dissertation pertaining to the Vanderbilt powered knee and ankle prosthesis, describing the development and evaluation of a daily-use running controller for the prosthesis, including a coordination or activity level controller as well as a supervisory controller to facilitate transitions into and out of the running controller/mode from a walking controller/mode. The manuscript was published in the *IEEE Transactions on Neural Systems and Rehabilitation Engineering*, published online in July 2014 and in print May 2015, Volume 23, Issue 3. A version of the manuscript describing results for the activity level controller only was presented at the *2012 Annual Confer-*

ence of the IEEE Engineering in Medicine and Biology Society (EMBC 2012). Chapter 3 describes a control approach which enables walking and standing for a powered ankle prosthesis, demonstrating the efficacy of the approach for a unilateral transtibial amputee subject walking with variable cadence and standing on various slopes. The manuscript contained within was published in the *IEEE Transactions on Neural Systems and Rehabilitation Engineering*, published online in April 2015 and in print April 2016, Volume 24, Issue 4. A version of the manuscript describing results for a healthy subject walking with an able-bodied adaptor at a single speed was presented at the *2013 IEEE International Conference on Robotics and Automation* (ICRA 2013). A version of the manuscript describing results for a below-knee amputee subject walking at multiple speeds only was presented at the *2014 Annual Conference of the IEEE Engineering in Medicine and Biology Society* (EMBC 2014). Chapter 4 describes development and evaluation of a unified control strategy for walking on both even and uneven terrain with a powered ankle prosthesis, informed by behavioral models for the healthy ankle developed based on a small healthy subject study also conducted as part of this effort. The manuscript contained in this chapter has been submitted for consideration for publication in the *IEEE Transactions on Neural Systems and Rehabilitation Engineering*. A similar work which describes a preliminary healthy subject study and initial development of such a controller was presented at the *2015 Annual Conference of the IEEE Engineering in Medicine and Biology Society* (EMBC 2015), for which I was an Open Finalist in the 2015 EMBC Student Paper Competition.

1.1 Background and Motivation

Zeigler-Graham et al. estimated that 1.6 million persons were living with limb loss in 2005, predicting an increase to 3.6 million by 2050 [1]. Of the 1.6 million in 2005, an estimated 623,000 had major lower extremity amputations–i.e., of the foot (below the knee) or above the knee–with approximately 60% of amputees being under 65 years of age [1].

Lower limb prostheses exist in large part to improve the mobility of the user, partic-

ularly with regard to activities of daily living. A study conducted by Hafner and Smith demonstrated that the use of a microprocessor-controlled knee (MPK) prosthesis improved ambulation down hills and stairs as well as on uneven terrain compared to a (passive) mechanical knee for Medicare Functional Classification Level (MFCL)-2 and -3 individuals [2]. Participants also experienced fewer uncontrolled falls, and approximately 41% of subjects increased their activity level while using the MPK prosthesis [2], all pointing toward the benefits provided by intelligent prostheses. However, most conventional lower-limb prosthetic devices, including the MPK from the above study, are energetically passive and/or optimized for a single type of activity or gait, with a daily-use prosthesis being optimized for walking on level ground. While this optimization does not necessarily preclude other types of activity and locomotion, an amputee would benefit from a prosthesis which facilitates multiple gaits/activities in a biomechanically healthy manner and which possesses intelligence to infer the type of activity the user intends to perform.

1.1.1 Running as an Activity of Daily Living

Humans generally locomote with one of two primary forms of gait–walking or running–depending upon the speed of locomotion. When running for exercise, the individual makes the decision to engage in running with enough time to prepare for the activity beforehand. For an amputee, this almost always entails doffing his or her daily-use prosthesis and donning his or her dedicated running prosthesis. However, a situation might arise during the course of daily activity which requires locomotion at a higher speed than can be effectively accommodated by a walking gait, calling suddenly for a brief period of running. Such circumstances might include running to catch a bus or to chase one's child or pet who is running toward the road.

Running and walking gaits differ in several ways. The percentage of stride which corresponds to stance is greater than 50% in walking–resulting in a double stance phase–and less than 50% in running–resulting in a double float phase. Further, the body center-of-mass

(CoM) is at its highest in mid-stance in walking, whereas it is at its lowest in mid-stance in running. These differences in gait characteristics correspond to differences in gait kinematics and kinetics–including the relative phasing of the joint behavior. In running, the stance phase is divided into two phases: absorption (shock loading) and propulsion. The knee and the ankle both participate in these phases, absorbing and generating power approximately synchronously [3]; during walking the knee and ankle do not absorb and generate power synchronously. A running controller was therefore developed and incorporated into the suite of activities provided by the Vanderbilt powered knee and ankle prosthesis, including a controller for the running gait itself and a method for quickly and reliably switching into and out of running when necessary.

1.1.2 Walking and Standing with a Powered Ankle Prosthesis

The intact human ankle joint exhibits a variety of behaviors, including adaptive passive behaviors (i.e., passive behaviors which vary as a function of activity), as well as active behaviors such as powered push-off [4], supplying net positive energy during gait initiation [5] and during steady-state walking, particularly in self-selected medium to fast walking [6]. Further, Morgenroth et al. found reduction in limb loading asymmetry that the use of prosthetic feet which perform more push-off could potentially reduce the risk and severity of knee osteoarthritis in below-knee amputees by reducing their limb loading asymmetry [7]. This range of behaviors cannot be supplied by a simple passive device, especially one with a fixed behavior, which describes the vast majority of conventional below-knee prostheses.

While the first stage in developing prostheses for below-knee amputees, including the prosthesis described in this work, is to focus on restoring gait functionality on level, even terrain, the terrain which humans traverse in daily life is often varied, particularly outdoors. In this work, the type of variation which receives focus is uneven terrain, or terrain for which each step results in a different stance phase foot configuration (or effective incline).

This terrain description might apply to broken sidewalks, wooded areas, etc. Voloshina et al. conducted a study with healthy subjects wherein the subjects walked on a treadmill with wooden blocks affixed to its belt to create stable terrain with variations in ground topography, described herein as uneven terrain. When compared to the same subjects walking on smooth terrain (unmodified treadmill belt), a number of differences arose, one of the most notable being increased variability in joint kinematics, particularly at the ankle, when walking on the uneven terrain [8]. This increased ankle variability introduced a new facet of design criteria which should be considered for an ankle/foot prosthesis to restore biomechanically healthy gait for a below-knee amputee. Control strategies were therefore developed which enable appropriate and stable walking and standing on even and uneven terrain.

1.2 State of the Art and Research Efforts

1.2.1 Running as an Activity of Daily Living for a Transfemoral Amputee

Conventional daily-use prostheses have traditionally been passive. In the case of prostheses for above-knee amputees, the knee is typically a damper which is designed to lock in (hyper) extension while the user is in stance and to swing freely once the user enters the swing phase. For a prosthesis to enable biomechanically healthy running for above knee amputees, it must be capable of generating significant torque (and power) at both joints simultaneously [3]. Recent advances in robotics technologies (battery, microprocessor, motor) have facilitated the emergence of powered prostheses which are capable of delivering power comparable to that which the biological joint generates during various gait activities. Össur's Power Knee™ [9] is capable of biomechanically significant levels of torque and power, and it can be paired with a powered ankle such as BiOM® or its its next generation emPOWER [10] to enable powered gait. In this case, however, the joints are not coordinated and do not communicate. Further, no information is available which

indicates that either device is equipped with a biomechanically healthy running function. Spring Active, Inc. describes a powered ankle prosthesis to enable running, particularly for military applications, similar to what is described by Hitt et al [11]. However, this device was neither available commercially nor evaluated in any publications at the time the running controller presented herein was developed [12, 13]; further, without a coordinating powered knee unit, this cannot enable such a running gait in above-knee amputees. To the knowledge of the author, other than the Vanderbilt Powered prosthesis described in this work, no powered knee and ankle devices capable of generating significant knee and ankle torque simultaneously have been shown to enable biomechanically healthy running in above-knee amputees.

1.2.2 Walking and Standing on Various Terrain for Transtibial Amputees

The research concerning prosthetic intervention for below-knee amputees described herein is a suite of controllers which enables walking with powered push-off on various surfaces and at various speeds, as well as stable standing with spring-like restoring torque/-support on various inclines and all without information about the activity or surface a priori, all within a single type of device: a powered controllable prosthesis. In order to enable all of these activities, a device must have hardware and software which enable delivery of net positive energy at the ankle joint and which enable appropriate modulation of ankle behavior depending upon the environment and user intent. Several devices and control methods (being developed in a research setting and/or available commercially) exist which fulfill some, but not all, of these requirements.

There are several devices [14, 15, 16, 17, 18, 19, 20, 21] and controllers, commercial and otherwise, which enable biomechanically healthy walking (including powered push-off) on level, even ground for below-knee amputees. A number of control methods for (level ground) walking with powered prosthetic ankles were reviewed by Jiménez-Fabián and Verlinden [22]. Among these, Holgate et al. discuss several strategies for control in-

cluding position control, velocity or stiffness control, impedance control, and proportional myoelectric control [23]. Additionally, two control strategies are proposed to augment position control, including one based on a continuous relationship between shank angle (relative to an inertial reference frame) and ankle angle [23, 24] in conjunction with a scaling factor based on speed, and one which continuously modulates the ankle period and amplitude based on stride time of the previous gait cycle [23]. Out of this group was formed SpringActive Inc., which has been developing various powered ankle technology. One of these devices, Odyssey [25], is a powered ankle which appears to use a control method similar to that previously described by Holgate et al. [23, 24]. The JackSpring™ ankle [26] incorporates an adjustable robotic tendon for energy efficiency; stiffness is adjusted by the addition and subtraction of coils of a spring which is used as a lead screw [27].

A powered ankle control strategy presented by Au et al. [28] describes both a neural network model and a neuromuscular model which rely on electromyogram (EMG) signal inputs from the amputee's residual limb to set the ankle angle. Another control strategy implements a four-state finite-state controller, where the control action within each state is a stiffness, a torque source, a position trajectory controller, or some combination of these [29]. This method is applied to both level ground walking and stair climbing [30], and EMG signals from the user enable switching between controllers [30]. Additionally, Eilenberg et al. present an approach based on a two-state model: one for swing and the other for stance [31]. The swing state employs position control, and the stance state incorporates a Hill-type muscle model which reacts with a force in proportion to position and speed [31]. From this group emerged the company iWalk, which has become BionX Medical Technologies, Inc., which created the BiOM® powered ankle/foot and now the emPOWER [10]. The BiOM® incorporates a powered push-off and can be optimized for walking at multiple speeds. The emPOWER website [10] describes the ability to adjust ankle power, resistance, and flexion in real-time as well as centering the balance of the user, without description of the control method for achieving this.

Sun and Voglewede present [32] and later evaluate [33] a finite-state controller comprised of four states: loading response, middle and terminal stance, pre-swing, and swing. During the stance phase (comprised of the first three finite states) output torque is controlled via PI feedback with a healthy subject torque profile as the reference, while the swing state is a PID position controller. Huang et al. present a proportional myoelectric controller for a pneumatic artificial plantar flexor muscle for a transtibial prosthesis [34, 35].

Össur offers a prosthetic foot called Pro-Flex® which has 27 degrees of ankle motion and which effects a mechanically powered push-off that has been shown to reduce the load on the contralateral side by 11%.

Prosthetic devices have also been created as research tools to test various behaviors by varying mechanical and control parameters which affect push-off [36, 37, 38]. One is an energy-recycling foot which stores energy from collision and releases that energy at push-off; this device has been shown to increase push-off work and, depending upon spring stiffness, reduce metabolic cost, compared with conventional prostheses [36, 39, 40]. A powered ankle-foot prosthesis emulator was developed in order to rapidly explore various prosthesis behaviors with human subjects as well as emulate candidate prosthetic interventions [37, 41, 42]. Kim et al. studied a control method wherein the magnitude of prosthetic ankle work was modulated for each step based on lateral velocity of the approximate center of mass (CoM) of the subject in order to increase stability. The stabilizing controller showed improvement, for example in metabolic energy consumption, compared to the other conditions tested [43]. Another prosthesis emulator prototype is presented which controller torque in both plantar-dorsiflexion and inversion-eversion [38].

The level walking controller described in this work incorporates a different control structure from the methods described above, including different state behaviors and switching conditions. A controller is introduced in this work which uses the absolute orientation of the shank to initiate push-off. Note that Lenzi et al. describe a controller which uses shank angle as a switching condition in a powered prosthesis for transfemoral amputees

which can accommodate changes in walking speed [44]. In the work presented herein, however, shank angle is used to accommodate ambulation over uneven terrain. Additionally, the controller presented in this work is for use with transtibial amputees, who naturally possess more direct control of shank angle, as the shank portion of the prosthesis is connected to the residual limb. Holgate et al. use shank angle to determine percentage of stride in order to execute an ankle angle trajectory; this inherently restricts ankle movement, which would likely prove to be a limitation when walking on uneven terrain, according to the data reported by Voloshina et al. [8, 23]. To the knowledge of the author, none of the previously developed controllers described here are specifically designed for walking on uneven ground. The BiOM® was evaluated on a different type of terrain, a loose rock surface, by Gates et al. [45] and showed improvements compared to a passive prosthesis. The BiOM® was also evaluated for use in climbing stairs [46] and was shown to restore powered push-off, compared to a passive prosthesis. However, there is no indication that the prosthesis detects and/or adapts to these various conditions and gaits. Further, while it is shown to provide improvement in terms of power delivery compared to a passive prosthesis, it has not shown that the BiOM® restores the function of the intact human ankle. Eilenberg et al. evaluates the neuromuscular model approach on level ground and ± 11 degree slopes [31]. While it is shown that the trend of net work done in terms of degree of incline is comparable to that of healthy walking [47], they do not show any comparison to healthy kinematics or kinetics for walking on the non-level surfaces (± 11 degree slopes).

Several passive or quasi-active devices (which cannot provide powered push-off) have been developed to improve stability while standing and/or walking on various slopes/uneven terrain. According to literature available on the internet, the Elan [48] from Endolite provides ground adaptive standing support and natural foot posture when sitting (or standing) in a manner similar to one of the methods presented by the author for the Vanderbilt powered ankle prosthesis [49]–by stiffening the ankle joint (in this case with hydraulic resistance) when ankle movement ceases. This device also modulates directional resistances

independently based on incline to assist in braking when walking downhill and in optimizing energy storage and return when walking uphill. The Echelon [50] and Echelon VT [51] from Endolite appear to have similar function to the Elan, but possibly without the adaptive hydraulic stiffening when standing. Both incorporate additional toe clearance during swing. Additionally, the EchelonVT offers ± 15 degrees axial shank rotation. The Proprio Foot® [52] from Össur incorporates a motor for use only when the device is not loaded–i.e. to increase ground clearance and to adjust the foot position for inclines, declines, and stairs. The traditional carbon fiber leaf spring stores and returns energy during the stance phase. The Kinterra™ Foot/Ankle System [53] by Freedom Innovations, LLC, combined hydraulic damping and carbon fiber leaf spring technology to improve stability (during walking and standing) on terrain which is uneven or sloped by increasing ground contact with 12 degrees of pivoting (10 degrees plantarflexive and 2 degrees dorsiflexive) while still providing energy return with the carbon fiber foot.

The ground adaptive standing controller described herein allows the user to set his or her posture in a static manner (similar to that used by the New Elan from Endolite); however, when the user's foot is flat on the ground but his or her movement is not static, this controller is still able to determine the appropriate ankle position about which to provide restoring torque. A control method for such ground slope adaptation has not yet been demonstrated in the literature for a powered transtibial prosthesis. Members of the Center for Intelligent Mechatronics (CIM) have demonstrated similar functionality in a previous publication with a powered transfemoral prosthesis [54]; however that method relies on measurement of ground reaction force, which is not measured in the system presented herein. This work additionally describes the supervisory method by which the system determines how to switch between the walking and standing controllers.

1.3 The Vanderbilt Powered Prosthesis

1.3.1 A Brief History

The Vanderbilt powered prosthesis began in Generation 0 as a tethered pneumatically actuated powered knee and ankle device which was controlled for walking using piecewise passive impedance functions [55]. The next major design iteration, Generation 1, along with each succeeding generation described herein, utilized the same basic activity-level control design of piecewise passive impedance functions but traded the pneumatic actuation for a motor and ball-screw transmission, as well as an onboard power source, making it the first self-contained powered knee and ankle prosthesis [56]. This generation included control for intent recognition for walking on level ground with variable cadence, walking on inclines and declines, and standing-sitting transitions [57, 58, 59]. This generation was also used for stumble detection and recovery control, ground adaptive standing control, preliminary stair ascent and descent control, and volitional knee control using electromyography [60, 54, 61, 62].

Generation 2 involved another major hardware design change, moving to a belt-chain-chain transmission, with the load sensing moving from a foot with heel and toe load sensors to a uniaxial load cell (implemented in line with the shank) and a standard carbon fiber prosthetic foot. It is with this generation that the running controller [13] described in Chapter 2 was developed and evaluated, as well as the stair ascent and descent controllers [61].

Generation 3 began with the first generation of the Vanderbilt powered transtibial prosthesis. The belt-chain-chain transmission type remained; however, since the ankle unit needed to stand alone and fit a population of below-knee amputees, build height minimization was an important design criterion. As such, there was no load cell incorporated into the generation 3 powered ankle prosthesis. A carbon fiber leaf spring was incorporated into the foot such that when engaged it would act in parallel with the transmission to increase maximum torque output during ankle dorsiflexion. The generation 3 powered knee and ankle

prosthesis incorporates two similar units which are connected via off-the-shelf prosthetic components. These design changes were largely aimed at improving inertial properties (mass distribution) and commercial viability.

1.3.2 Mechanical/Electrical Design

For all prostheses used in this work, each joint has a brushless DC motor driving a three-stage (belt-chain-chain) transmission. Each joint employs absolute angle measurement at the output in the form of a magnetic encoder as well relative position measurement at the motor. The prostheses each have a 6-axis inertial measurement unit (IMU) on the shank portion–i.e., the limb segment whose distal joint is the ankle–which contains an accelerometer and a gyroscope. Each prosthesis has a custom embedded system with a 16-bit digital processing chip which performs low-level control functions, such as commutation and current control of the motor as well as sensor signal conditioning, integrated with a 32-bit microcontroller for execution of high-level control code and sensor fusion at 500Hz. The prostheses are also each self-contained, powered by an onboard battery.

1.3.2.1 Powered Knee and Ankle Prosthesis

The Vanderbilt Powered Knee and Ankle Prostheses (Generation 2) used in the work described in Chapter 2 is shown in Fig. 1.1. The knee and ankle prosthesis axial load cell is located at the connection of the knee and ankle portions of the prosthesis. An optional custom bridge piece connects the load sensor to the ankle portion in order to add length depending upon the user's height. Additionally, the motor joint position sensors for this prosthesis are simply the Hall effect sensors (used for commutation) from the motor itself, and the power source is a lithium polymer battery. This prosthesis weighs approximately 5 kg.

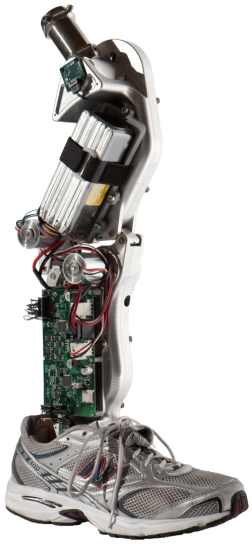

Figure 1.1: Generation 2 Vanderbilt powered knee and ankle prosthesis prototype.

1.3.2.2 Powered Ankle Prosthesis

There were two versions of the Vanderbilt powered ankle prosthesis used in this work: revisions 1 and 2 of the Generation 3 powered prosthesis. Gen 3.1 (Fig. 1.2a) was used in the development and assessment of the level ground variable cadence walking and ground adaptive standing controllers discussed in Chapter 3. Gen 3.2 (Fig. 1.2b) was used in the work discussed in Chapter 4.

a) b)

Figure 1.2: Photos of the Vanderbilt Powered Ankle Prosthesis prototype a) Generation 3.1 and b) Generation 3.2.

The powered ankle prostheses incorporate an additional magnetic encoder at the motor

to measure relative position. The Generation 3.1 ankle is powered by a lithium polymer battery, while the Gen 3.2 ankle is powered by a lithium ion battery. The same embedded system was used for the Gen 3.1 ankle and its knee and ankle prosthesis counterpart. However, the circuit board for the Gen 3.2 powered ankle received a new layout design which eliminated circuitry pertaining only to the knee joint and which fit into the desired envelope; this is discussed in greater detail in Chapter 4. The ankle-foot complex of the powered ankle prostheses additionally incorporates a carbon-fiber leaf spring into the foot; since the foot segment is easily removed and replaced, various foot sizes (typically between 26 and 28) and spring stiffnesses (typically between 3.5 Nm/deg and 6 Nm/deg) can be accommodated. The spring engages (in parallel with the transmission) at approximately 0 deg, biasing the output capabilities of the ankle toward plantarflexion, which is consistent with the biomechanical characteristics of the human ankle during locomotion. The spring stiffness and engagement angle are calibrated for each foot-spring when it is installed for the purposes of torque compensation and data analysis. Each of these prostheses weigh approximately 2.3 kg.

1.3.3 Control Design

1.3.3.1 Finite State-Based Impedance Control

The control system for the powered prostheses is structured into three levels, the lowest of which commands joint torque and controls motor current. The torque reference is generated by the mid-level controller (specific to a type of gait), which is implemented as a finite-state machine (FSM) where each state is defined by passive joint impedance characteristics, modified from that developed by Sup et al. [63]. The ankle joint impedance within each state is given by

$$\tau = k_i(\theta - \theta_{e,i}) + k_{5,i}(\theta - \theta_{e,i})^5 + b_i\dot{\theta} \tag{1.1}$$

where k_i, $k_{5,i}$, b_i, and $\theta_{e,i}$ denote linear stiffness, fifth-order stiffness coefficient, damping coefficient, and equilibrium angle, respectively, for the i^{th} state during a gait cycle. Note that the fifth-order stiffness coefficient $k_{5,i}$ is nonzero only during the middle stance state of the walking controller (for the powered ankle prosthesis), where it acts as a stiffening spring term to increase ankle support as the user's CoM passes over the ankle joint. The fifth-order term was implemented as an approximation of the nonlinear stiffening behavior (between ankle angle and torque) observed in healthy subjects during the middle stance phase of walking [4, 64], where middle stance takes place from the time the foot becomes flat on the ground until the initiation of powered push-off. Transitions between finite states are triggered by pre-selected thresholds in sensor measurements. The top-level control is a supervisory controller which selects which FSM–.e., activity mode–is active based on the current activity mode and controller state, as well as sensor data.

1.3.3.2 Mid-Level Controller Development

When first designing a controller for a type of gait–i.e. running with the powered knee and ankle prosthesis–the number of states and impedance parameters for each state within an FSM are initially determined by an iterative least-squares regression of (4.2) applied to joint position (θ), velocity ($\dot{\theta}$), and torque (τ) data from relevant biomechanical literature, in this case [3]. In the case of a powered ankle controller for a gait for which a controller had already been implemented on the powered knee and ankle prosthesis–i.e. standing and walking–the original controller was adapted to use only the states required for and signals available to an ankle-only prosthesis. For each of the controllers described herein, a base set of impedance parameters was implemented, and the controller was first tested for efficacy and initial parameter tuning with an able-bodied subject equipped with an adaptor to attach the prosthesis in approximately the location of the most proximal corresponding anatomical joint location, as well as immobilize that joint in a position which does not impede the function of the prosthesis. Fig. 1.3 shows such a device for use with the

powered and passive ankle prostheses. Note that during use, there are a foot shell and a shoe on the powered prosthesis, with the battery pack attached to the adaptor boot using velcro.

Figure 1.3: Sample able bodied adaptor setup for powered and passive ankle prostheses.

Impedance parameters and transition conditions/thresholds are adjusted experimentally (first with an able-bodied individual, and then with an amputee subject), as the participants are trained to use (and become accustomed to) the controller. Parameter adjustment is based on user feedback–in order to achieve user comfort and confidence in the action of the prosthesis–and on prosthesis joint angle data and qualitative video analysis–in order to achieve biomechanical characteristics representative of a particular gait, smooth transitions between modes of the FSM, and reliable and natural transitions between activity modes when applicable. Most of these parameters are stored on an SD card which is used by the embedded system at startup. These parameters can be modified in MATLAB via a custom graphical user interface (GUI).

CHAPTER 2

RUNNING WITH A POWERED KNEE AND ANKLE PROSTHESIS

While running for exercise with above-knee amputation may be best accomplished with a dedicated running prosthesis, circumstances in the course of daily life occasionally demand a brisk gait which must be accommodated by the amputee's daily-use prosthesis. Since running is the gait of choice for higher speeds in healthy individuals, logic dictates that a daily-use prosthesis which can accommodate brief periods of running would improve locomotion for an above-knee amputee. Running and walking are fundamentally different types of gait. Most commercially available daily-use prosthetic interventions for above-knee amputees are energetically passive and/or optimized for walking rather than running. Even interventions which are capable of generating power do not have a control setting to facilitate a running gait. This chapter describes the development and evaluation of a daily-use running controller for the Vanderbilt powered knee and ankle prosthesis, including a controller for the running gait as well as a one to facilitate transitions into and out of running from a walking gait. The following manuscript was published in the *IEEE Transactions on Neural Systems and Rehabilitation Engineering*, published online in July 2014 and published in print May 2015, Volume 23, Issue 3. Included in an addendum are clarifications to some of the content of the published manuscript.

2.1 Manuscript 1: Running with a Powered Knee and Ankle Prosthesis

2.1.1 Abstract

This paper presents a running control architecture for a powered knee and ankle prosthesis that enables a transfemoral amputee to run with a biomechanically appropriate running gait, and to intentionally transition between a walking and running gait. The control architecture consists firstly of a coordination level controller, which provides gait biomechanics

representative of healthy running, and secondly of a gait selection controller that enables the user to intentionally transition between a running and walking gait. The running control architecture was implemented on a transfemoral prosthesis with powered knee and ankle joints, and the efficacy of the controller was assessed in a series of running trials with a transfemoral amputee subject. Specifically, treadmill trials were conducted to assess the extent to which the coordination controller provided a biomechanically appropriate running gait. Separate trials were conducted to assess the ability of the user to consistently and reliably transition between walking and running gaits.

2.1.2 Introduction

Humans generally locomote with one of two primary forms of gait–walking or running. Although a number of differences exist between walking and running, among the most salient are the phasing of the vertical excursion of the body center-of-mass (CoM) during the stance phase of gait and the proportion of time the feet are on the ground relative to in the air. Specifically, walking is characterized by a body CoM trajectory that is highest at mid-stance, while running is characterized by a body CoM trajectory that is lowest at mid-stance (see Fig. [65, 66]. Additionally, the stance phase exists for more than 50% of the stride in a walking gait, such that a portion of the gait cycle is comprised of a double-support phase (e.g., see [67]). Conversely, the stance phase exists for less than 50% of the stride in a running gait, such that a portion of the gait cycle is comprised of a double-float phase [67]. Walking is more efficient means of locomotion (in terms of metabolic cost of transport) at low to moderate speeds (approximately 2.5 m/s, according to a simple model proffered by [67]), while running becomes a more efficient means of locomotion at higher speeds [67, 68].

A typical transfemoral prosthesis is designed to provide gait biomechanics corresponding to walking but does not generally provide knee and ankle joint biomechanics corresponding to a running gait [69]. As a result, when a transfemoral amputee requires a higher

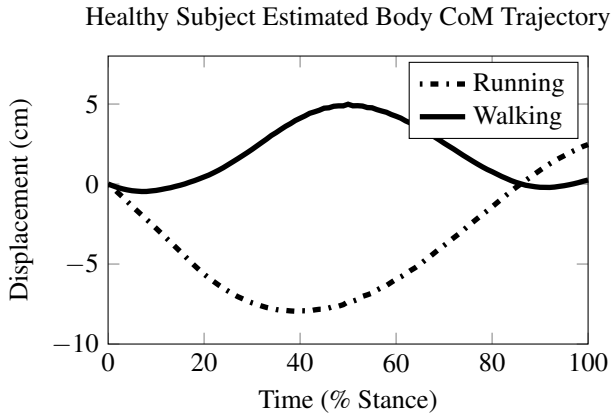

Figure 2.1: Estimated body vertical center of mass (CoM) for walking and running in healthy subjects.

Body CoM is estimated as the centroid of the pelvis, as is detailed later in the work.

gait speed than a walking prosthesis can provide, he or she generally employs a "hop-skip" gait, which is a highly asymmetric and energy-intensive gait comprised of both double-support and brief double-float phases [69, 70, 71]. Specialized transfemoral prostheses have been designed for running (e.g., [72]), but such prostheses are not multipurpose, and as such compromise the biomechanics of walking.

Recently, powered lower limb prostheses have begun to emerge. Powered prostheses–particularly those designed with low open-loop output impedance joints–have the ability to emulate a wide range of physical behaviors. Such devices are thus capable of emulating the biomechanical attributes of the healthy knee and ankle joints during walking or running, provided: 1) the prosthesis is endowed with a coordination-level controller that provides appropriate joint behaviors during walking and running, and 2) the prosthesis can recognize when the user wishes to transition between the walking and running gaits. The authors have previously presented a coordination-level controller that provides knee and ankle joint biomechanics representative of a healthy walking gait with a transfemoral amputee [55, 56, 58]. The authors note that Hitt, et al. have demonstrated the use of a powered ankle prosthesis to facilitate running in transtibial amputees [11], but are unaware of any prior research conducted to enable biomechanically healthy running in a transfemoral am-

putee with a powered knee and ankle prosthesis. As such, in this paper, the authors present a coordination-level running controller as well as a control methodology that enables user-controllable transitions between walking and running. Following a description of the controllers, the control approach is implemented on a powered knee and ankle transfemoral prosthesis, and the efficacy of the controller is assessed in a series of treadmill-based running trials.

A typical transfemoral prosthesis is designed to provide gait biomechanics corresponding to walking but does not generally provide knee and ankle joint biomechanics corresponding to a running gait [69]. As a result, when a transfemoral amputee requires a higher gait speed than a walking prosthesis can provide, he or she generally employs a "hop-skip" gait, which is a highly asymmetric and energy-intensive gait comprised of both double-support and brief double-float phases [69, 70, 71]. Specialized transfemoral prostheses have been designed for running (e.g., [72]), but such prostheses are not multipurpose, and as such compromise the biomechanics of walking.

Recently, powered lower limb prostheses have begun to emerge. Powered prostheses–particularly those designed with low open-loop output impedance joints–have the ability to emulate a wide range of physical behaviors. Such devices are thus capable of emulating the biomechanical attributes of the healthy knee and ankle joints during walking or running, provided: 1) the prosthesis is endowed with a coordination-level controller that provides appropriate joint behaviors during walking and running, and 2) the prosthesis can recognize when the user wishes to transition between the walking and running gaits. The authors have previously presented a coordination-level controller that provides knee and ankle joint biomechanics representative of a healthy walking gait with a transfemoral amputee [55, 56, 58]. The authors note that Hitt, et al. have demonstrated the use of a powered ankle prosthesis to facilitate running in transtibial amputees [11], but are unaware of any prior research conducted to enable biomechanically healthy running in a transfemoral amputee with a powered knee and ankle prosthesis. As such, in this paper, the authors present

a coordination-level running controller as well as a control methodology that enables user-controllable transitions between walking and running. Following a description of the controllers, the control approach is implemented on a powered knee and ankle transfemoral prosthesis, and the efficacy of the controller is assessed in a series of treadmill-based running trials.

2.1.3 Biomechanical Characteristics of Running

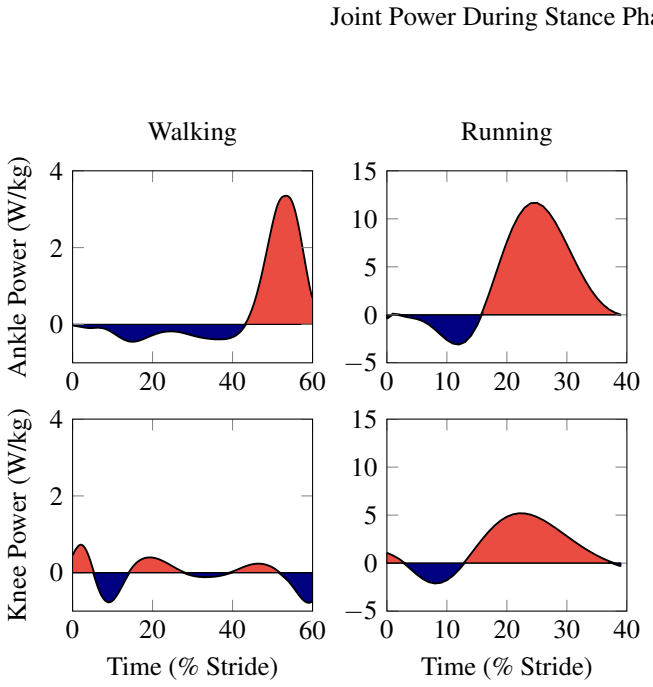

Figure 2.2: Power during running (right) and walking (left).

Blue (dark) area represents negative or absorbed power. Red (light) area represents positive or generated power [3, 64].

As previously mentioned, unlike walking, running is characterized by a body CoM trajectory that is lowest at mid-stance, and a stance phase that comprises less than 50% of the stride, resulting in a double-float portion of the gait cycle. Specifically, the double float phase of running comprises approximately 10% to 20% of the running stride, while the double support phase of walking comprises approximately the same proportion of the

walking stride. Biomechanically healthy running is further characterized by net positive power generation at both the knee and ankle joints (see Fig. 2.2), and also by a substantially greater degree of stance knee flexion and a correspondingly greater degree of stance ankle dorsiflexion, relative to walking.

The stance phase of running consists of two sub-phases: an absorption phase, which comprises approximately the first half of stance, and a propulsion phase, which comprises approximately the second half. During the absorption phase the knee and ankle joints function synchronously to absorb energy following foot strike, during which time the body CoM is increasingly lowered. This phase is followed by a propulsion phase during which the knee and ankle joints synchronously generate power (see Fig. 2.2), raising the body CoM, and subsequently leading to the double float phase of the stride [3, 73]. Note that the synchronous phasing of power absorption and generation in the knee and ankle joints characteristic of a running gait is in contrast with the generally asynchronous phasing exhibited during walking, also shown in Fig. 2.2 [64].

2.1.4 Controller Design

2.1.4.1 Coordination-Level Running Controller

The coordination-level running controller implemented in this paper is based on a control structure previously presented by the authors for level and sloped walking [55, 58, 56]. Specifically, coordination for a given activity is provided by an appropriately designed finite-state machine (FSM), wherein the physical behavior of each joint within each state (or mode) is characterized by a passive (emulated) impedance of the form:

$$\tau = k_i(\theta - \theta_{ei}) + b_i\dot{\theta} \tag{2.1}$$

where k_i, b_i, and θ_{ei} denote the linear stiffness, damping coefficient, and equilibrium angle, respectively, for a given joint (i.e., knee or ankle) for the i^{th} state during a gait cycle.

An iterative least squares regression of (2.1) was applied to joint position (θ), velocity ($\dot{\theta}$), and torque (τ) to healthy biomechanical running data from [3] (for both the knee and ankle) in order to determine the minimum number of finite states which could emulate the function of the leg during running, as well as a base set of parameters from which to begin a manual tuning process. This procedure resulted in a finite-state machine with four distinct gait modes, each with a corresponding set of impedance parameters, as shown in Fig. 2.3. Note that although the FSM derived here is characterized by common knee and ankle states, the knee and ankle FSMs need not incorporate an equal number of states, nor a synchronous set of states.

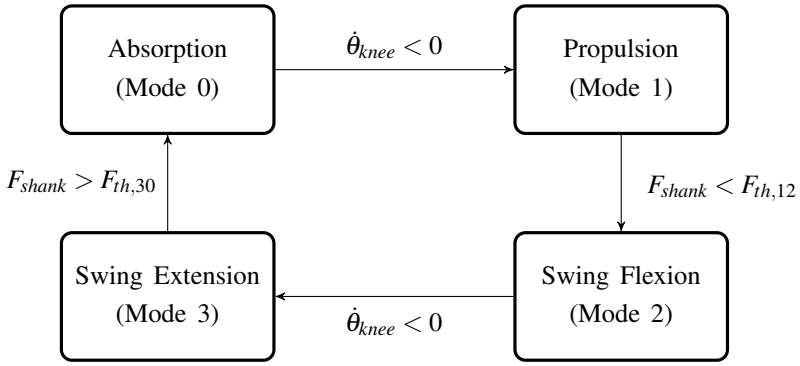

Figure 2.3: The finite state machine executed by the prosthesis for the running activity mode.

$\dot{\theta}_{knee}$ is the knee joint angular velocity. F_{shank} is the axial load in the prosthetic shank, which is compared to some predetermined threshold, $F_{th,xx}$, where xx represents the particular mode transition.

The four common states of the running controller correspond biomechanically to the absorption phase of stance (mode 0), the propulsion phase of stance (mode 1), swing flexion (mode 2), and swing extension (mode 3). A typical running gait cycle begins with foot strike, indicated by the shank load exceeding a given threshold, which places the FSM into mode 0, the energy absorption mode. In mode 0, both the knee and ankle predominantly exhibit relatively high stiffnesses. In this mode, the knee flexes under the load of the user's body mass, while the ankle dorsiflexes (following a brief initial plantarflexion to achieve foot flat). Energetically, both joints absorb the kinetic energy of the body CoM, as the

CoM is decelerated toward the nadir of its vertical excursion. At this point, indicated to the controller by the knee velocity approaching zero, the controller enters mode 1, the propulsion mode. While in mode 1, the knee and ankle actively extend and plantarflex, respectively, in order to propel the user forward and upward. Upon entering the double-float phase, the knee becomes unloaded, and as it nears its equilibrium point, the velocity of knee extension nears zero, signaling the controller to switch to mode 2, swing flexion mode. Mode 2 is characterized by knee flexion and ankle dorsiflexion. Once the knee moves through its equilibrium angle, knee angular velocity will again near zero, which moves the FSM into mode 3, during which the knee extends in preparation for foot strike (and entry into mode 0). Although not explicitly shown in the state chart in Fig. 2.3, a safety condition exists such that if during any aerial mode (mode 2 or 3) a load is detected by the prosthesis, the controller immediately transitions into the absorption mode (mode 0).

2.1.4.2 Transitions into and out of the Running Controller

In addition to providing a gait biomechanics representative of running, a prosthesis capable of both walking and running must enable the user to safely, intentionally, and consistently transition into and out of running when desired. Several studies have been conducted regarding the walk-run and run-walk transition in humans, although most of these are concerned with the factors that influence the gait speed at which people transition between walking and running gaits. Segers et al. [74] studied the kinematics of these transitions, including that of the transition stride as well as the preceding and subsequent strides. The study defined a walk-run transition (WRT) as the first stride (after walking) in which a double-float phase is observed, and a run-walk transition (RWT) as the first stride (after running) in which a double-support phase is observed [74]. The authors suggest that a WRT incorporates a pre-transition phase, where the subject adapts his or her configuration prior to landing for the first running step, and that the RWT incorporates a post-transition

phase, during which the trunk re-orients itself. Furthermore, the adaptation to walking was shown to take place mainly during the stance phase of the RWT transition stride. [74]

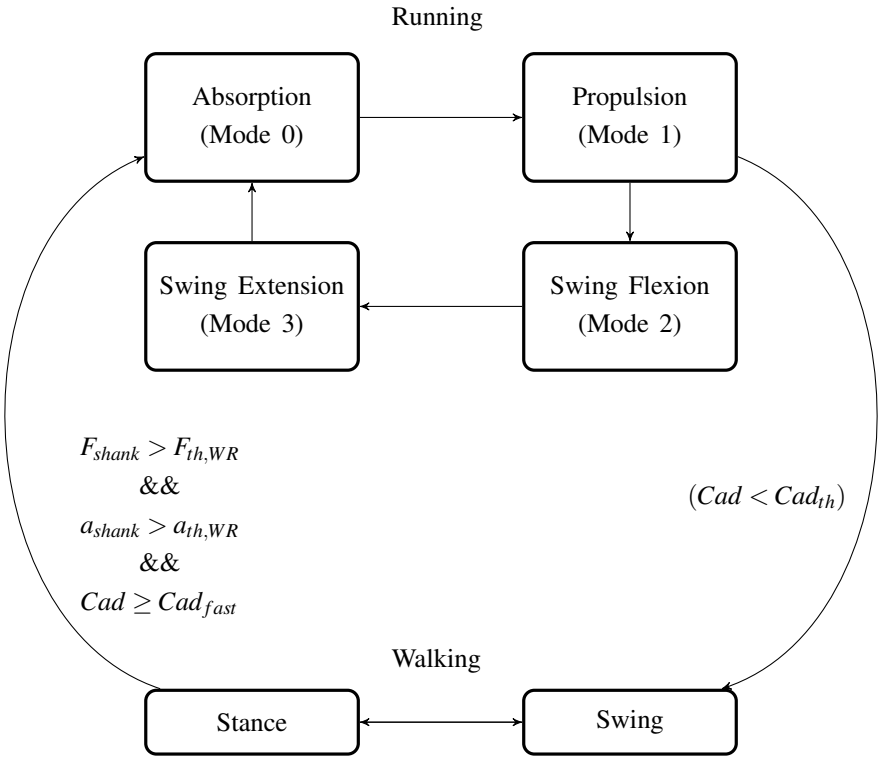

Figure 2.4: The finite state machine executed by the prosthesis for activity mode control between walking and running.

F_{shank}, a_{shank}, and Cad are shank load, acceleration along the shank, and estimated cadence, respectively, which are compared to predetermined thresholds, $F_{th,WR}$, $a_{th,WR}$, and Cad_{fast} for the transition to running from a walking gait. Note that Cad_{fast} denotes a cadence which characterizes a fast walking gait in the prosthesis walking controller. Cad is also compared to Cad_{th}, a predetermined threshold for the minimum acceptable cadence for a running stride.

Based on the observations presented in [74] regarding WRT and RWT, controller conditions for transitioning between walking and running coordination-level controllers were established, as diagrammed in Fig. 2.4. A WRT occurs at the transition from the swing phase of a fast walk to the absorption phase of running (mode 0). This transition technically takes place in the stance phase of the walking controller, since the load condition for the WRT will be met after the load condition for the stance phase of walking has been met; however, this condition is met very quickly after heel strike, giving the impression that the

transition took place from the swing phase of walking. A RWT is restricted to occurring at the transition from the propulsion phase of running (mode 1) to the swing phase of walking.

In the case of the WRT, consistent with the pre-transition phase observed by [74], the WRT condition requires that, from a fast walk, the user impose simultaneously a significant load and acceleration on the shank at heel strike, which is perceived by the prosthesis after the user enters the stance phase of the walking controller. Note that this transition is initiated by the user's sound leg by propelling the body upward such that the requisite force and acceleration are present after the user lands on the prosthesis. This action is deliberate and somewhat exaggerated but is also intuitive and natural, since it is consistent with the WRT observed in healthy subjects. The requirement of a deliberate action in general helps confirm intent of the user to transition into the running controller. Since the behaviors of the knee and ankle in running are similar to those in walking at the beginning of the stride, the transition can occur in a smooth and natural manner. Additionally, false positives are minimized since the user must be walking at an unnaturally fast cadence (for a walk) in order to transition into running (i.e., failure to trigger a transition into the running gait is more likely than unintentionally triggering it). Note that failure to trigger the transition will result in a limping stride, but will not otherwise become an adverse event.

The condition for a RWT requires that the running cadence falls below a minimum threshold. Cadence is determined by measuring the time between entries into each gait mode for adjacent strides. After the condition for the RWT has been met, the controller sends vibrational feedback to the user during mode 1, which indicates to the user that the prosthesis will transition to the walking controller immediately following the stance phase. Since the user is notified of a transition prior to its occurrence, the user is able to reenter a walking gait even in the case of an unintended RWT, and therefore a false positive will not result in an adverse event.

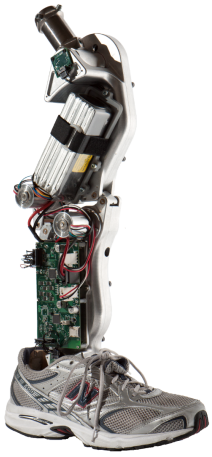

Figure 2.5: Vanderbilt powered prosthesis prototype.

2.1.5 Experimental Assessment

In order to assess the ability of the previously described controller to provide running biomechanics and controllable transitions between walking and running, the control approach was implemented on a powered knee and ankle prosthesis, which was then used in running trials performed by a transfemoral amputee subject. The powered prosthesis prototype on which the controller was implemented is shown in Fig. 2.5. This prosthesis is the second-generation Vanderbilt powered knee and ankle prosthesis, as described in [61]. The amputee subject who performed the controller assessment trials was a male age 24, 7 years post-amputation; the amputation resulted from a traumatic injury. His daily use (walking) prosthesis was an Otto-Bock C-Leg with a Freedom Innovations Renegade foot. Approval for this study was granted by the Vanderbilt University Institutional Review Board; the subject gave informed consent, including permission for publication of photographs and video.

2.1.5.1 Subject Training and Experimental Tuning of Impedance Parameters

As previously described, the impedance parameters of the running coordination controller were derived from a least-squares fit to healthy subject running data. That process

provided a set of nominal parameters, which do not account for individual differences in people, or for differences between the native limb and the powered prosthesis. As such, the impedance parameters were manually tuned to the prosthesis and amputee subject prior to conducting the running experiments. Specifically, the impedance parameters and transition conditions/thresholds were adjusted experimentally during treadmill running, as the subject was trained to use (and became accustomed to) the running controller. This training/learning/adjustment period occurred over nine sessions of running, each lasting approximately 30 min to one hour. Parameter adjustment was based on user feedback–in order to achieve user comfort and confidence in the action of the prosthesis–and on knee and ankle joint angle prosthesis data and qualitative video analysis–in order to obtain biomechanical characteristics representative of a running gait, smooth transitions between modes of the finite state controller, and reliable and natural transitions between walking and running activity modes.

2.1.5.2 Evaluation of the Coordination-level Running Controller

As previously mentioned, two of the distinguishing features of a running gait (from a walking gait) are 1) the existence of a double-float phase, and 2) a phasing between the vertical excursion of the CoM and the stance phase, in which the former is at a minimum at mid-stance. As such, the running controller was evaluated on its ability to produce these features as well as the extent to which it provided sagittal plane joint kinematics representative of healthy running. In order to assess these features, representative data was collected in experimental trials in which the amputee subject ran on a treadmill while the subject's movement was recorded with a motion capture system. Motion capture was performed using a twelve-camera OptiTrack S250e infrared camera system (NaturalPoint, Inc.) to track a full skeletal marker set (similar to the Helen Hayes marker set) consisting of thirty-four reflective markers. Motion capture data was sampled at 120 Hz using ARENA software (NaturalPoint, Inc.) and subsequently exported to and processed in MATLAB in

order to extract lower limb sagittal joint angles and motion of the estimated CoM.

For this assessment, the amputee subject ran with the powered prosthesis on a treadmill set to 2.25 m/s (5 mph), as shown in Fig. 2.6, which corresponded to a cadence of 133 steps/min for the subject. The subject was permitted to utilize the treadmill's handrails as necessary. Data was recorded over two trials, each trial consisting of approximately one minute of continuous, steady-state running, from which 15 strides were selected and used for analysis. Reference data representative of healthy running was collected using the same protocol on a small set of healthy subjects. Specifically, five healthy subjects (males ages 24 to 26) each ran on a treadmill at a speed of 2.25 m/s for two trials, approximately forty-five seconds each. Twenty consecutive strides from each healthy subject trial were selected and used for analysis.

Figure 2.6: Photo from single speed treadmill running.

The periodic data were parsed into single strides and normalized to a time base of 100%. Note that, in lieu of force plate data, the strides were parsed based on kinematic data in a manner similar to that presented in [75, 76]. Specifically, a sharp inflection of the ankle angle was used to determine heel strike–which marks beginning of the stance phase of gait–in lieu of the minimum position of the heel marker used in [75]. Toe off–which marks beginning of the swing phase of gait–was determined via the same marker used in [76], however using the vertical position of the toe marker rather than the acceleration

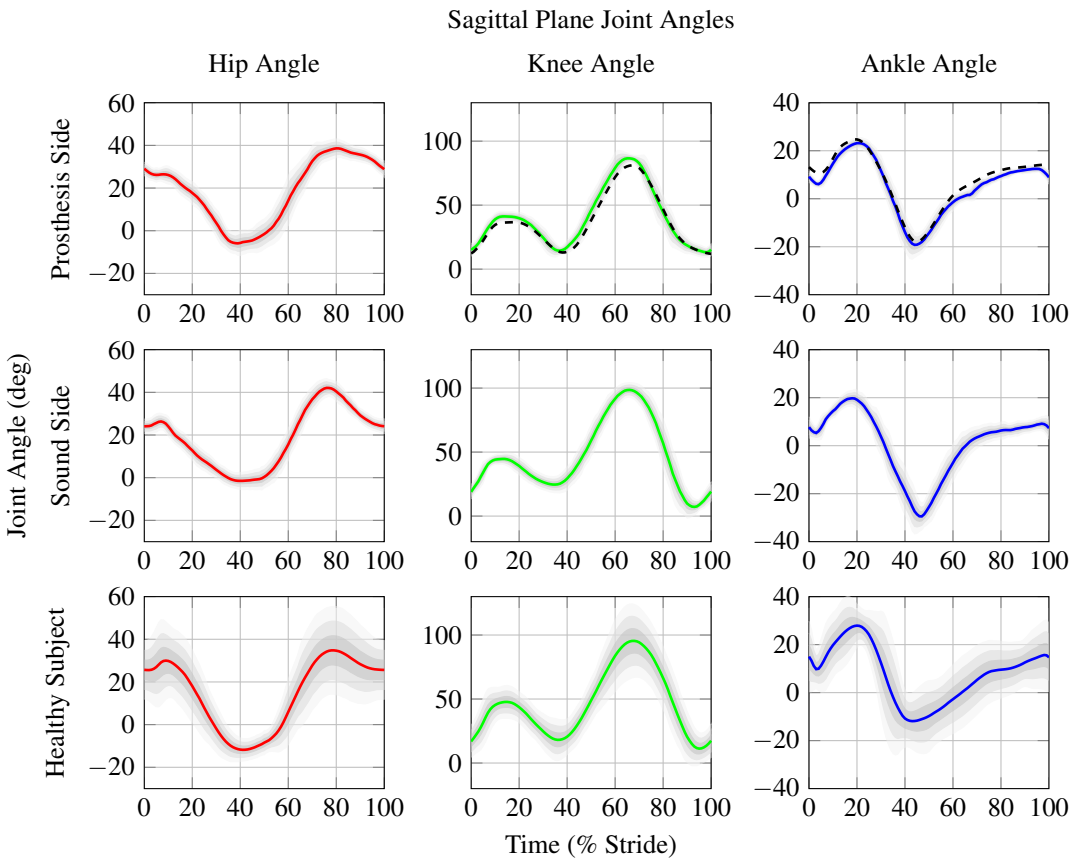

Figure 2.7: Lower Limb sagittal plane joint angles during running at 2.25 m/s.

For 1) amputee subject powered prosthesis (right) side, 2) amputee subject sound (left) side for powered prosthesis trials, and 3) healthy subject right side (averaged from 5 healthy subjects). The solid colored lines represent the mean joint angle data acquired via motion capture with 3 standard deviations shown in shades of gray. These data were taken from 15 consecutive strides for the amputee subject and 20 consecutive strides for the healthy subject, each in 2 trials. The dashed black lines represent the mean data recorded from the prosthesis for the same strides and trials as the motion capture data.

data. Periodic data for the amputee running measurements corresponds to the average of 30 strides taken over two trials, while the periodic data corresponding to healthy subject reference data corresponds to the average of 200 strides, taken from five subjects and two trials per subject.

Note also, since the "zero" position of the ankle angle is dependent on choice of reference between the foot and floor, an offset was applied to the ankle angle of each healthy

subject based upon the angle of the foot with respect to the ground plane during a period where each subject's foot was known to be flat on the ground. For the amputee subject, since the relative offset between the motion capture and prosthesis data sets was related to calibration and marker placement, an offset was applied to the ankle such that the two data sets had approximately the same mean value. Finally, note that the motion capture data was specifically used to compute the bilateral sagittal plane joint angles for the hip, knee, and ankle joints, in addition to the vertical excursion of the body CoM. The latter was approximated for this work by measuring the vertical displacement of the centroid of the pelvis.

Figures 2.7 - 2.10 show measurements derived from the motion capture data corresponding to these running trials. Specifically, Fig. 2.7 shows the averaged sagittal plane hip, knee, and ankle angles for both the prosthetic and sound side legs of the amputee while running with the powered prosthesis as well as the averaged (bilaterally symmetric) hip, knee, and ankle joint angles for the set of healthy subjects running at the same speed. Note that the figures also show the standard deviations in shading. The standard deviations for the single amputee subject are small (for both prosthesis and sound sides), indicating a consistent running gait. The standard deviations across healthy subjects are considerably greater, indicating some degree of natural variation between the running gaits of healthy subjects. With regard to the prosthesis joint angles, one can observe that the hip, knee, and ankle joints all exhibit the salient features of the corresponding healthy subject data. Despite this, one can also observe that the peak knee flexion angles are slightly smaller in the prosthesis in both stance and swing relative to the sound side and healthy norm, presumably due to power limitations in the prosthesis. Specifically, the powered prosthesis was operating at or near its maximum torque capabilities in stance and its maximum velocity capabilities in swing during the running trials. Consequently, the impedance parameters were set such that a smaller degree of knee flexion is achieved in each instance, thus reducing the amount of torque and velocity, respectively, required but not substantially

compromising the running gait.

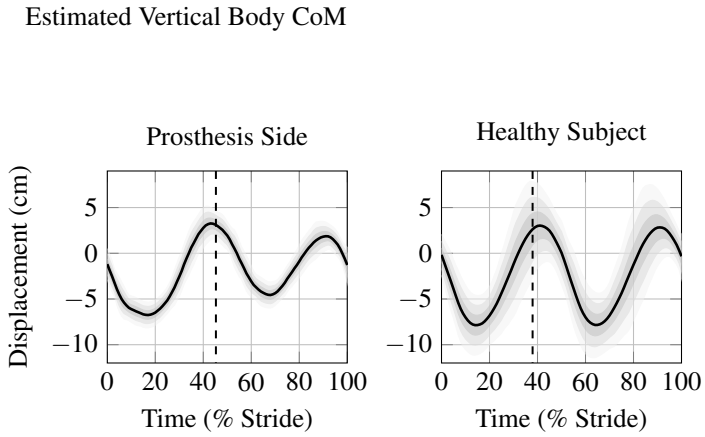

Figure 2.8: Estimated vertical body CoM (measured vertical displacement of the pelvis) during running at 2.25 m/s.

For 1) amputee subject powered prosthesis (right) side and 2) healthy subject right side (averaged from 5 healthy subjects). The solid lines represent the mean displacement data acquired via motion capture with 3 standard deviations shown in shades of gray. Each user's standing pelvis height (estimated vertical body CoM) was used as the zero offset.

Figure 2.8 depicts the vertical motion of the estimated CoM of the amputee subject while running, relative to stride percentage of the prosthesis, and also shows the corresponding averaged healthy subject data. The data indicates that the CoM is lowest near mid-stance (i.e., approximately 20%) of the prosthesis stride, and demonstrates a clear similarity of character to the pattern of CoM excursion in the healthy subject. Recall that this pattern of CoM movement is one of the defining characteristics of a running gait. Despite the similarity, one can also observe that, unlike the healthy subject data, the CoM excursion when running with the powered prosthesis is not bilaterally symmetric. Specifically, the amplitude of vertical excursion during sound-side stance is less than the corresponding amplitude during prosthesis-side stance. Although one could enumerate several potential factors underlying the bilateral asymmetry, the authors believe that the decreased vertical excursion during and following sound-side propulsion is substantially related to the subject's preference to minimize socket and prosthesis loading when landing on the prosthetic foot. Since the prosthetic leg must absorb at foot strike an amount of potential energy di-

rectly related to the vertical excursion of the body CoM, decreasing the vertical excursion of the body CoM during prosthetic swing phase will decrease the impact loading between the foot and ground, on the joints of prosthesis, and similarly between the socket and the load-bearing portions of the user/socket interface.

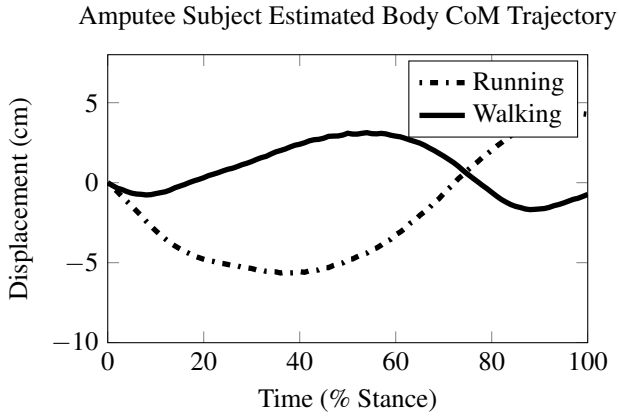

Figure 2.9: Estimated body vertical center of mass (CoM) for walking and running in amputee subject.

Running data are taken from single speed running trials. Walking data is taken from the third stride after a RWT in the walk-run transition trials described later in the work.

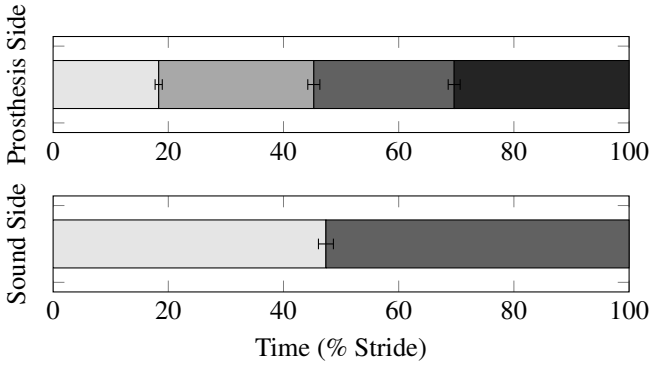

Figure 2.10: Mean prosthesis gait mode transition times (top) and sound side toe-off times (bottom) with error bars representing one standard deviation.

Figure 2.10 shows the proportion of the stance and swing phases for both the prosthetic and sound side legs during the running trials. Note that stance was measured as the period between heel strike and toe-off, both of which were extracted from the motion capture data for the sound leg according to the kinematic markers described previously, and were

measured by the load cell of the powered prosthesis for the prosthetic leg. As indicated in the figure, since the stance phase of both legs ends at approximately 45% of stride (45% and 47% respectively for the prosthetic and sound legs), the running gait includes a double-float phase comprising approximately 10% of the stride cycle. As a point of reference, the stance phase of running in healthy subjects has been reported to last between 39% and 45% of stride in [3, 73], and was an average of 38% in the group of healthy subjects used in this study. Recall that the existence of this double-float phase is one of the defining characteristics of a running gait. As such, Figs. 2.8 and 2.10 collectively validate that the powered prosthesis and running controller provide the two primary defining characteristics of a running gait. Finally, note that Fig. 2.10 also depicts the standard deviation of the controller modes with respect to stride, demonstrating a high degree of the consistency of gait mode transitions in the running controller which further fosters a consistency of stride on the sound side, as also indicated in the figure. A video depicting a set of representative steady-state running strides is included in the supplemental material.

2.1.5.3 Evaluation of the Transition Control Structure

In order to validate the walk/run and run/walk gait transition algorithm, a series of trials were conducted requiring the amputee subject to volitionally transition between gaits, while the transition from one gait to the other was captured in order to evaluate the ability of the controller to transition in a fluid and consistent manner. Specifically, motion capture data was recorded during five gait transition trials in which the subject was instructed to transition from a walking to a running gait on the treadmill, and subsequently from the running gait back to the walking gait.

For each transition trial, the subject started in the walking controller at his self-selected walking speed of 1.35 m/s (3 mph), and subsequently selected a treadmill speed of 2.25 m/s, which was the speed for which steady-state running was assessed. As the treadmill speed increased from 1.35 to 2.25 m/s, the subject initiated a walk-to-run transition (WRT).

Recall that the controller condition for the WRT requires that, from a fast walk, the user impose simultaneously a significant load and acceleration on the shank at heel strike, which initiates the stance phase of the running controller. Once in the running controller, the subject continued running for approximately five full running strides, after which he selected a treadmill speed of 1.35 m/s again. As the treadmill speed decreased, the user's running cadence decreased correspondingly, which initiated a run-to-walk transition (RWT). Recall the RWT is initiated based on the cadence falling below a given threshold, at which time the user is provided with vibrational feedback through the prosthesis, indicating that the controller will revert to a walking gait on the subsequent stride. This WRT/RWT treadmill trial was repeated five times. Note that the tachometer signal from the treadmill was also recorded during these trials, such that relationships between gait speed (i.e., treadmill speed) and gait transitions (i.e., as indicated by motion capture data) could be assessed.

These transition trials were conducted with the amputee subject only (i.e., not with the healthy subjects). The transition stride is defined for the prosthesis side as the stride during which the device begins to use the controller for the new gait mode. For example, for a WRT, the transition stride is defined as the stride during which the running controller is first used. A transition stride as defined from the perspective of the sound side was the first stride with characteristics corresponding to the new gait to which the subject transitioned. For example, the first stride to exhibit a double float phase on the sound side is the WRT stride. This stride would also share other gait characteristics with running, particularly sagittal plane joint angles as well as vertical body CoM, especially by the end of the stride. For each of the five trials, seven strides were identified and analyzed–the transition stride, three strides immediately preceding the transition, and three strides immediately following the transition–corresponding to each transition. For each stride identified, sagittal plane joint angles and estimated CoM were computed. The strides were normalized to a time base of 100% of stride and then grouped according to their temporal location relative to the transition stride–e.g. the five strides immediately following the WRT (one from each

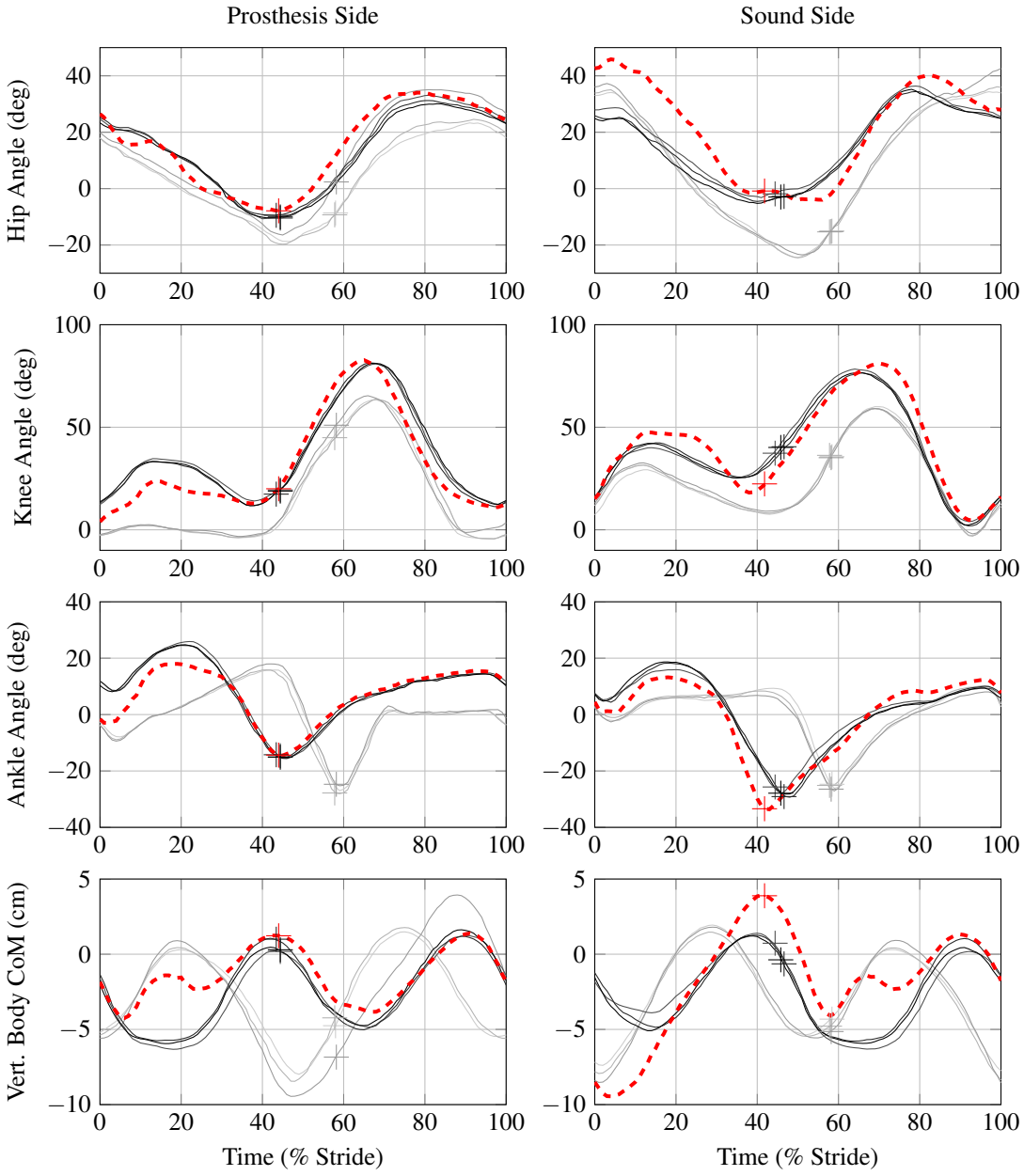

Figure 2.11: Lower limb sagittal joint angles and estimated vertical body CoM (measured vertical displacement of the pelvis) for the prosthesis and sound sides for the WRTs.

The transition stride $\pm$ 3 strides from each of the 5 trials were each averaged and plotted. Shown in light gray are the walking strides, shown in dark gray to black are the running strides, and shown by a red dashed line is the transition stride. The lightest gray curve represents the walking stride temporally furthest away from the transition stride, and the black curve represents the running stride temporally furthest away from the transition stride. A crosshair on each curve marks toe-off, separating stance from swing.

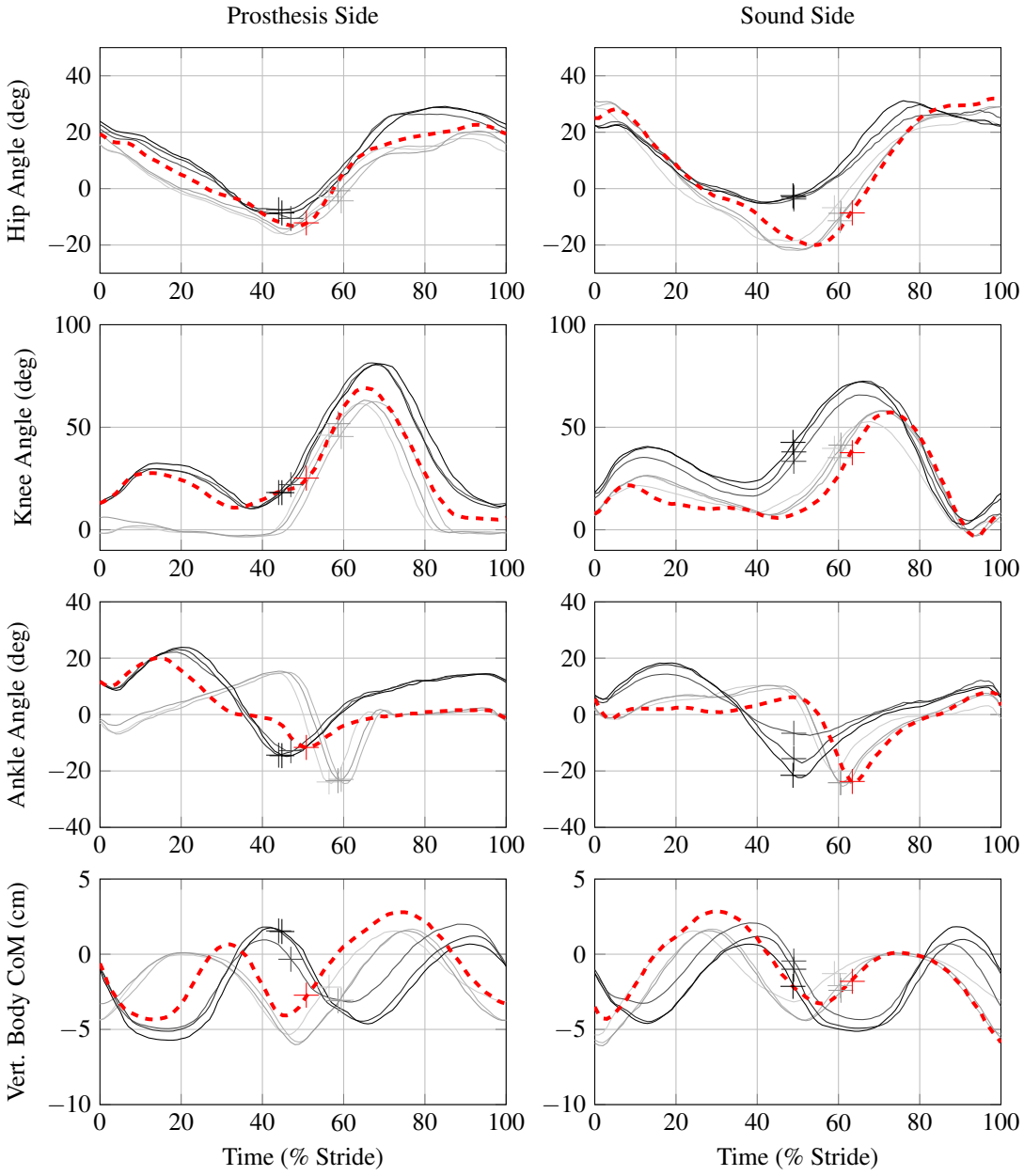

Figure 2.12: Lower limb sagittal joint angles and estimated vertical body CoM (measured vertical displacement of the pelvis) for the prosthesis and sound sides for the RWTs.

For legend, see Fig. 2.11.

trial) were grouped. The stride data in each group were averaged to produce representative data for that type of stride–e.g. for a stride immediately following a WRT. Joint angle and estimated CoM data for the WRT and surrounding strides are shown in Fig. 2.11, while corresponding data for the RWT are shown in Fig. 2.12.

Consider first the WRT depicted in Fig. 2.11. This transition is initiated by the sound side leg, and in particular by an exaggerated push-off phase (reminiscent of the propulsion phase in running) on the sound side, which results in an exaggerated heel strike on the prosthesis, initiating a transition to the running controller on the prosthesis. Note that the hip and knee joint movements exhibited by the sound side during the transition stride are exaggerated compared to those of the succeeding running strides, which is similarly the case for the estimated vertical body CoM for the WRT stride. Notice also that the estimated CoM trajectory begins the WRT stride similar to a typical walking stride and ends as a typical running stride, not exhibiting similarity to either in the middle of the stride. Finally, note that the stance phase duration of the transition stride, as indicated by the crosshair on the curve, has the characteristic shape of a running stride, but is also shorter than the other running strides, perhaps resulting from the users attempt at an extreme landing in order to ensure that transition conditions are met.

Though the controller switches to running almost immediately upon this exaggerated landing, since the user landed with the prosthesis in a configuration characteristic of walking, the kinematics do not immediately conform to a typical running stride. In particular, the knee and ankle exhibit less stance flexion and dorsiflexion, respectively, than the running strides which follow, but more than the preceding walking strides. Regarding the estimated vertical body CoM, the WRT curve initially follows a typical trajectory for a walking stride but begins to transition into one typical of a running stride by about 15% of stride and conforms to a typical running trajectory by approximately 30%. The hip angle curve for the WRT also resembles that of a typical running stride by approximately 30% of stride. The beginning of the stride resembles neither a walking nor a running stride. The oscillation shown may be related to stabilization at the hip during the transition between the walking and running controllers. Notice also that the hip angle curve of one of the walking strides resembles that of a running stride in the last 40%. In all trials, the WRT occurred after the treadmill had reached 2.25 m/s, as per the subjects preference. Specifi-

cally, the subject stated he felt more confident attempting the transition once the treadmill had reached a steady-state speed.

Figure 2.12 depicts data in a similar format to Fig. 2.11, but for the five trials corresponding to RWTs. For each trial, the RWT occurred at a treadmill speed between 1.35 m/s and 1.55 m/s (3.5 mph). Unlike the WRT, the RWT is initiated by the prosthesis side. On the prosthetic side, the RWT stride is characterized by a stance phase which lasts just over 50% of stride, which is characteristic of a walking stride. Regarding the sagittal plane joint angles, each RWT curve resembles a running stride for the stance phase and a walking stride for the swing phase. One can note in Fig. 2.12 the decrease in the peak of the ankle plantarflexion angle on the sound side in the three running strides preceding the transition. Specifically, the ankle plantarflexion associated with push-off decreases monotonically as the subject approaches the transition stride, which presumably is reflective of a general deceleration as the subject reduces speed and cadence ahead of the transition to walking, particularly since the transition to walking occurs at a lower velocity for the amputee subject than is seen for healthy subjects. The estimated vertical body CoM trajectory falls between the walking and running curves until approximately 30% of stride and then begins to resemble a walking stride. On the sound side, the RWT curves closely resemble those of a walking stride for their duration, since the prosthesis has already entered the walking controller by this time. The curves deviate slightly during the stance phases but match well the subsequent walking strides. In all cases of WRT and RWT, the consistency of data between trials, as depicted in Figs. 2.11 and 2.12, provides a clear indication that the subject was able to predictably and reliably execute transitions between the two forms of gait. A video depicting a representative WRT and RWT is included in the supplemental material.

2.1.6 Conclusion

This paper described and demonstrated a control approach for a powered knee and ankle prosthesis that enables a biomechanically appropriate running gait for transfemoral

amputees as well as transitions into and out of the running gait. The running controller was implemented in a powered prosthesis prototype and evaluated via treadmill trials on a transfemoral amputee subject. Motion capture data recorded during these trials indicates that the resulting gait characteristics are representative of a healthy running gait, including the presence of a double-float phase and a pattern of CoM motion in which the vertical excursion of the CoM reaches a minimum near mid-stance. The experimental assessments also demonstrated the ability of the user to consistently perform volitional transitions between the running and walking controllers and to execute these transitions in a fluid and predictable manner.

2.2 Addendum to Manuscript 1

2.2.1 Stability of the Coordination-Level Running Controller

The coordination-level (activity-level) running controller is designed such that once state 0 is initiated, the state machine will cycle through sequentially to state 3 according to the transition conditions which are met due to the natural motion of the user. However, the next gait cycle is not triggered until the user loads the prosthesis again. Therefore, should the user wish to stop suddenly (before transitioning to the walking gait), he or she should to avoid loading the prosthesis by using the sound side to bear weight and handrails for balance. This was the method used by the amputee subject to terminate his running gait prior to the development of the walk-run and run-walk transition controller.

2.2.2 Clarifications to Manuscript 1

The following is intended to provide clarification to some portions of the above manuscript and to address potential questions readers might have.

2.2.2.1 Target Population

Though it was not specifically stated in the above manuscript, the coordination and supervisory controllers presented in this work were intended for use with unilateral above-knee amputees only.

2.2.2.2 Walk-Run and Run-Walk Transition Analysis

Figures 2.11 and 2.12 were intended to depict each the seven phases of the transition from one type of gait to the other. Each for each set of axes, each plotted curve represents one phase, where the mean is taken of the one stride from each of the five trials which represents that phase. In summary, 35 strides are represented in each figure, where there are seven phases of the transition, with five individual strides averaged for each phase.

2.2.2.3 Running Powered Versus Passive Prostheses

The passive running prosthesis owned and used by the amputee subject in this work was comprised of a four-bar knee and a c-shaped carbon fiber blade-type foot. The subject was not comfortable running on a treadmill with either his running prosthesis or his daily-use (walking) prosthesis, especially for an extended period of time. Therefore, a direct comparison between passive and powered devices for running as well as walk-run and run-walk transitions was omitted from the above manuscript. The fact that the subject could achieve and sustain a running gait as well as return to a walking gait when desired with the powered prosthesis demonstrated the superiority of the powered prosthesis for running in an emergency or as an activity of daily living.

CHAPTER 3

VARIABLE CADENCE WALKING AND GROUND ADAPTIVE STANDING WITH A POWERED ANKLE PROSTHESIS

This chapter describes a controller which enables variable cadence walking and stable ground adaptive standing on various inclines for a powered ankle prosthesis. The walking controller incorporates varied passive behaviors and active power generation very similar to that seen in healthy subjects, while the standing controller enables the prosthesis to conform to the ground according to the user's input and subsequently provides support with the use of adaptive passive behaviors. Finally, the controller is able to distinguish the intent/need to use each controller based on biomechanical cues from the user, switching to the required function. While several prosthetic interventions exist which offer a subset of this functionality, this is the first to offer the entire suite. The following manuscript was published in the *IEEE Transactions on Neural Systems and Rehabilitation Engineering*, published online in April 2015 and published in print April 2016, Volume 24, Issue 4. Included in an addendum are clarifications to some of the content of the published manuscript.

3.1 Manuscript 2: Variable Cadence Walking and Ground Adaptive Standing with a Powered Ankle Prosthesis

3.1.1 Abstract

This paper describes a control approach that provides walking and standing functionality for a powered ankle prosthesis, and demonstrates the efficacy of the approach in experiments in which a unilateral transtibial amputee subject walks with the prosthesis at variable cadences, and stands on various slopes. Both controllers incorporate a finite-state structure that emulates healthy ankle joint behavior via a series of piecewise passive impedance functions. The walking controller incorporates an algorithm to modify impedance param-

eters based on estimated cadence, while the standing controller incorporates an algorithm to modulate the ankle equilibrium angle in order to adapt to the ground slope and user posture, and the supervisory controller selects between the walking and standing controllers. The system is shown to reproduce several essential biomechanical features of the healthy joint during walking, particularly relative to a passive prosthesis, and is shown to adapt to variable cadences. The system is also shown to adapt to slopes over a range of $\pm$ 15 deg and to provide support to the user in a manner that is biomimetic, as validated by quasi-static stiffness measurements recorded by the prosthesis. Data from standing trials indicate that the user places more weight on the powered prosthesis than on his passive prosthesis when standing on sloped surfaces, particularly at angles of 10 deg or greater. The authors also demonstrated that the prosthesis typically began providing support within 1 s of initial contact with the ground. Further, the supervisory controller was shown to be effective in switching between walking and standing, as well as in determining ground slope just prior to the transition from the standing controller to the walking controller, where the estimated ground slope was within 1.25 deg of the actual ground slope for all trials.

3.1.2 Introduction

Transtibial amputees typically utilize passive dynamic elastic response (DER) foot/ankle prostheses, which are relatively stiff leaf springs, typically configured nominally with a 90 deg angle between the foot and the shank. The behaviors of the intact human ankle joint, however, are considerably more varied than those provided by the passive DER prosthesis. Among the behaviors which might be exhibited by the intact ankle are adaptive passive behaviors (i.e., passive behaviors that vary as a function of activity), as well as active behaviors such as powered push-off [4]. Regarding the latter, the intact human ankle joint supplies net positive energy during gait initiation [5] and during steady-state walking, particularly in self-selected medium to fast walking [6]. A passive DER prosthesis is inherently unable to produce net power generation in these instances, and is therefore deficient

relative to the healthy joint.

Additionally, persons with below knee amputations walking on passive prosthetic devices have been shown to require up to 20% more oxygen uptake relative to healthy individuals [77], and their walking speed is significantly reduced [78] (between 10% and 22% [79, 80]). Walking speed and efficiency are substantially related to powered push-off (see, for example, [81, 82]), and as such, it is reasonable to hypothesize that restoring powered push-off could decrease cost of transport and increase walking speed for these individuals.

3.1.2.1 Prior Work

Recent advances in robotics technologies (battery, microprocessor, motor) have facilitated the emergence of powered prostheses which are capable of delivering power comparable to that which the biological joint generates during walking. Several such powered ankle designs are described in [14, 15, 16, 17, 18, 19, 20]. The extent to which such a device can restore the biomechanical functionality of the absent ankle, however, is dependent on the ability of a control system to coordinate the action of the powered prosthesis with both the movement and the movement intent of the user.

A number of control methods have emerged in conjunction with powered prosthetic ankle designs, several of which are reviewed in [22]. Among these, Holgate et al. discuss several strategies including position control, velocity or stiffness control, impedance control, and proportional myoelectric control [23]. Additionally, two control strategies are proposed to augment position control, including one based on a continuous relationship between shank angle (relative to an inertial reference frame) and ankle angle [23, 24], in conjunction with a scaling factor based on speed, and one which continuously modulates the ankle period and amplitude based on stride time of the previous gait cycle [23]. A powered ankle control strategy presented by Au et al. [28] describes both a neural network model and a neuromuscular model which rely on electromyogram (EMG) signal inputs from the amputee's residual limb to set the ankle angle. Another control strategy imple-

ments a four-state finite-state controller, where the control action within each state is a stiffness, a torque source, a position trajectory controller, or some combination of these [29]. This method is applied to both level ground walking and stair climbing in [30], and EMG signals from the user enable switching between controllers [30]. Additionally, [31] presents an approach based on a two state model, one for swing and the other for stance. The swing state employs position control and the stance state incorporates a Hill-type muscle model which reacts with a force in proportion to position and speed. Sun and Voglewede [32] present a finite-state controller comprised of four states: loading response, middle and terminal stance, pre-swing, and swing. During the stance phase (comprised of the first three finite states) output torque is controlled via PI feedback with a healthy subject torque profile as the reference, while the swing state is a PID position controller. Finally, Huang et al. present a proportional myoelectric controller for a pneumatic artificial plantar flexor muscle for a transtibial prosthesis [34].

This paper presents a walking controller which enables a biomimetic walking gait in a transtibial amputee with a powered ankle prosthesis prototype. The method incorporates a different control structure from the methods described above (i.e., [22, 29, 30, 31, 32]), including different state behaviors and different switching conditions. Further, the paper describes a control methodology for ground adaptive standing–namely, a controller that provides adaptation to various ground slopes regardless of the user's posture (the orientation of the shank with respect to the ground). A control method for such ground slope adaptation has not yet been demonstrated in the literature for a powered transtibial prosthesis. The authors have demonstrated similar functionality in a previous publication with a powered transfemoral prosthesis [54], although that method relies on measurement of ground reaction force, which is not measured or utilized in the system presented here. This work additionally describes the supervisory method by which the system determines how to switch between the walking and standing controllers. After a brief description of the powered ankle prosthesis prototype utilized herein, the authors describe the pow-

ered ankle prosthesis control structure for level walking with variable cadence and ground adaptive standing. Following the control description, the paper describes an experimental implementation and assessment of the prosthesis and each controller (variable slope standing, variable cadence walking, and the supervisory controller for switching between), and presents data demonstrating the ability of the prosthesis and controller to provide desired functionality during these activities and to select between them.

3.1.3 Prosthesis Design

3.1.3.1 Mechanical Design

The Vanderbilt powered ankle prosthesis prototype, shown in Fig. 3.1, has a range of motion of 45 deg of plantarflexion and 20 deg of dorsiflexion. Note that the electronics and battery shown in Fig. 3.1 are temporary, as a (more compact and better integrated) custom embedded system and battery pack will be implemented at a later date. The prosthesis incorporates a Maxon EC60 14-pole brushless motor, which is speed reduced by a factor of 116:1 through a 3-stage belt/chain/chain transmission in order to produce a peak ankle joint torque of approximately 100 Nm. The ankle-foot complex additionally incorporates a carbon-fiber leaf spring into the foot, which is characterized by a stiffness of approximately 4.2 Nm/deg and engages at approximately 1.6 deg (dorsiflexion). The spring biases the output capabilities of the ankle toward plantarflexion, which is consistent with the biomechanical characteristics of the human ankle during locomotion. At typical peak (dorsiflexive) ankle angles in middle to late stance, the spring provides up to 50 Nm of supplemental torque, such that the prosthesis is capable of providing a (combined active and passive) plantarflexive torque in middle to late stance of up to 150 Nm. A custom embedded system integrates a 32-bit microcontroller for execution of high-level control code with a 16-bit digital signal processing chip, which performs low-level control functions, such as commutation and current control of the brushless motor, and signal conditioning

of an absolute encoder at the joint, an incremental encoder at the motor, and a 6-axis inertial measurement unit (IMU) on the control board. Sensor information available to the high-level controller therefore includes ankle joint position and velocity (provided by the encoders), as well as shank absolute orientation and angular velocity information (provided by the IMU). The prosthesis is powered by an on-board lithium-polymer battery and attaches to a user's socket via a standard pyramid connector. The mass of the prosthesis as shown in Fig. 3.1, including electronics and battery, is 2.3 kg. Note that this prosthesis is based on an earlier version of the Vanderbilt powered ankle prosthesis prototype, described in [83].

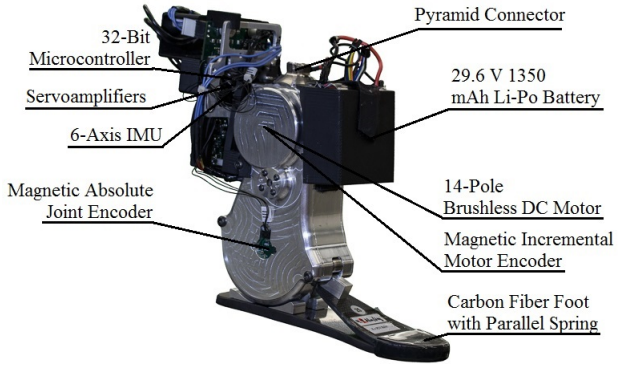

Figure 3.1: Vanderbilt powered prosthesis prototype.

3.1.3.2 Impedance-Based Control Design

Similar to the structure described by the authors for the control of a transfemoral prosthesis [63], the ankle control system consists of a finite-state machine (FSM) for each activity (e.g., walking, standing), where the behavior within each state is characterized by passive stiffness and damping terms. Specifically, for the controller described here, the ankle joint impedance within each state is given by

$$\tau = k_i(\theta - \theta_{e,i}) + k_{5,i}(\theta - \theta_{e,i})^5 + b_i\dot{\theta} \tag{3.1}$$

where k_i, $k_{5,i}$, b_i, and $\theta_{e,i}$ denote linear stiffness, fifth-order stiffness coefficient, damping coefficient, and equilibrium angle, respectively, for the i^{th} state during a gait cycle. The fifth-order stiffness coefficient $k_{5,i}$ is nonzero only during the middle stance state of the walking controller, where it acts as a stiffening spring term to increase ankle support as the user's center of mass (CoM) passes over the ankle joint. The fifth-order term was implemented as an approximation of the nonlinear stiffening behavior (between ankle angle and torque) observed in healthy subjects during the middle stance phase of walking [4, 64]. Transitions between finite states are triggered by pre-selected thresholds in sensor measurements. A supervisory controller selects which FSM (i.e., activity mode) is active based on the current activity mode and controller state, as well as sensor data. This paper describes the activity-level controller developed by the authors for walking at various cadences, the activity-level controller for ground adaptive standing, and the supervisory controller that switches between the two.

3.1.3.3 Walking Activity Mode Controller

In the walking activity mode controller, the ankle behavior over a gait cycle can be characterized by four basic functions, which map directly to states in the FSM, presented as a state chart in Fig. 3.2. During the early stance phase of gait (state 3), the joint behaves essentially as a damper, allowing plantarflexion upon heel contact to provide shock absorption (i.e., corresponding to the loading response). The powered prosthesis emulates a nonlinear spring during middle stance (state 0), which may be initiated either by foot flat detection (foot angular velocity sufficiently close to zero) or by the detection of ankle dorsiflexion immediately following heel strike. Since the prosthesis neither incorporates a load cell nor measures ground contact, heel strike is detected by a negative (plantarflexive) ankle angular velocity during state 3 which occurs when the ankle angular position is dorsiflexed relative to the equilibrium position for that state. Late stance (state 1) is initiated when the ankle is dorsiflexed past a predetermined angle. This state effects power deliv-

ery (push-off in healthy walking) by emulating a stiffness with a virtual equilibrium point in a plantarflexed position. At this transition, the rate of change of the torque reference is limited such that the power delivery is less abrupt and better mimics that which is observed in healthy gait. Once push-off is complete (the ankle angle reaches a predetermined threshold), the controller enters early swing (state 2), during which the ankle returns to a near-neutral although slightly dorsiflexed position to facilitate toe clearance during swing. Late swing (state 3) begins once the ankle has reached equilibrium (indicated by an ankle angular velocity that is sufficiently close to zero). In this state, as described previously, the ankle behaves essentially as a damper (with a light spring to maintain its nominal configuration) in preparation for heel strike.

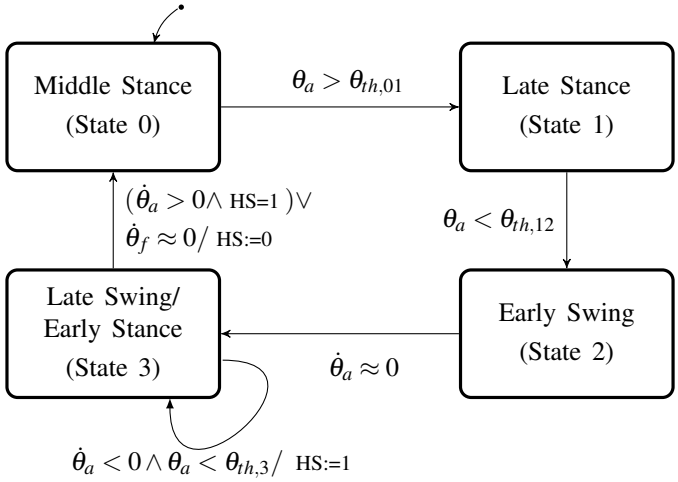

Figure 3.2: The FSM executed by the prosthesis for walking.

θ_a is the ankle angle, which is compared to predetermined thresholds $\theta_{th,01}$, $\theta_{th,12}$, and $\theta_{th,3}$, respectively. $\dot{\theta}_a$ is the angular velocity of the ankle, and $\dot{\theta}_f$ is the angular velocity of the foot with respect to the ground. HS is a flag which when set to 1 indicates a heel strike event.

Note that all transitions in the state machine associated with ground contact (i.e., all those except termination of late stance (push-off) and entrance into the damping state) require active user input. Specifically, to achieve foot flat the user must load the foot after

heel strike, and to initiate push-off (late stance), the user must continue to load the prosthesis as his center of mass moves forward over the foot. Late stance (state 1) will terminate automatically, based on either an angle or time condition, and as such this state is an inherently transient state that provides bounded movement and energy delivery. Ankle return (state 2) will also terminate once it has been completed. Therefore, in the absence direct user input, the prosthesis will default to passive behavior, and come to rest in either state 0 or 3. The dependency on user input to progress through the state machine, specifically during stance states, ensures that the user maintains control of ankle behavior, and that the device will default to passive behavior in the event that the user is not actively engaged in walking.

Note also that the walking controller does not enforce a specific walking speed, allowing the user to control his or her speed or cadence. Varied walking speeds, however, may be better accommodated by variation in power delivery in late stance and stiffness in middle stance. The controller accommodates such variation by measuring cadence, selecting one of three cadence ranges–slow, normal, or fast–and applying a corresponding set of controller parameters that provides increased push-off and stiffness with increasing cadence, in order to better match the biomechanical characteristics of the healthy ankle within those respective ranges of cadence. Cadence is measured by recording the time between each heel strike, with a moving window average of three strides. The controller switches between appropriate cadence regimes with a 2 step/min hysteresis in the switching in order to mitigate chatter between sets of control parameters.

3.1.3.4 Ground Adaptive Standing Activity Mode Controller

A powered prosthesis also benefits from a ground adaptive standing controller. This functionality is provided by the control structure depicted in Fig. 3.3, which is comprised of two impedance-based finite states: a support state and a conformal damping state, which are similar to the middle stance and late swing/early stance states, respectively, in the walk-

ing controller. The support state of the standing controller emulates a spring with light damping and is designed for use when the prosthesis is loaded; the conformal damping state is designed for use when the device first contacts the ground in order to facilitate foot flat according to the user's posture and ground topology. Adaptation to the ground is achieved by establishing the support state equilibrium angle based on the configuration of the ankle and/or foot following foot flat. This adaptation mechanism facilitates standing on a surface which is not perpendicular to gravity–i.e. inclines and declines. This functionality is also beneficial when standing or sitting in a relaxed pose where foot flat is desired regardless of the orientation of the shank. This controller is designed to accommodate both circumstances.

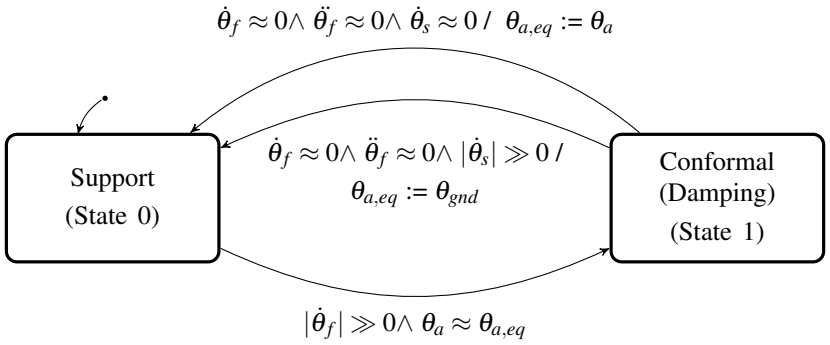

Figure 3.3: The FSM executed by the prosthesis for the standing activity mode.

$\ddot{\theta}_f$ is the angular acceleration of the foot. $\dot{\theta}_s$ is the angular velocity of the shank, and $\dot{\theta}_f$ is the angular velocity of the foot. θ_a is the ankle angle, which is compared to the ankle virtual equilibrium position $\theta_{a,eq}$. Additionally, θ_{gnd} is the estimate of the ground slope.

3.1.3.5 Supervisory Controller

A supervisory controller, depicted in Fig. 3.4, determines which of the two activity controllers, walking or standing, should be active. Switching from the standing activity controller to the walking activity controller is essentially equivalent to the push-off (late stance) trigger in walking–dorsiflexion of the ankle past a predetermined angle. In this case, the ankle must exceed a predetermined angle offset from the equilibrium position.

The transition to the walking controller can only be made from the support state (state 0) of the standing controller to the late stance state (state 1) of the walking controller. A walking gait, however, can be initiated by a step with either the sound leg or the prosthesis. In the case of the former, as the sound leg swings forward to heel strike, push-off is triggered on the prosthesis when the ankle angle (dorsiflexion) threshold is met. In the case of the latter, since the conformal damping and support states of the standing controller are similar in function to the early stance and middle stance states, respectively, of the walking controller, the prosthesis can remain in the standing control during the early and middle stance phases of the first stride, while exhibiting biomechanical functionality similar to that of the walking controller. Specifically, the user will initiate a step with the prosthesis in the standing controller, in which case the prosthesis will reside in the conformal damping state during heel strike; the controller will transition to support state at foot flat with an equilibrium position set according to ground slope, and finally will enter the walking activity controller and trigger push-off in late stance. Therefore, a stride initiated with the prosthesis is essentially the same as one initiated with the sound leg, although middle stance is characterized in the first step by a linear rather than nonlinear stiffness. Additionally, in both cases, the strength of the first push-off after switching to the walking controller is diminished relative to that of subsequent steps.

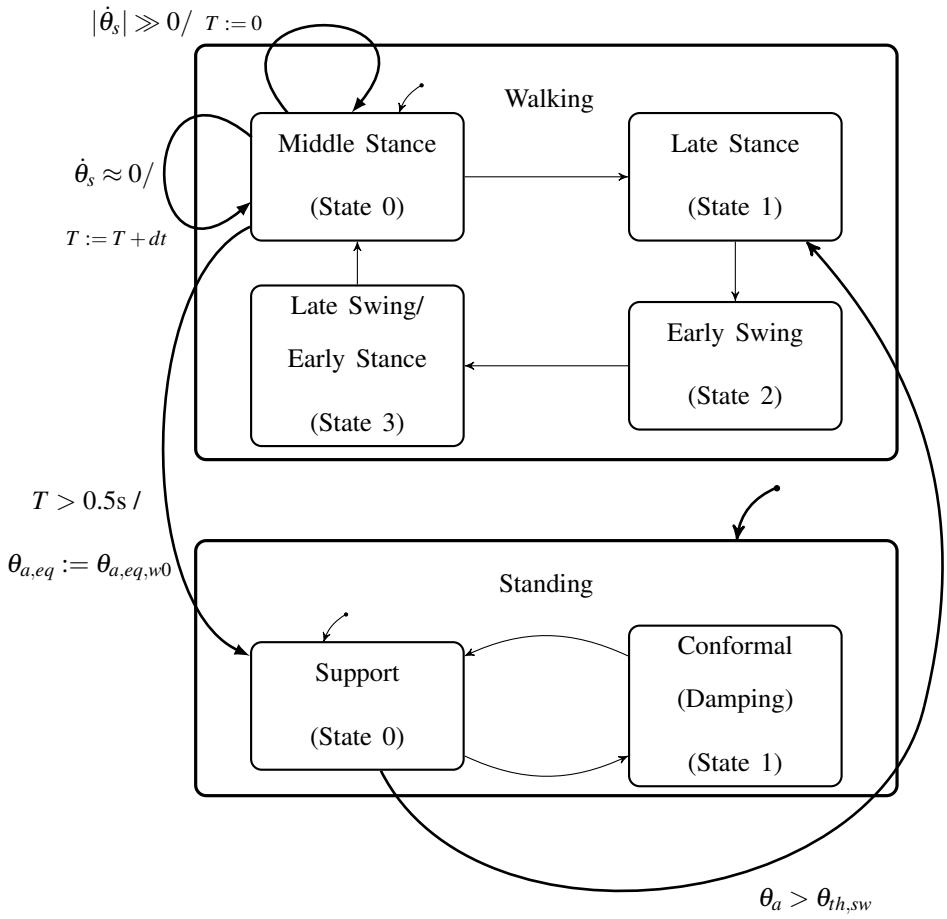

Figure 3.4: The supervisory controller executed by the prosthesis.

θ_a is the ankle angle, which is compared to a position threshold offset from the ankle equilibrium angle, represented here by $\theta_{th,sw}$. $\dot{\theta}_s$ is the angular velocity of the shank, T represents the amount of time that $\dot{\theta}_s$ is approximately zero, and dt is the sample time of the controller. $\theta_{a,eq}$ is the ankle equilibrium position for the subsequent state (State 0 of Standing), and $\theta_{a,eq,w0}$ is the ankle equilibrium position of State 0 of Walking, which is the previous state.

Switching from the walking controller to the standing controller takes place from middle stance (walking) to support (standing). While in middle stance (state 0), if the absolute angular velocity of the shank is near zero–i.e., magnitude less than 5 deg/s–for 0.5 s, the controller transitions into the support state of the standing controller, where the equilibrium position of the ankle persists from the middle stance state of walking.

The controller executes a transition from the support state to the conformal damping

state if the angular velocity of the foot is greater than 30 deg/s while the ankle angle is within 1.5 deg of the equilibrium position. These conditions are intended to establish that the user is not loading the prosthesis and may subsequently contact the ground. The controller transitions from the conformal damping phase to the support phase if the estimated (sagittal plane) foot angular velocity and foot angular acceleration are both approximately zero (magnitudes are less than 5 deg/s and 50 deg/s^2, respectively). These conditions indicate that the foot is essentially stationary with respect to the inertial reference frame, and thus is either on the ground and loaded, or in the air and immobile, in which case it need not conform to the ground and can enter support state.

A new equilibrium position is established at each transition from conformal damping to support. The new equilibrium angle is established by either the ground slope or the user's posture, depending upon the nature of the movement preceding the transition. In the case that the shank is rotating at the transition from conformal damping to support, as indicated by a magnitude of shank angular velocity greater than or equal to 10 deg/s, the new equilibrium angle is established as the mean of the estimated ground slope (orientation of the foot in the sagittal plane) during the 50 ms prior to the transition. These conditions might be met, for example, if the user is in prosthetic-side single support, while the sound-side foot is adjusting to the ground topology. Alternatively, these conditions might be met when the user initiates walking with the sound side, a circumstance which is discussed in more detail in the following subsection. In the case that the shank is essentially stationary at the transition from conformal damping to support, as indicated by a magnitude of shank angular velocity less than 10 deg/s, the new equilibrium angle is established as the mean of the ankle angle during the 50 ms prior to the transition. These conditions might be met if the user is in sound-side single support and the prosthetic foot is conforming to the ground, such as when sitting or when stepping onto a slope first with the sound side, followed by the prosthesis. Note that foot orientation is calculated as the sum of the sagittal plane shank orientation and ankle angle, and foot angular velocity as the sum of shank angular velocity

and ankle angular velocity, where the shank orientation and angular velocity are provided by the IMU.

3.1.4 Experimental Assessment

The two activity level controllers–variable cadence walking and variable slope standing–were implemented in the powered prosthesis prototype, along with the supervisory controller, and the collective behavior was assessed in experimental trials with a unilateral transtibial amputee subject. The subject was male, 44 years of age, 3 years post-amputation, with a body mass of 85.7 kg (189 lb). His limb loss was the result of a traumatic injury. Controller efficacy during walking and standing was assessed by comparing the behavior of the powered prosthesis to that of the subject's passive prosthesis (an Össur Vari-Flex XC carbon fiber foot) and to that of the healthy limb, as well as by determining the ability of the controller to select the appropriate behavior for a given activity in a timely manner; the details of these assessments are provided in subsequent subsections. Approval for these assessments was granted by the Vanderbilt University Institutional Review Board; the subject gave informed consent, including permission for publication of (non-de-identified) photographs and video. A video is included in the supplemental material that depicts walking and standing activities representative of the experimental trials described below.

3.1.4.1 Controller Parameters

A nominal set of controller parameters (i.e., impedance values and transition conditions) for the walking controller were initially established using ankle joint angle, angular velocity, and torque data from healthy subjects [64], and these parameters were iteratively tuned for the amputee subject during treadmill and overground walking. Control parameters were specifically adjusted based on a combination of quantitative (ankle joint kinematic and kinetic data) and qualitative (user feedback, external observation) information, in order to provide appropriate kinematics and kinetics as well as reliable and natural state tran-

sitions. The process of parameter tuning is similar to the manner in which a prosthetist iteratively adjusts passive components during prosthesis fitting in order to achieve comfortable, stable, and functional walking and standing. While there are a relatively large number of parameters associated with the walking controller presented in this work (16 per cadence mode), the authors hypothesize that the set which would require tuning in a clinical setting would be significantly reduced and would be intuitive for the prosthetist. Firstly, the four parameters associated with early swing as well as the equilibrium position in late swing/early stance are assumed to be independent of the subject or patient. Further, damping and linear and nonlinear stiffness parameters could likely eventually be coupled and thus adjusted by a single mechanism for each state. Additionally, the equilibrium and stiffness/damping of push-off, or late stance (state 1), can be coupled and adjusted as the strength of push-off. Therefore, establishing the control parameters for the intermediate cadence regime essentially entails tuning five gait parameters: 1) the stiffness/damping parameter in middle stance (analogous to selecting stiffness of a DER foot); 2) the equilibrium angle in middle stance (analogous to adjusting alignment of a DER foot); 3) the strength of push-off; 4) the trigger angle for push-off; 5) the speed (rate limiting) of push-off. Further, once these parameters are established, the parameters that would require modification for the slow and fast cadence regimes are 1) the spring stiffness in early stance; 2) the spring stiffness in middle stance; 3) push-off strength; 4) push-off trigger angle; 5) speed of push-off. As such, an additional ten parameters establish all controller function for the remaining cadence regimes. Thus, despite the existence of 48 total parameters, tuning of 15 parameters at three cadence regimes is sufficient to establish control functionality. The authors note also that, once a larger number of subjects have been fitted with the device, it is likely that height and weight can be correlated to certain parameters, such that the controller could be tuned in a clinical setting by adjusting only a few nominal controller characteristics.

3.1.4.2 Evaluation of the Walking Controller

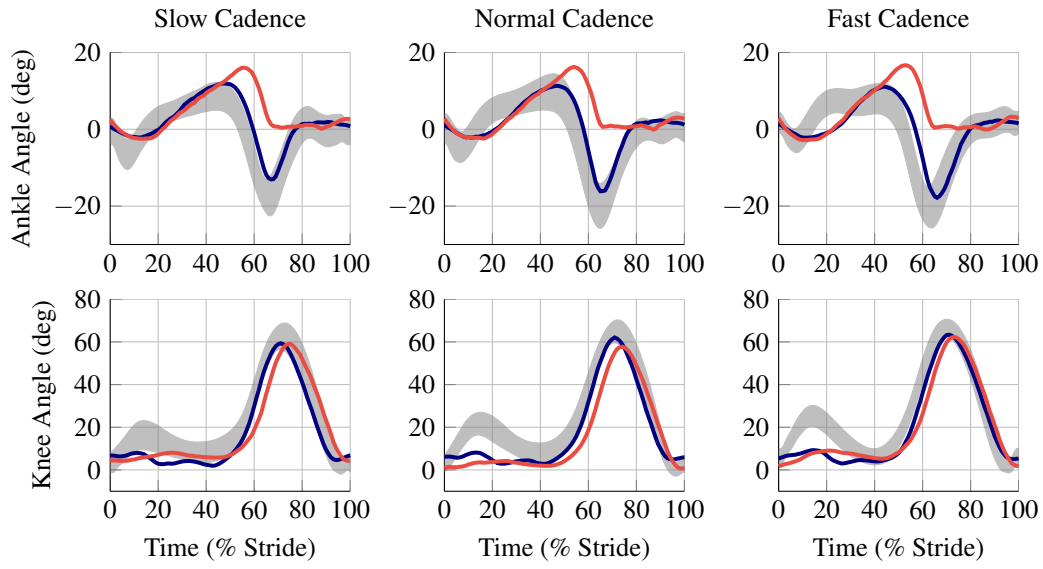

Figure 3.5: Kinematics (knee and ankle angles) for slow, normal, and fast cadences.

Healthy subject data $\pm$ 1 standard deviation are shaded in gray, powered prosthesis data are shown by blue (dark) lines, and passive prosthesis data are shown by red (light) lines. The maximum standard deviations of the mean at the ankle for the passive prosthesis are 1.90 deg at 65% stride, 1.48 deg at 62% stride, and 2.17 deg at 62% stride for slow, normal, and fast cadences respectively. The maximum standard deviations of the mean at the ankle for the powered prosthesis are 1.82 deg at 75% stride, 4.11 deg at 61% stride, and 4.28 deg at 62% stride for slow, normal, and fast cadences respectively. The maximum standard deviations of the mean at the knee for the passive prosthesis are 3.88 deg at 65% stride, 3.15 deg at 90% stride, and 4.24 deg at 85% stride for slow, normal, and fast cadences respectively. The maximum standard deviations of the mean at the knee for the powered prosthesis are 4.42 deg at 86% stride, 6.33 deg at 61% stride, and 6.60 deg at 89% stride for slow, normal, and fast cadences respectively.

In order to assess the efficacy of the walking controller, the amputee subject walked on a treadmill at three speeds–0.98, 1.13, and 1.35 m/s–which represent the slow, self-selected, and fast cadence regimes, respectively, with the powered prosthesis, and subsequently with his passive prosthesis. The subject walked at each speed, and with each prosthesis, for a period of approximately 90 s, during which ankle and knee joint angle data were collected via a motion capture system. Motion capture was performed using an OptiTrack S250e infrared twelve-camera system (NaturalPoint, Inc.) to track a full skeletal marker set (similar

to the Helen Hayes marker set) consisting of thirty-four reflective markers. Motion capture data were sampled at 120 Hz using ARENA software (NaturalPoint, Inc.) and subsequently exported to and processed in MATLAB in order to extract lower limb sagittal-plane joint angles. For each prosthesis and walking speed, 20 consecutive strides were selected from steady-state walking for analysis. The periodic data were parsed into strides in a manner similar to that presented in [75], using the inflection in ankle angle to determine heel strike in lieu of the minimum vertical position of the heel marker.

Figure 3.5 shows the knee and ankle kinematics for the subject walking with the powered prosthesis and the passive prosthesis, respectively, and also shows for reference the corresponding kinematic data for healthy subjects walking at similar cadences [64]. Specifically, the gray shaded area represents a plus and minus one standard deviation band around the healthy mean, the blue (dark) line is mean powered prosthesis data, and the red (light) line is mean passive prosthesis data, all at comparable cadences. Specifically, the three treadmill speeds used in the previously described experiments corresponded to respective cadences of 91, 101, and 112 steps/min with the powered prosthesis and 93, 104, and 110 steps/min for the passive prosthesis, respectively, while the healthy subject data corresponds to average cadences of 85, 105, and 125 steps/min.

As shown in the top row of Fig. 3.5, the ankle kinematics for the powered prosthesis falls largely within the healthy data band for all three speeds, while the kinematics of the passive prosthesis are much less representative of healthy patterns. Among the notable differences, powered push-off is not provided by the passive prosthesis, as evidenced by the absence of a plantarflexive peak in late stance/early swing. Additionally, notice that (for all three cadences) the peak dorsiflexion provided by the passive prosthesis in stance occurs at least 10% later in the stride than that of the powered prosthesis or healthy data.

One can observe in the healthy subject data a significant ankle dorsiflexion around 20% of stride, particularly for normal and fast cadences, and that neither prosthesis exhibits a similar pattern of dorsiflexion. Further, as shown in the bottom row of Fig. 3.5, the

subject achieves a significantly smaller degree of stance knee flexion with both prostheses, compared to healthy. Because the trajectory of the ankle is highly influenced by that of the knee during stance, this deviation in knee behavior (presumably due to compensatory behaviors that are trained into the amputee) causes the ankle to exhibit less dorsiflexion (compared to healthy) during the same portion of the stride.

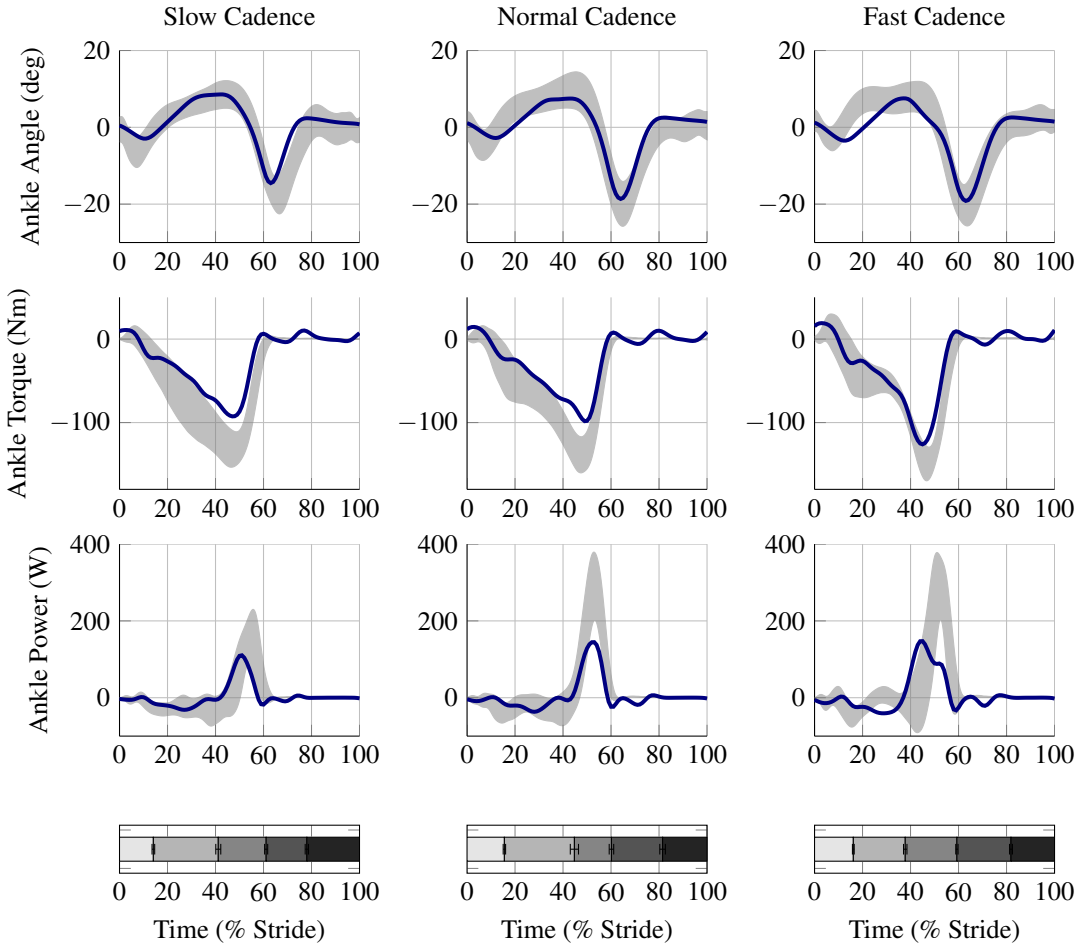

Figure 3.6: Kinematics and kinetics for slow, normal, and fast cadences.

Healthy subject data $\pm$ 1 standard deviation are shaded in gray, and powered prosthesis data are shown by blue (dark) lines. 1.35 deg at 68% stride, 7.12 Nm at 54% stride, and 16.54 W at 46% stride for slow cadence; 2.59 deg at 70% stride, 9.90 Nm at 47% stride, and 44.34 W 48% stride for normal cadence; and 1.14 deg at 69% stride, 6.88 Nm at 51% stride, and 15.29 W at 41% stride for fast cadence. State transition times (in percent of stride) with error bars representing $\pm$ 1 standard deviation are also shown in the bottom row of this figure.

For the powered prosthesis, ankle angle, angular velocity, and motor current data were recorded by the embedded system on the prosthesis during another set of trials. For these data, heel strike was determined as the point during State 3 when the ankle angular velocity became substantially nonzero (i.e., by the heel strike flag described in Fig. 3.2). The joint torque experienced by the user was calculated using the recorded motor current in combination with a model of the known or estimated passive characteristics of the motor, transmission, and parallel spring (i.e. inertia, friction, and stiffness) according to:

$$\tau_{jnt} = \begin{cases} \tau_{mot} - J\ddot{\theta} - b\dot{\theta} - c \cdot \text{sgn}(\dot{\theta}) - k(\theta - \theta_0) & \text{if } \theta \geq \theta_0 \\ \tau_{mot} - J\ddot{\theta} - b\dot{\theta} - c \cdot \text{sgn}(\dot{\theta}) & \text{if } \theta < \theta_0 \end{cases} \tag{3.2}$$

where τ_{mot} represents the motor torque (transformed into joint space), J is rotor inertia (transformed into joint space), b is viscous damping coefficient, c is Coulomb friction, k is the spring constant for the parallel spring, and θ_0 is the equilibrium position (contact angle) for the parallel spring. The motor torque is calculated using the motor current, torque constant (from the motor datasheet), and the transmission ratio from the motor to the joint output. The parallel spring stiffness and engagement angle, k and θ_0, respectively, were determined experimentally and were implemented in the control code to offset the motor torque command and are therefore known for the purpose of this analysis. Rotor inertia J was derived from motor manufacturer specifications and the known transmission ratio. The remaining parameters, c and b, were determined using least squares estimation of a set of data taken from driving the prosthesis with the motors through a state space comparable to level ground walking with no external load. The calculated torque was then multiplied by joint velocity to obtain joint power. Note that joint position, velocity, and acceleration data were filtered in post-processing in MATLAB in order to avoid phase lag in the velocity and acceleration signals. Specifically, the ankle position was filtered using a Fast Fourier Transform (FFT) to remove the frequency content above 10 Hz and reconstructed with an inverse FFT; the velocity and acceleration were obtained by differentiation of the zero-

phase-filtered position.

Figure 3.6 shows the powered ankle kinematic and kinetic data corresponding to the amputee subject walking with the powered prosthesis at the three cadences evaluated in this work, along with corresponding data representative of healthy subject walking, excerpted from [64]. In each plot, data characterizing plus and minus one standard deviation around the healthy mean are shaded in gray, providing a standard for comparison which incorporates inter-subject variability for healthy individuals, while the blue line is the mean data (over 20 strides) from the powered prosthesis. The respective cadences for healthy and prosthesis data are as listed previously.

The top row of Fig. 3.6 shows the ankle angle versus stride for the powered prosthesis and healthy norm, for the three respective walking speeds, while the second row of Fig. 3.6 shows the sagittal plane ankle torque for the powered prosthesis, relative to the healthy norm. The joint torque profiles for the powered are highly representative of healthy data, but with slightly lower magnitude. The third row of Fig. 3.6 shows the sagittal plane ankle joint power for the powered prosthesis, relative to the healthy norm, for the three walking speeds. The power delivery falls within the band of healthy subject data for slow walking (for the corresponding body weight), but is somewhat under-powered at normal and fast cadences. Note that in fast walking, the power pulse observed in the powered prosthesis leads that of healthy fast walking. Due to the aforementioned power limitations in the powered prosthesis, the authors chose to initiate power delivery slightly earlier than what is observed in healthy data in order to increase net energy delivery over the stride. Note that, while torque and power data are not available for the passive prosthesis, by nature it cannot deliver net positive power and will actually dissipate net power over a stride. The bottom row of Fig. 3.6 shows the state transition times in terms of percent of stride with error bars indicating $\pm$ one standard deviation, demonstrating a high degree of consistency in the transitions, thus indicating consistent, repeatable, and predictable prosthesis behavior during walking.

Average electrical power consumption of the powered prosthesis, as measured at the battery for the experimental trials conducted here, was 40.7 W, 69.8 W, and 88.2 W while walking at slow, normal (self-selected), and fast cadences, respectively. The battery currently implemented in the prosthesis, as shown in Fig. 1, has a capacity of 40 Wh (i.e., 1350 mAh @ 29.6 V), and as such, will provide approximately 3500 steps of walking on a battery charge at the self-selected walking cadence (i.e., 101 steps/min). Note that, as reported in [84, 85] an active amputee takes approximately 3000 - 4200 steps per day, and as such, the powered prosthesis as currently configured is estimated to provide a full day of walking on a battery charge. It should be noted, however, that an active healthy adult takes approximately 9500 steps per day [86], and providing this amount of activity would require either an increased battery capacity or replacement/charging of the battery during a day of use.

Note that the system is presently configured with a 4.2 Nm/deg parallel spring incorporated into the foot, which serves to effectively bias the torque capability of the device toward plantarflexion, reflecting the torque curve for walking in healthy subjects. A larger spring constant and/or a more plantarflexed engagement angle for this parallel spring would further bias the system toward plantarflexion, presumably reducing power consumption during walking, the extent to which has not yet been determined by the authors. Note, however, that as level ground walking is not the only activity supported by the powered prosthesis in this work, optimization of the spring stiffness and engagement angle should be based on power consumption in other activities, such as standing on inclines.

3.1.4.3 Evaluation of the Variable Cadence Control Algorithm

The performance of the variable cadence algorithm was assessed in a series of five trials during which the subject began walking on the treadmill at 0.78 m/s, after which the speed of the treadmill was increased at approximately 0.09 m/s increments to 1.7 m/s, and then subsequently decreased to the starting speed of 0.78 m/s. Cadence and cadence

mode data from the prosthesis were collected from the embedded system on the prosthesis and synchronized with video from which cadence was later extracted as the time between apparent heel strikes. The first two strides were removed from each data set, since the cadence measurement onboard the prosthesis averages that of the current and two preceding strides. Figure 3.7 shows a plot from one representative trial of cadence estimated by the prosthesis (red or light-colored marks) and measured from the video footage (blue or dark-colored marks), and also indicates the cadence mode at each time step by shading to various degrees. The mean and standard deviation of the absolute value of the cadence error (measured versus estimated) were 2.64 and 3.36 steps/min, respectively, for the trial depicted in Fig. 3.7, and 3.00 and 5.36 steps/min for all five trials combined. Note that, as can be seen in Fig. 3.7, the largest errors in each trial are at the beginning and end of the trial, where the subject was walking so slowly that the controller did not detect a heel strike during some strides. Since the controller still selected the correct cadence regime, however, these estimate errors did not affect the performance of the device.

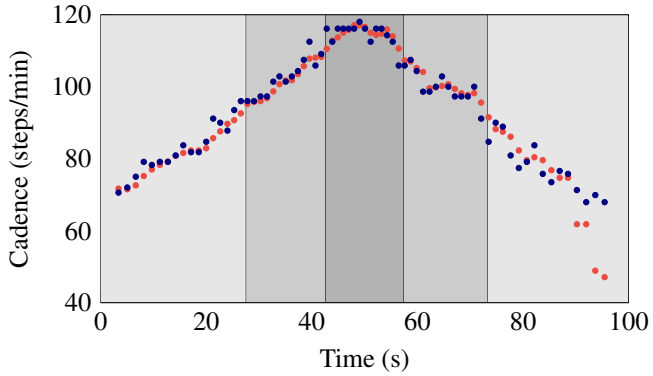

Figure 3.7: Cadence for a single variable cadence trial.

The red (light-colored) marks are the cadence measured by the prosthesis, and the blue (dark-colored) marks are the cadence extracted from the video. The gray shaded areas indicate the cadence mode of the prosthesis. The lightest-colored area represents the slow cadence mode, and the darkest-colored area represents the fast cadence mode.

3.1.4.4 Evaluation of the Ground Adaptive Standing Controller

The ground adaptive standing controller was evaluated based on its ability to select the appropriate equilibrium position according to the slope and/or preference of the user, and then to provide support at that position. In a first experiment, the subject stood on various ground slopes while the average weight distribution between the sound and prosthetic legs was measured by force plates. This experiment was conducted with the powered and passive prostheses, respectively for slopes of ± 15, ± 10, ± 5, and 0 deg, respectively. For the 0 deg slope, the subject stood directly on the force plates–one under each foot. For nonzero slopes, a corresponding wooden wedge with non-slip tape was placed on top of each force plate. For this assessment, the subject was instructed to stand on the wedges as though he were going to be doing so for an extended period of time.

Figure 3.8 shows the relative load on each foot for the affected and sound sides with the powered and passive prostheses, respectively. Notice that for the passive prosthesis, the subject did not load the prosthesis as much as his sound side for the more extreme inclines and declines (± 15 and ± 10). Since the passive prosthesis maintains a 90-deg equilibrium angle between the foot and shank, the subject must stand with a bent knee (and therefore shortened leg) on the prosthetic side when standing on the downslope, and must stand on the toe of the prosthesis on the upslope, slightly posterior to his center of mass. This can be seen clearly in Fig. 3.9a-b, which depicts the subject standing with his passive prosthesis on negative and positive 15 deg slopes, respectively. In both cases, the amputee is unable to comfortably place equal weight on the prosthesis, as indicated by Fig. 3.8. In the case of the powered prosthesis, the subject loaded the prosthesis more than the sound leg on extreme inclines, perhaps because it alleviated muscle loading on the sound side at extreme ends of the muscle length/tension curve. Figure 3.9c-d depicts the subject standing on negative and positive 15 deg slopes, respectively, with the powered prosthesis, demonstrating the ability of the prosthesis to conform to the slope, which enables the subject to stand with a straight knee and with the prosthetic foot fully flat on the sloped surface.

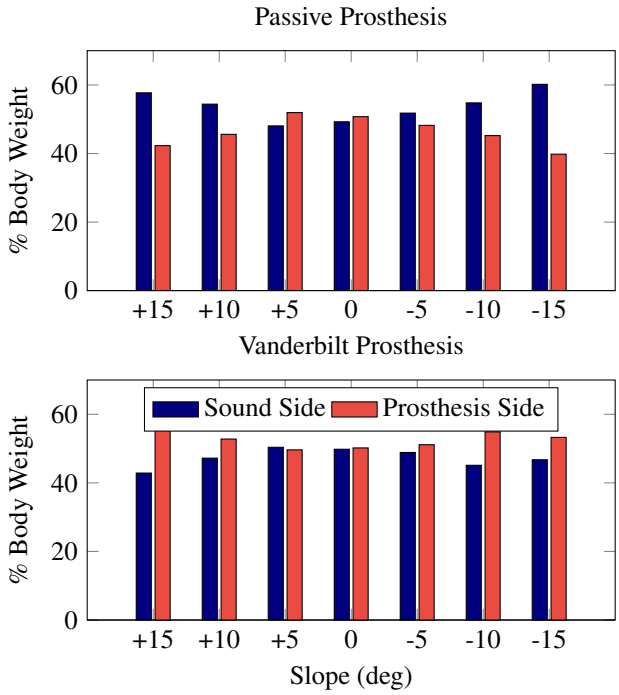

Figure 3.8: Plot of percent body weight on the sound side and prosthesis side, respectively, during standing on slopes of ± 15, ± 10, ± 5, and 0 degs with the passive prosthesis (top) and powered prosthesis (bottom).

The ability to conform to a ground slope can of course be provided with a simple articulated ankle (e.g., a simple or damped revolute joint), without the associated powered prosthesis or standing controller. In that case, however, the user would not receive the benefit of postural support provided by ankle joint stiffness, which is one of the primary biomechanical roles of the ankle during standing. In order to demonstrate that the powered prosthesis is providing ankle stiffness around the desired equilibrium, a second experiment was conducted in which the subject stood on the same sets of slopes with the powered prosthesis, and was instructed to sway slightly forward and backward, during which time the prosthesis recorded the ankle torque and angle. Figure 3.10 shows a plot of the ankle angle versus torque for each slope on which the subject stood. The data were calculated from measurements taken and recorded by the prosthesis and filtered in post-processing in MATLAB using the same method described previously for the walking data. This plot verifies the ankle stiffness and equilibrium point, demonstrating that the ankle was supporting

a)  b)  c)  d) 

Figure 3.9: Photos of the amputee subject standing on a 15-deg decline and incline with the powered and passive prostheses.

From left to right: a) passive prosthesis, -15-deg slope; b) passive prosthesis +15-deg slope; c) powered prosthesis, -15-deg slope; d) powered prosthesis +15-deg slope.

the user at the appropriate equilibrium position for each slope. Note that while the data shown indicate an equilibrium position approximately equal to the incline of each slope, the subject preferred increased dorsiflexion when standing on an incline, demonstrating the utility in allowing the user to position the ankle where comfortable prior to establishing an equilibrium angle.

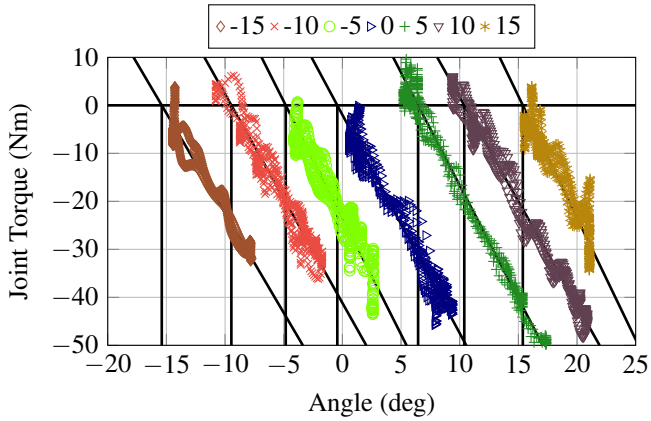

Figure 3.10: Plot of stiffness (torque versus angle) for the passive prosthesis during standing on slopes of ± 15, ± 10, ± 5, and 0 deg.

A third experiment was conducted to measure the time from initial contact between the prosthesis and the ground to the transition into the support state. All seven slope conditions listed previously were assessed, initially for stepping onto the slope with the prosthesis first, and then with the sound leg first. For this assessment, the force plate and wedges were used, and the prosthesis standing state was recorded by the embedded system and

synchronized with force plate data. For each slope condition, the subject was instructed to step onto the force plate/wedge first with his prosthetic side and then with his sound side, pause until the prosthesis provided support, then dismount, repeating the procedure five times. The subject was then instructed to repeat this sequence five times beginning with the sound side instead. The subject was permitted to readjust the prosthesis once he stood on the wedge if desired.

From these trials, the time of initial ground contact of the prosthesis and of the transition to support state were recorded. Any trials for which the prosthesis entered support state before initial contact or for which the prosthesis entered damping state after the prosthesis was fully loaded were considered ineligible for assessment and discarded, since no meaningful value for response time in these cases could be extracted. Such trials might include ones wherein the subject paused just before contacting the wedge or force plate and chose not to reposition the foot, or repositioned the foot so quickly that the force plate signal did not return to zero before it was loaded once more by the subject. Response time was then calculated as the difference between the time at transition into support state and the time of initial contact of the prosthesis with the force plate. The mean and standard deviation of this response time for eligible trials wherein the subject stepped with his prosthesis side first were 786 and 306 ms, respectively, and for trials where the subject stepped with his sound side first were 535 and 207 ms, respectively. The mean response time of all eligible trials was 663 ms, and the condition with the smallest mean response time was the -5 deg slope, sound side stepping first, at 284 ms.

3.1.4.5 Evaluation of the Supervisory Controller

The supervisory controller was evaluated in a series of 11 trials during which the subject started from sitting, stood, took two strides leading with the sound side, paused, turned around, took two strides leading with the prosthesis side (wherein for the first step the equilibrium position during support state was established according to estimated ground

slope), paused, turned around, and sat. This assessment procedure is somewhat similar to the timed-up-and-go test, although with the constraint that the sound side lead in the first two steps and the prosthetic side lead in the second two. Transition from standing to walking was expected at the beginning of each set of two strides, and transition from walking to standing was expected during each pause. Recall that the transition from walking to standing is based on a timer of inactivity (of shank motion).

In 10 of the 11 trials, the supervisory controller selected the expected activity modes. In the single trial in which the supervisory controller did not select the expected activity modes, the single error was a failure to select standing mode between the two-stride walking subsets. In this case, standing mode was not selected because the subject did not pause (standing quietly) long enough to reenter the standing mode. This error, however, was not noticeable to the subject, since the prosthesis remained in middle-stance state during the brief standing period, and thus provided essentially the same functionality. Had the subject stood on a sloped surface during that brief period, however, he would have noticed that the ankle would not have conformed to the surface. Since the second expected standing transition (which was the one to be initiated by the prosthesis side) could not take place in the aforementioned trial, it was considered ineligible for assessment of the equilibrium angle selection. For this series of trials, the expected equilibrium angle is the slope of the ground–in this case 0 deg. For the 10 eligible trials, the mean and standard deviation of the selected equilibrium angles were 0.67 and 0.44 deg, respectively, indicating that the controller was highly effective in selecting both an appropriate equilibrium angle, and the correct activity mode.

In addition to these trials, video was taken of the subject completing a series of tasks to demonstrate the functionality of the controllers presented in this work, including the supervisory controller and cadence mode selection. This video is included in supplemental material

3.1.5 Conclusion

A variable cadence walking controller and ground adaptive standing controller for a powered ankle prosthesis were described in this paper. The prosthesis and controller were demonstrated on an amputee subject, and shown to provide several features of healthy walking and standing biomechanics, which were not provided by the subject's passive prosthesis. The authors hope that this improved functionality in such a prosthesis can improve the extent of mobility, quality of life, and musculoskeletal health. Although clearly subjective, the single subject involved in the assessments presented here indicated a preference for functionality provided by the powered prosthesis, relative to his passive prosthesis, for the standing and walking activities characterized here. Future work will include the further development of prosthesis controllers for activities such as walking on uneven terrain, upslope and downslope, and for facilitating stair ascent and descent. Additionally, future work includes assessment of metabolic energy consumption while walking with a powered prosthesis, relative to walking with a passive prosthesis, and assessment of stresses on intact joints. Such studies will provide insight to support the extent to which such devices might provide health benefit relative to existing passive prostheses.

3.2 Addendum to Manuscript 2

This addendum serves to provide greater detail regarding the manner in which ankle position data were filtered for use in the output torque calculation. In order to obtain the most accurate estimate for the the output torque at the ankle joint, the model described by Eq. 3.2 in the manuscript above should use signals from the output of the joint, rather than the motor, in order to avoid influence from transmission dynamics. Further, this signal should also have minimal noise content and minimal phase lag. Since this analysis was performed in post-processing rather than in real time, a zero phase filtering method was used on the joint encoder signal to obtain the desired signal.

First, a Fast Fourier Transform (FFT) was performed on the joint encoder signal (the function. The the frequency content above the cut-off frequency was removed by setting all of the values corresponding to frequencies between the cut-off and the sampling frequency less the cut-off to 0. Then an inverse FFT was performed on the remaining frequency content to reconstruct the signal, of which the real part was set as the filtered signal. The following MATLAB code was used to accomplish this.

```
fs = 500; % sampling frequency (Hz)
fc = 10; % cut-off frequency (Hz)
rawSig = ankleMagEnc; % output encoder signal
N = length(rawSig);
fftSig = fft(rawSig); % FFT
freq = ((0:1/N:1-1/N)*fs).';
fftSig(freq >= fc & freq <= fs-fc) = 0; % remove frequency content (above 10Hz)
filtSig = ifft(rawSig); % reconstruct signal
filtSig = real(filtSig); % use real part only
```

CHAPTER 4

A UNIFIED CONTROLLER FOR WALKING ON EVEN AND UNEVEN TERRAIN WITH A POWERED ANKLE PROSTHESIS

Walking on flat or even, level terrain has received the most attention regarding development for powered prostheses thus far, with very little investigation into human gait while walking on uneven terrain, where changes in ground topography change the angle of the foot with respect to the ground from one step to the next. Consequently, there has been little to no investigation into control strategies for accommodating changes in terrain. This chapter describes development and evaluation of a unified control strategy for walking on even and uneven terrain with a powered ankle prosthesis, informed by behavioral models for the healthy ankle which were derived from a small healthy subject study for walking on even and uneven terrain. The following manuscript is being submitted for consideration for publication in the *IEEE Transactions on Neural Systems and Rehabilitation Engineering*. An addendum is included following the manuscript which provides some additional results from the aforementioned healthy and amputee subject studies, details the preliminary work done in preparation for that described in the manuscript, and presents some related technical development which has not been published.

4.1 Manuscript 3: A Unified Controller for Walking on Even and Uneven Terrain with a Powered Ankle Prosthesis

4.1.1 Abstract

This work describes the development of a controller for a powered ankle prosthesis that is intended to provide appropriate biomechanical behavior for walking on both even and uneven terrain without having to explicitly detect local slope to do so. In order to inform development of the controller, the authors conducted a small study of five healthy

subjects walking on even and uneven terrain. Data from the healthy subject study were used to formulate behavioral models for the healthy ankle, which were in turn used to develop controller behaviors intended to replicate various aspects of healthy ankle behavior in the powered prosthesis. The controller behaviors were implemented in a powered ankle prosthesis prototype and comparatively assessed on an amputee subject.

4.1.2 Introduction

Individuals with below-knee amputation who ambulate with the aid of a prosthesis typically use a passive dynamic elastic response (DER) prosthetic foot, which is constructed as a relatively stiff leaf spring. While such prostheses restore the ability to walk, they cannot provide net energy to the user, nor can they change their behavior to better accommodate different functions, activities, or changes in the environment. Robotic prosthetic interventions have begun to emerge which offer the potential to adapt behavior based on a given activity or terrain. Several control strategies have been proposed for such prostheses [23, 31, 28, 29, 30, 49, 35], although most of these have focused on providing walking on level, even terrain.

In this paper, the authors investigate and propose a controller for walking on level uneven terrain, which is defined here as terrain with substantial variation in local slope, with little to no variation in ground height between steps. For ambulation on uneven terrain, one would expect a body center of mass trajectory similar to that of even, level terrain, but with wide variations in step-to-step stance foot angle relative to the inertial reference frame. Examples of such terrain include broken sidewalks and rocky terrain. Walking on this type of terrain has not generally received attention in the literature describing powered prosthesis control strategies. Some recent studies, however, have examined related issues. For example, a recent study investigated kinematic differences in subjects with transtibial amputation when walking on uneven terrain (i.e., a loose rock surface) with powered (BiOM) versus an unpowered (DER) prostheses [45], reporting some differences in body

kinematics between the two interventions, such as in self-selected walking speed and toe clearance during swing.

Another recent study was conducted to examine healthy subjects walking on uneven terrain [8], specifically to assess changes in kinematics, kinetics, muscle activation, and metabolic energy expenditure when walking on uneven terrain, relative to walking on even terrain. One conclusion from the study was that healthy subjects experienced a large increase in the variation in ankle angle, particularly during the middle stance portion of the stride, on uneven terrain relative to even terrain [8]. This increase in ankle variability suggests potential problems for an ankle prosthesis which enforces a trajectory, which significantly restricts ankle movement, and/or which relies on measurement of ankle position to initiate key transitions within a stride–such as powered push-off. The aforementioned study [8] prompted the authors to conduct a follow-on study in order to gain more insight into the manner in which healthy subjects adapt to such changes in terrain, with the aim of designing a controller for a powered prosthesis which accommodates changes in terrain while maintaining proper function on even terrain.

4.1.3 Healthy Subject Experiments

Two studies were conducted over the course of this research; the first was conducted with five healthy subjects to provide data upon which to model control behaviors, while the second was conducted with a single amputee subject to assess the efficacy of the control behaviors derived from the first. Approval for these studies was granted by the Vanderbilt University Institutional Review Board, and all subjects gave informed consent, including permission for photo and video publication. This section describes the conduct and results of the first study.

4.1.3.1 Experimental Protocol

The healthy subject study was conducted with five male subjects, ages 25 to 32, with body masses ranging from 63.4 to 95.0 kg. This study was conducted to better understand movement and control strategies used by healthy subjects when walking on uneven terrain, and to establish a control objective for controller design for the powered prosthesis. These studies consisted of having healthy subjects walk repeatedly across first even and subsequently uneven terrain at a self-selected speed, during which whole-body kinematics and kinetics were recorded. In order to measure kinematic and kinetic data, synchronized motion capture and force data collection were performed using a 10-camera (T40) system from Vicon, one Bonita 720c video camera, and six AMTI OPT400600 force plates in a 6×1 configuration. The hardware was integrated and controlled via Vicon Nexus 2.5 software. A custom 42-marker skeleton was used to capture lower body and trunk motion. Terrain tiles for both the even and uneven terrain were created to fit on top of the force plates, and were also used to form a walkway leading to and from the force plates. Terrain very similar to that used in [8] was created for the uneven terrain used in these studies. In this work, uneven terrain is defined as terrain which is stable–i.e., does not shift or change while the foot is in contact with the ground–but which may result in a different local slope at each step. Here, local slope is defined as the orientation of the foot, particularly in the sagittal plane, while it is flat on the ground (during middle stance). Each terrain tile was created from a plywood base, and each uneven terrain tile held a repeating pattern of 4" $\times$ 6" $\times$ 1/2" plywood blocks stacked 0, 1, or 2 high. All tiles were covered with a foam sheet material, using spray adhesive, in order to prevent the subjects from encountering the sharp edges of the blocks or slipping. A foam mesh material was affixed to the bottom of the tiles using double-sided tape in order to prevent slippage relative to the force plates during normal walking. Two sets of uneven terrain tiles were created, each with the same repeating pattern but one set shifted relative to the other. Since each terrain tile could also be rotated 180 degrees when placed in the walkway, there were effectively four possible tile

types which could be interchanged to randomize the terrain pattern in the walkway. Figure 4.1 depicts a healthy subject (left) and an amputee subject (right) traversing two different configurations of the uneven terrain walkway.

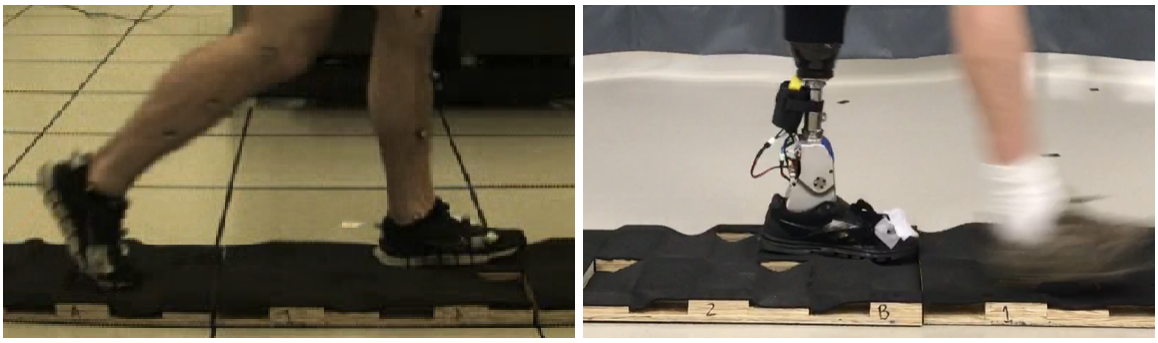

Figure 4.1: Photos of a healthy subject (left) and the amputee subject (right) each traversing a different configuration of the uneven terrain walkway.

For each data collection session, after the cameras were calibrated and markers placed on the subject, static and functional calibration files were collected for use in post-processing. Motion capture data were collected at 100 Hz for healthy subjects and 200 Hz for amputee subject trials. Force data were collected at 1000 Hz for all trials. In all trials, the even terrain portion of the study was completed before the uneven terrain portion.

For each terrain type, each subject took several trial passes along the walkway in order to familiarize himself with the terrain and to determine the ideal starting position for achieving a sufficient number of clean heel strikes. In order to achieve a stride for which all of the desired data could be analyzed following was required: 1) four successive instances of foot contact (two from each foot), 2) foot from first contact connected with force plates only at time of second foot contact (heel strike), and 3) no force plates shared between feet for first, second, or third foot contact. Subjects were instructed to walk as naturally as possible, at whatever pace was most comfortable, not targeting for clean foot strikes. The subjects completed between 50 and 80 passes for each terrain type–until the author conducting the study was convinced that a sufficient number of full strides had been captured.

For even terrain, after every 5 passes, the terrain tiles were inspected for shift and

repositioned if necessary. For the uneven terrain, every three passes, one terrain tile was reconfigured–uneven terrain tile type and/or orientation was changed–in a predetermined sequence which was identical for every subject, such that no combination of the 6 tiles was repeated for up to 69 passes. The other tiles were also inspected for shift at this time. Each time the terrain was reconfigured, the force plates were zeroed. Each subject switched his starting foot for every pass on uneven terrain. Further, subjects were allowed to take breaks as requested.

4.1.3.2 Data Analysis

The motion capture marker data post-processing was performed in Vicon Nexus 2.5, including file trimming, skeleton creation, static and functional subject calibration, marker filling, and deletion of erroneous marker captures. Next the force and marker data were processed in Visual3D, including skeletal model creation and functional calibration, data filtering, and performance of inverse dynamics. Some manual force-foot segment reassignment was required for accurate heel strike and foot contact data. All desired signals–i.e. kinematic and kinetic data–were calculated and exported from this software to MATLAB, where the data were parsed into acceptable strides according to the rules previously described, and further analyses performed. For each subject, a total of 40 strides were used, including strides for right and left sides.

Figure 4.2 shows representative data from a single healthy subject for walking on both even and uneven terrain. Specifically, the first column shows data from 40 strides of walking on even terrain, while the second column shows the equivalent data from 40 strides on uneven terrain. For both columns, the three rows show ankle angle, shank angle (relative to the vertical), and ankle moment (or torque), respectively, versus stride, for the 40 overlaid strides. Based on foot angle data (not shown in the figure), the range of slopes incurred by this subject during middle stance for the 40 strides on uneven terrain was -5.8 degrees to 10.0 degrees. As can be seen in the first column, the ankle angle, shank angle, and ankle

moment are all highly consistent when walking on even terrain, while the ankle angle is considerably less consistent when walking on uneven terrain. Figure 4.3 shows the data plotted in Fig. 4.2 during the middle stance portion of stride (i.e., 15-40% stride), plotted as ankle moment versus ankle angle (first row), and as ankle moment versus shank angle (second row) for the even (first column) and uneven (second column) terrain, respectively. In this paper, the relationship between ankle moment and angle during middle stance (as shown in Fig. 4.3 (a) and (c)) are referred to as the internal quasistiffness of the ankle, while the relationship between ankle moment and shank during middle stance (as shown in Fig. 4.3 (b) and (d)) are referred to as the external quasistiffness of the ankle. As evident in Fig. 4.3, while both the internal and external quasistiffnesses of the ankle appear to be invariant during even terrain walking, only the external quasistiffness remains invariant while walking on uneven terrain. Specifically, when walking over uneven terrain, ankle angle varies considerably from stride to stride, while the ankle moment remains relatively invariant. As a result, the internal quasistiffness relationship between ankle moment and angle observed in even terrain walking is no longer present. As observed in the plot of ankle moment versus shank angle for uneven terrain, however, the external quasistiffness relationship between ankle moment and shank angle is nearly fully preserved. Thus, the healthy behavior of the ankle during middle stance can be described by an external quasistiffness relationship that appears to be nearly invariant with respect to local ground slope.

Note that data is shown in Figs. 4.2 and 4.3 are for a single representative subject because intersubject variation obfuscates the invariance of the relationship in external quasistiffness, and thus ensemble averages act to wash out the subject-specific quasistiffness invariance. The invariance in external quasistiffness was consistent among subjects, however, which can be shown by comparing the quasistiffness residuals across all subjects. Specifically, the internal and external quasistiffness for both even an uneven terrain for each subject was fit to the function

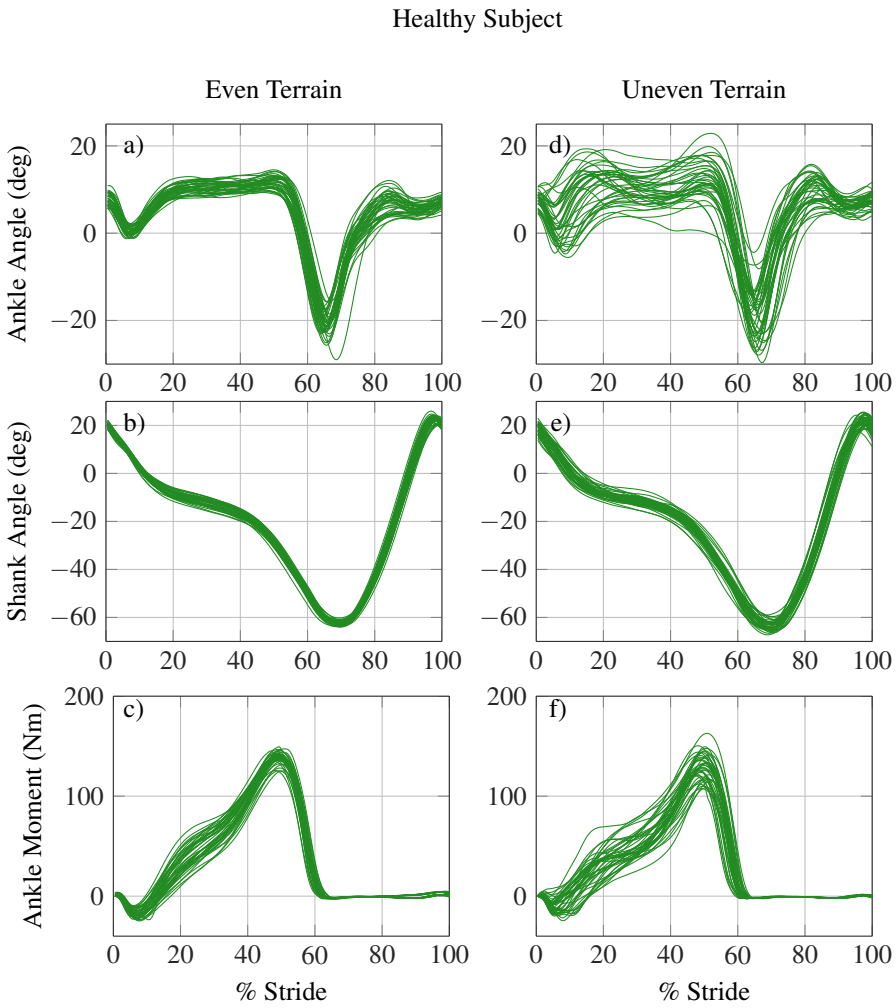

Figure 4.2: Sagittal plane ankle angle, shank angle, and ankle moment from a representative healthy subject (subject 4) walking on even (left) and uneven (right) terrain.

$$\tau = k(\theta - \theta_e) + k_5(\theta - \theta_e)^5 \tag{4.1}$$

using a linear regression of ankle moment in terms of ankle angle and then shank angle, where k, k_5, and θ_e were all coefficients in the regression. The residuals (and their respective standard deviations) corresponding to each for all five subjects are shown in Fig. 4.4. As can be observed in the figure, all subjects exhibited similar behavior. Note that the subject corresponding to the data shown in Figs. 4.2 and 4.3 is subject 4 (in Fig. 4.4), which is (as previously stated) representative of the group for both even and uneven terrain.

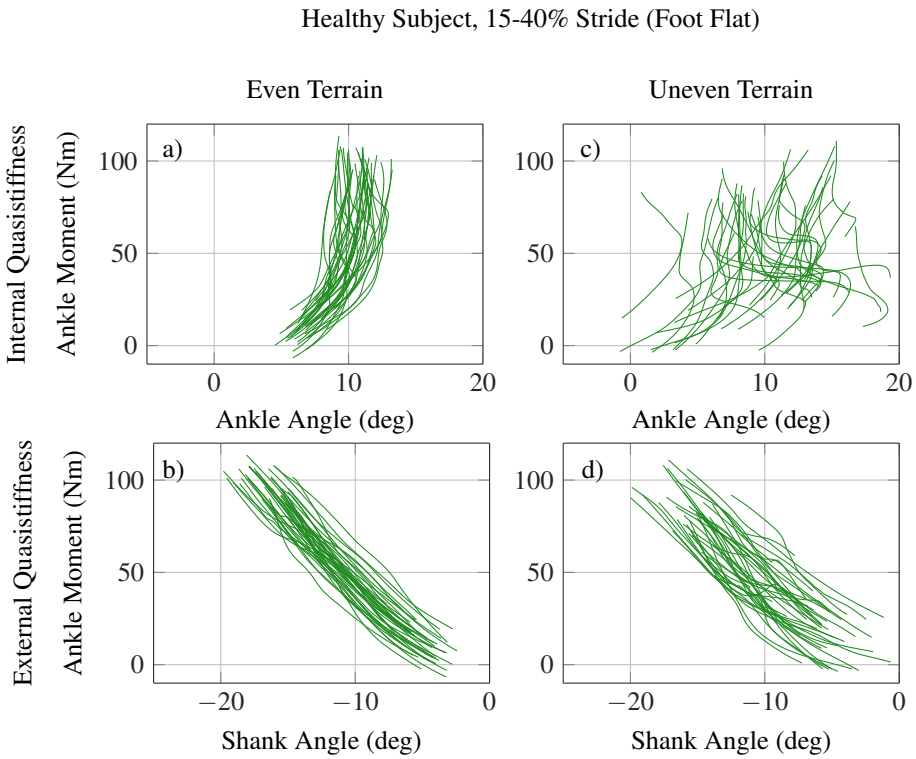

Figure 4.3: Internal (top) and external (bottom) ankle quasistiffness during middle stance for a representative healthy subject (subject 4) walking on even (left) and uneven (right) terrain.

As shown in Figs. 4.3 and 4.4, one can infer that the purpose of the behavior illustrated by these data is to provide an adaptive suspension of sorts, where the ankle provides an adaptive interface between the inconsistent ground topology and the relatively consistent kinetics and kinematics of the more proximal limb segments (i.e., it allows the foot to conform to the uneven surface, yet provides a consistent movement kinetics when viewed in the shank movement space). This observation of biomechanical behavior during walking on uneven terrain, along with other related observations subsequently discussed, motivated the prosthesis controller development and assessment that follows.

4.1.4 Toward A Unified Even/Uneven Terrain Walking Controller

A conventional DER (e.g., carbon fiber) prosthetic foot/ankle provides an invariant internal stiffness, which provides middle stance behavior observed in healthy walking on

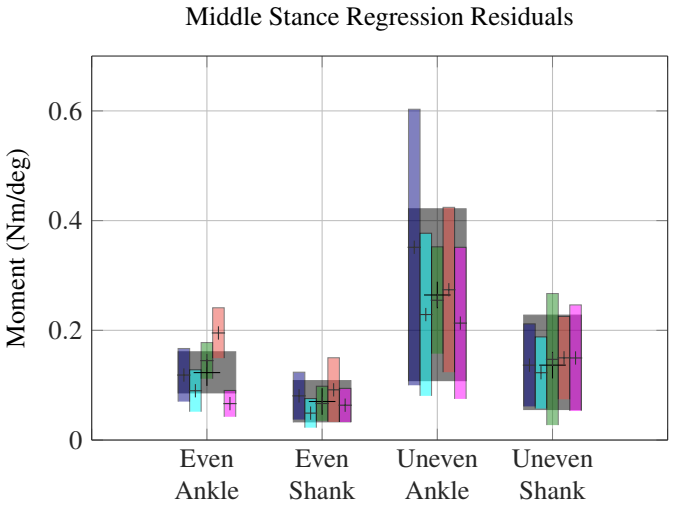

Figure 4.4: Root mean square (RMS) of the residuals from the linear regression performed for torque versus ankle and shank angle, respectively, for Eq. 4.1 (during middle stance/foot flat) for healthy subjects.

The crosshairs and translucent bars represent the mean $\pm$ 1 standard deviation, respectively; the narrow bars represent individual subjects, and the wide bars represent the mean of the standard deviations from the various subjects. The two groups on the left represent even terrain, and the two on the right represent uneven terrain. In each group of two, the one on the left is the ankle angle and the one on the right is the shank angle.

even terrain, but deviates from the behavior observed in healthy subjects on uneven terrain. As such, a conventional DER foot does not provide the adaptive interface observed in healthy walking on uneven terrain. Based on the aforementioned observation of external ankle quasistiffness invariance in healthy walking on even and uneven terrain, it follows that a prosthetic ankle that provides similar (mid-stance) behavior would provide improved functionality to the amputee user when walking on uneven surfaces. Such behavior can potentially be provided through energetically passive ankle mechanisms, as was the nominal objective in the device prototypes described in [87] and [88], both of which used gravitational forces to effect locking mechanisms in an ankle prosthesis. Rather than use mechanical design, this paper focuses on providing improved uneven terrain functionality through mechatronic means, specifically by implementation in a powered ankle prosthesis. Since the control behavior provided by a powered prosthesis is software programmable

(for the class of powered prostheses considered here), implementing such behaviors and investigating variations on these behaviors, as is done here, is greatly simplified relative to a mechanically-implemented design.

This paper specifically assesses the relative functionality for walking on even and uneven terrain provided by four controller variations, each of which consists of a single modification to the previous. The first is a controller which was previously published by the authors, developed strictly in the context of even terrain walking which provides an invariant internal stiffness during middle stance, and which was previously shown to functional effectively on even terrain. The second controller also provides an invariant internal stiffness during middle stance, but triggers push-off based on shank angle rather than ankle angle. The third provides an invariant external rather than internal ankle stiffness during middle stance. And the fourth provides a push-off behavior which accounts for ankle configuration at the onset of push-off. These controller variations, and the rationale for proposing them, are discussed in the following subsections.

4.1.4.1 C1: Previously Presented Walking Controller

The authors have previously described a walking controller for a powered ankle prosthesis [49] that was developed and previously assessed in the context of even terrain walking. That controller is used as the foundation for the controller variations presented here, and also used as a benchmark against which to assess the relative value of the proposed controller variations. As such, that controller is described in this section.

The basic structure of the walking controller employs an impedance-based finite-state machine (FSM) structure based on the powered prosthesis controller described in [63], where the commanded behavior within each state is characterized by passive stiffness and damping terms. The commanded ankle joint impedance within each state is given specifically by

$$\tau_i = k_i(\theta_a - \theta_{e,i}) + k_{5,i}(\theta_a - \theta_{e,i})^5 + b_i\dot{\theta}_a \tag{4.2}$$

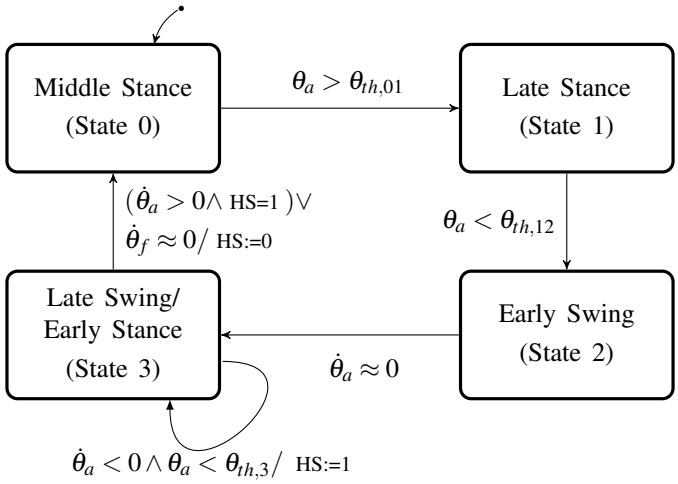

Figure 4.5: The FSM executed by the prosthesis for the C1 controller.

θ_a is the sagittal plane ankle angle which is compared to predetermined threshold $\theta_{th,01}$ to trigger push-off. θ_a is compared to thresholds $\theta_{th,12}$ and $\theta_{th,3}$, respectively, for other mode transitions. $\dot{\theta}_a$ is the angular velocity of the ankle, and $\dot{\theta}_f$ is the angular velocity of the foot with respect to the ground. HS is a flag which when set to 1 indicates a heel strike event.

where k_i, $k_{5,i}$, b_i, and $\theta_{e,i}$ denote linear stiffness, fifth-order stiffness coefficient, damping coefficient, and equilibrium angle, respectively, for the i^{th} state during a gait cycle; θ_a and $\dot{\theta}_a$ are sagittal plane ankle angle and angular velocity, respectively. The fifth-order term was implemented as an approximation of the nonlinear stiffening behavior (between ankle angle and torque) observed in healthy subjects during the middle stance phase of walking [4, 64] and is therefore only nonzero in the middle stance state. Transitions between finite states are triggered by pre-selected thresholds in sensor measurements. The ankle behavior over a walking gait cycle can be characterized by four basic functions, which map directly to states in the FSM, presented as a state chart in Fig. 4.5. The four states are late swing/early stance (state 3), middle stance (state 0), late stance (state 1), and early swing (state 2). Specifically, in late swing and early stance (i.e., state 3), the ankle provides damping, allowing passive plantarflexion and shock absorption upon heel contact. Since the prosthesis neither incorporates a load cell nor explicitly detects ground contact, heel strike is detected

by a plantarflexive ankle angular velocity during state 3 which occurs while the ankle is dorsiflexed relative to its equilibrium position. Note that heel strike need not be detected precisely at ground contact, since the behavior of the ankle does not change during heel strike. The powered prosthesis next transitions to middle stance (state 0), either by foot flat detection (foot angular velocity and acceleration sufficiently close to zero) or by the ankle dorsiflexion following heel strike. In the middle stance state, the ankle emulates a nonlinear spring behavior. Late stance (state 1) is initiated when the ankle is dorsiflexed past a predetermined angle. The late stance state delivers power (as in push-off in healthy walking) by setting the virtual equilibrium point of the ankle stiffness to a plantarflexed position with a relatively high stiffness. At this transition, the rate of change of the torque command is limited in order to better mimic the power delivery observed in healthy gait (i.e., the state behavior is a quasi-passive-impedance). Once the ankle angle reaches a predetermined position, the controller enters early swing (state 2), during which the ankle returns to a slightly dorsiflexed equilibrium position to facilitate toe clearance relative to the ground. Late swing (state 3) begins once the ankle has reached equilibrium (i.e. when ankle angular velocity is near zero). In this state, as described previously, the ankle behaves as a damper in preparation for heel strike. This controller (Fig. 4.5) is subsequently referred to as the C1 controller. As has been described in a prior publication, the C1 controller was shown to provide ankle motion, torque, and energy transfer more representative of the healthy ankle, relative to a DER ankle, when walking on even level terrain [49].

4.1.4.2 Variations on the C1 Controller for Uneven Terrain

Although the C1 controller was shown to provide behavior representative of the healthy ankle during level walking on even terrain, it is not necessarily well suited to walking on level uneven terrain. As such, controller variants were developed with the objective of providing appropriate behavior on both even and uneven terrain. Note that all differences between the C1 controller and the subsequently described variations are limited to the middle

and late stance control states only (i.e., the swing and heel strike states remain as described in the previous subsection and shown in Fig. 4.5).

4.1.4.3 Variations on the C1 Controller for Uneven Terrain – C2: Push-Off Trigger Modification

As previously described, the push-off state (state 1) is initiated in controller C1 when the ankle angle crosses a predetermined threshold of dorsiflexion. Although C1 was shown to provide appropriate push-off behavior on even terrain, preliminary experiments with this controller resulted in inconsistent push-off timing when walking on uneven terrain [89]. An analysis of data from the previously described healthy subject experiments suggests that the consistency of push-off initiation would be improved by initiating push-off based on shank angle, rather than ankle angle. The onset of push-off was identified in healthy-subject data as the moment at which the ankle power becomes and remains positive in late stance (i.e., the onset of the positive power pulse in late stance). The average variability in angle at push-off initiation was similar for the shank and ankle on even terrain, as well as the shank on uneven terrain, while the variability was much greater for the ankle on uneven terrain. Further, the push-off timing in healthy subjects was more robustly indicated by changes in shank angle relative to changes in ankle angle. Specifically, an event is most robustly indicated by a large and/or sudden change in an associated variable or quantity (e.g., the sudden increase in load corresponding to heel strike). Subtle changes in a variable are more difficult to detect and are more susceptible to variation or perturbation in the system. As such, a measure of robustness of indication is the local slope or gradient in the variable of detection, where a larger gradient indicates increased robustness of detection. Analysis of healthy subject push-off indicated that the mean gradients in ankle angle corresponding to initiation of push-off for walking on even and uneven terrain were 0.19 and 0.22 deg/% stride, respectively, while the mean gradients in shank angle were 1.32 and 1.38 deg/% stride, respectively. As such, the shank angle in healthy subjects provides a considerably

more robust indication of push-off initiation than does the ankle angle.

This observation of healthy ankle behavior on even and uneven terrain indicates that the transition from the middle stance state (state 0) to the late stance state (state 1) could be more robust if initiated by shank rather than ankle angle, particularly on uneven terrain. In order to test this assumption, a variation on controller C1 is proposed in which the only change is that the shank angle is used for push-off initiation, rather than ankle angle. Specifically, in the condition to switch from state 0 to state 1 shown in Fig. 4.5, θ_a is substituted by $-\theta_s$, or the negative of the sagittal plane shank angle, with a slightly modified threshold $\theta_{th,01}$. Note that this version of the controller preserves all other aspects of controller C1. As such, controller C2, the first controller variation, is similar to C1 in nearly all respects (see Fig. 4.5), but initiates push-off based on shank angle reaching a predetermined threshold, rather than ankle angle.

4.1.4.4 Variations on the C1 Controller for Uneven Terrain – C3: Middle Stance Impedance Modification

Recall that the healthy ankle provides an invariant internal and external quasistiffness during even terrain walking, but provides invariance only in external quasistiffness during uneven terrain walking (see Figs. 4.3 and 4.4). The middle stance behavior in the C1 (and C2) controllers provide an invariant internal quasistiffness (i.e., see Eq. 4.2 and its context), which provides behavior representative of healthy ankle behavior on even terrain (e.g., Fig. 4.3 (a)), but not on uneven terrain (e.g., Fig. 4.3 (c)). Similar to the invariant external quasistiffness behavior observed in healthy subjects (e.g., Figs. 4.3 (b) and (d)), the C3 controller variation replaces the middle stance internal stiffness behavior with a middle stance external stiffness by replacing the ankle angle terms in Eq. **??** with shank angle terms. Specifically, in controller C3, the reference angle for the virtual spring in middle stance (state 0) becomes the (negative of the) shank angle rather than the ankle angle, as

described in Eq. 4.3.

$$\tau_0 = k_{s,0}(-\theta_s - \theta_{s,e,0}) + k_{s,5,0}(-\theta_s - \theta_{s,e,0})^5 + b_0\dot{\theta}_a \tag{4.3}$$

where τ_0 is the torque command for middle stance; $k_{s,0}$, $\theta_{s,e,0}$, and $k_{s,5,0}$ are the linear stiffness, equilibrium position, and fifth-order stiffness coefficients, respectively, for the shank in middle stance; b_0 is the damping coefficient for middle stance; and θ_s and θ_a are the sagittal plane shank and ankle angles, respectively. Note that, aside from the difference in middle stance impedance behavior, the C3 controller preserves all other aspects of the C2 controller.

4.1.4.5 Variations on the C1 Controller for Uneven Terrain – C4: Push-Off Impedance Modification

Another observation of healthy subject data that informs a potential prosthesis controller for uneven terrain is that the push-off torque observed in healthy subjects when walking over even and uneven terrain was better modeled when the impedance (i.e., torque) equation included a term describing the ankle configuration at the onset of push-off. Specifically, an analysis similar to that conducted for middle stance (and shown in Fig. 4.4) was performed for push-off mode in order to compare the accuracy of various models of ankle torque on even and uneven terrain during push-off. The push-off state for healthy subjects was defined as the portion of the stride after push-off initiation until power delivery is completed (i.e., the duration of the positive power pulse in late stance). Four possible independent variables were considered for this analysis: ankle angle, shank angle, ankle angle with offset, and shank angle with offset. For each case with an offset, the offset was comprised of the (ankle or shank) angle at which push-off was initiated and a constant offset, such that on even terrain the mean difference between the spring reference and the equilibrium position at the initiation of push-off mode would be equivalent to that of C3.

Equation (4.4) describes the regression equation, where α was known, and k and θ_e were coefficients in the regression.

$$\tau = k(\theta - \alpha - \theta_e) \tag{4.4}$$

Figure 4.6 shows the RMS of the residuals of the linear regression of the measured torque based on the push-off impedance equation with and without an ankle offset term, demonstrating that inclusion of the offset term was the better predictor of torque during push-off for both even and uneven terrain with lower mean and standard deviation of the residuals. Note that the shank, ankle with offset, and shank with offset conditions performed very similarly, and therefore only the version using ankle angle as offset is shown, since ankle angle is a higher-quality real-time measurement than shank angle (as subsequently discussed). Accordingly, in order to better replicate healthy ankle behavior in a powered prosthesis, the C3 controller was further modified to implement an impedance behavior during push-off (state 1) given by

$$\tau_1 = k_1(\theta_a - (\theta_{e,1} + \alpha)) + b_1\dot{\theta}_a \tag{4.5}$$

where α is equal to the ankle angle at push-off with a predetermined constant offset. Note that the nonlinear stiffness term is omitted here since k_5 is equal to 0 in all controller variations during push-off. Further, α is applied to the transition from state 1 to state 2 in the following manner:

$$\theta_a < \theta_{th,12} + \alpha \tag{4.6}$$

A summary of features of the four controllers (i.e., original controller and three variations) is given in Table 4.1.

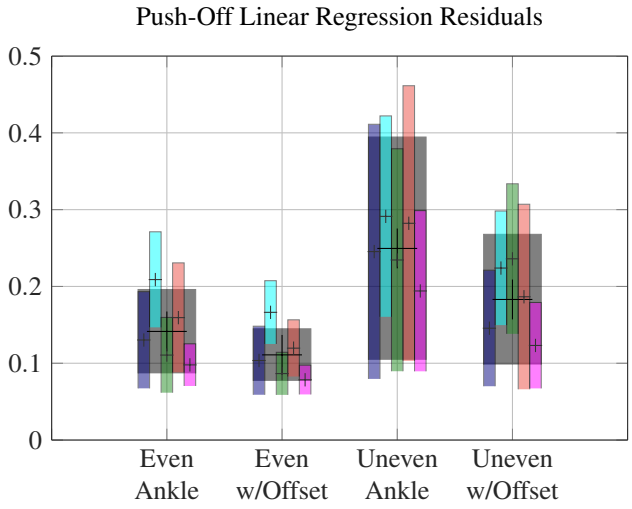

Figure 4.6: Root mean square (RMS) of the residuals from the linear regression performed for torque versus ankle angle and ankle angle with offset, respectively, for Eq. 4.4 (during push-off) for healthy subjects.

The crosshairs and translucent bars represent the mean $\pm$ 1 standard deviation, respectively; the narrow bars represent individual subjects, and the wide bars represent the mean of the standard deviations from the various subjects. The two groups on the left represent even terrain, and the two on the right represent uneven terrain. In each group of two, the one on the left is the ankle angle and the one on the right is the ankle angle with offset.

4.1.5 Controller Assessment: Methods

In order to assess the prospective value of the controller variations, relative to the previously-proposed controller and relative to a DER prosthesis, the authors conducted experiments in which an amputee subject walked over even and uneven terrain with a powered prosthesis controlled by each of the four controller variations, and also with a daily-use DER prosthesis. The amputee subject in this work was a male, age 50, ten years post-amputation, with body mass of 82.5kg (with his daily use prosthesis). His daily use prosthesis was a Fillauer AllPro Foot. The experimental protocol, setup, and instrumentation for these experiments were the same as the previously-discussed healthy subject experiments. As in the healthy-subject experiments, 40 (clean) strides were recorded from the prosthetic side for each controller for the powered prosthesis and for the daily-use prosthesis, with the exception of the daily-use prosthesis on even terrain, for which only 36

Table 4.1: Controller Summary

		C1	C2	C3	C4
Push-Off	Ankle Angle	✓			
Trigger	Shank Angle		✓	✓	✓
State 0	Ankle Angle	✓	✓		
Spring Ref	Shank Angle			✓	✓
State 1	Ankle Angle	✓	✓	✓	
Spring Ref	Ankle Angle w/Offset				✓

strides could be parsed and used. The experiments were conducted in the following order: Daily-Use, C3, C4, C2, C1, with no more than one experiment per week. Before each uneven terrain experiment, the subject was allowed to walk back and forth across the uneven terrain until he felt comfortable traversing the walkway. The subject received training with several variations of the prosthesis walking controller over the course of several months of controller development. He received training with the specific controller versions, including parameters and thresholds, during two to five, two-hour sessions in the weeks prior to the experiments.

4.1.5.1 Powered Prosthesis Prototype

The previously discussed controllers (i.e., Fig. 4.5 and Table 4.1) were implemented in the Vanderbilt powered ankle prosthesis prototype, which is similar to that described in [49], but with an integrated embedded system and battery pack and improved form factor. The prosthesis range of motion is 45 deg of plantarflexion and 20 deg of dorsiflexion. The prototype incorporates a Maxon EC60 14-pole brushless motor, with a transmission ratio of 116:1 via a 3-stage (belt-chain-chain) transmission in order to produce a peak ankle joint torque of approximately 100 Nm. A parallel carbon-fiber leaf spring incorporated into the foot biases the output capabilities of the ankle toward plantarflexion; the spring is characterized by a stiffness of approximately 3.7 Nm/deg and engages at approximately 1 degree of plantarflexion. The prosthesis is powered by a 6-cell lithium-ion battery which is attached

Figure 4.7: Amputee subject walking with Vanderbilt powered ankle prosthesis prototype.

via a hinge mechanism near the proximal end of the prosthesis such that its position and orientation can be adjusted to fit the user's pylon or socket profile. The prosthesis attaches to a user's socket via a standard pyramid connector. The mass of the prosthesis, including integrated electronics, battery, and foot shell, is 2.4 kg. A custom embedded system integrates a 32-bit microcontroller for execution of high-level control code with a 16-bit digital signal processing chip, which performs low-level control functions–commutation and current control of the brushless motor, signal conditioning of an absolute encoder at the joint, an incremental encoder at the motor, and a 6-axis inertial measurement unit (IMU) on the control board, etc. Sensor information available to the high-level controller therefore includes ankle joint position and velocity (from the encoders), as well as shank absolute orientation and angular velocity (from the IMU). The prosthesis as used by the amputee subject in this work is shown in Fig. 4.7.

4.1.5.2 Powered Prosthesis Prototype – Shank Angle Measurement

Precise measurement of the orientation of the shank is important for three of the controller variations discussed previously. The sagittal plane shank angle is calculated using

a complimentary filter which fuses the high frequency content of one axis of the gyroscope with the low frequency content of two axes of the accelerometer, accounting also for tangential acceleration about the ankle joint axis. The precision of the shank angle measurement with respect to motion capture was assessed for an amputee walking on both even and uneven terrain during the C3 data collection trials for this study. The difference between the motion capture measurement and the prosthesis measurement for shank angle during foot flat (25% - 43% of stride) was found for 18 strides on each terrain type. For even terrain, the mean of the standard deviation of this difference was 0.49 degrees; for uneven terrain, the mean of the standard deviation of the difference was 1.44 degrees.

4.1.5.3 Powered Prosthesis Prototype – Control of Ankle Torque

Note also that the finite-state-based impedance controller commands motor current, and the motor, transmission, and parallel spring introduce additional dynamics to the system. The spring stiffness and engagement angle as well as the Coulomb friction are calibrated prior to use and incorporated into the current reference in a dynamic manner. However, the inertia–due mainly to the rotor inertia of the EC60 motor reflected through the 116:1 transmission–is significant and cannot be accounted for dynamically due to lag in the calculation of ankle angular acceleration. During early and middle stance this inertia causes some oscillation of the ankle joint which delays foot flat. Therefore, a set of feed-forward cosine current pulses–tuned manually for duration and amplitude–were introduced to counteract this inertia. These pulses were tuned for even terrain to approximately half of the amplitude required to completely attenuate the oscillation and then applied to both even and uneven terrain. This was implemented in order to achieve foot flat more quickly and to provide the most accurate demonstration of the capabilities of the controllers presented herein given the hardware limitations.

4.1.6 Controller Assessment: Results and Discussion

Recall that the three controller variations (C2, C3, and C4) were intended to provide improved consistency in push-off, improved behavior in middle stance, and improved consistency of push-off torque, respectively and collectively, relative to the C1 controller.

4.1.6.1 Consistency in Powered Push-Off: C1 vs C2

Recall that controller C2 implemented a shank-angle-based initiation of powered push-off, relative to the ankle-angle-based initiation in C1, in order to provide improved consistency of push-off. For C2, the standard deviation of net ankle energy transfer on uneven terrain at 0.061 J/kg was almost identical to that of the healthy norm, while the mean net energy transfer was slightly higher than that of C1. The C1 controller resulted in 10% of push-offs missed completely, with the standard deviation of the percentage of stride at which push-off occurred for the remaining strides being 7.4% for uneven terrain. C2 showed improvement in that the standard deviation for uneven terrain was 5.2%, with zero missed push-offs. The variation in the magnitude of sagittal plane ground reaction force saw significant improvement, at 0.069G, approximately equal to that of healthy subjects (0.075G). The variation in shank and knee angle during foot flat on uneven terrain remained close to that of C1. In summary, C2 demonstrated improvements relative to C1 in terms of emulating healthy subject energy transfer and both percentage of stride and ground reaction force at push-off.

4.1.6.2 Consistency in Middle Stance Stiffness: C2 vs C3

Figures 4.8 and 4.9 show the internal and external middle stance quasistiffnesses, respectively, for even and uneven terrain walking for the cases of the daily-use prosthesis, C2, and C3 controllers, as well as a representative healthy subject (reprinted from Fig. 4.3). One can observe from the plots that all provide similar behavior on even terrain (i.e.,

the left column of all are similar), while the behavior on uneven terrain differs notably between them. In particular, considering the internal stiffness on uneven terrain (plots (e), (f), (g), and (h) from Fig. 4.8), ordering the plots from the daily-use prosthesis to C2, C3, and finally healthy data (top to bottom), the plots show a monotonic progression from a well-defined internal stiffness (e.g., in the daily-use prosthesis and C2 controller), to a highly-disordered relationship between ankle angle and torque (e.g., in the C3 and healthy subject data). Similarly, considering the external stiffness on uneven terrain (plots (e), (f), (g), and (h) from Fig. 4.9), the plots show a monotonic progression from a bimodal external stiffness behavior (e.g, in the daily-use prosthesis and C2 controller), to a unimodal external stiffness behavior (e.g., in the C3 and healthy subject data). Thus, relative to both the daily-use prosthesis and the C2 controller, the middle stance behavior implemented in C3 appears to better represent the observed character of the healthy ankle.

4.1.6.3 Consistency in Energy Transfer: C3 vs C4

The standard deviation of body-mass-normalized (BMN) energy transfer (i.e., integrated ankle power per stride) for walking on uneven terrain was calculated to be 0.09 and 0.085 J/kg for the C3 and C4 controllers, respectively. The corresponding standard deviation for the healthy subjects was 0.064 J/kg. As such, although the C4 controller may have reduced the variation in energy transfer slightly relative to the C3 controller, the difference was not significant.

4.1.6.4 Further Discussion and Study Limitations

Several hardware limitations exist which contributed to deficiencies in the performance of the powered prosthesis. Perhaps the most significant is the rotor inertia of the Maxon EC60 motor, as it affects the performance of the prosthesis throughout the entire stride. The inertia of the rotor delays foot flat by approximately 5% of stride compared to both healthy subjects and the daily-use prosthesis, which delays the transition into the middle stance

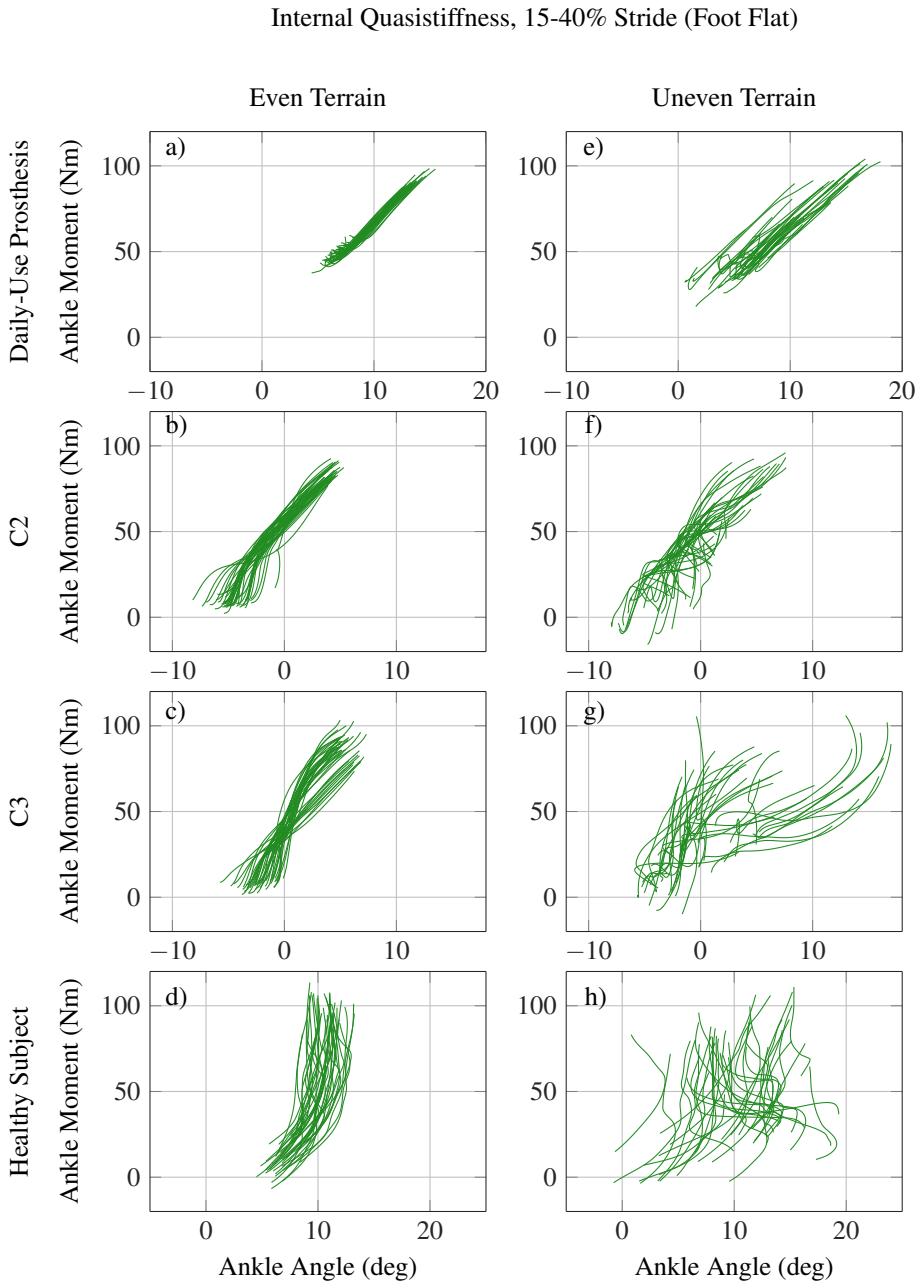

Figure 4.8: Internal ankle quasistiffness (ankle moment versus ankle angle) during middle stance for the amputee subject walking with the daily-use prosthesis (top), C2 controller (second row), C3 controller (third row), and a representative healthy subject (bottom) on even (left) and uneven (right) terrain.

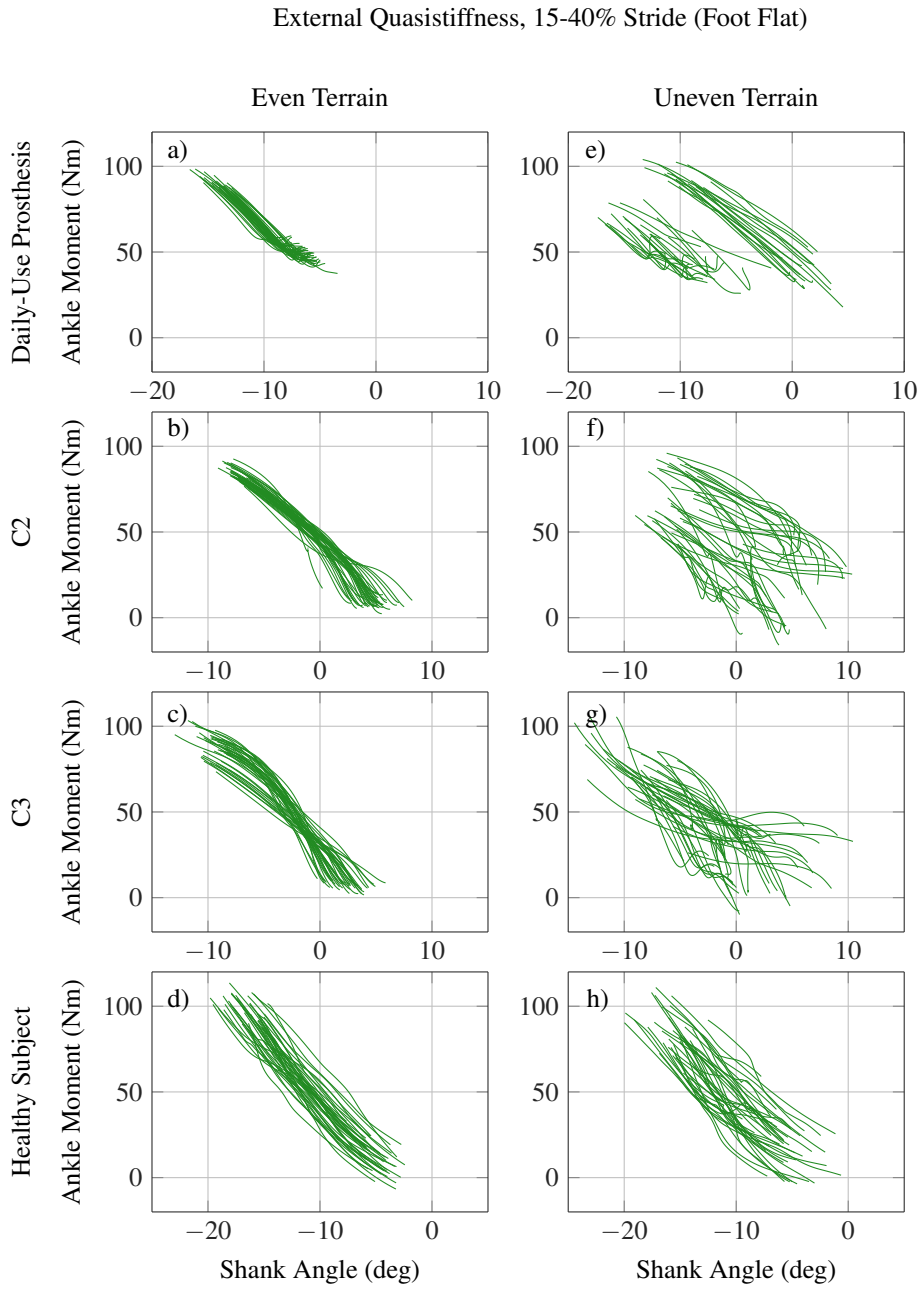

Figure 4.9: External ankle quasistiffness (ankle moment versus shank angle) during middle stance for the amputee subject walking with the daily-use prosthesis (top), C2 controller (second row), C3 controller (third row), and a representative healthy subject (bottom) on even (left) and uneven (right) terrain.

state of the controller. As the foot flattens, the rotational inertia causes an oscillation–from about 15-25% of stride–in output ankle torque (and consequently ankle angle) which cannot be accounted for in real-time, as discussed previously. Even with the aforementioned feedforward current cosine pulses, the oscillatory effect is still observable on both even and uneven terrain, and the feedforward pulses actually exacerbate the effect of the rotational inertia at times on uneven terrain.

Any external or un-modelled force which distorts the relationship between shank angle and ankle torque, particularly in a variable manner, undermines the controller improvements introduced here. The rotor inertia affects the torque output to some degree during foot flat; further, the (albeit small) error in the measurement/calculation of shank angle affects both the timing of push-off and the torque during middle stance (state 0).

Recall the lack of value added in the performance of C4 relative to C3. A significant, but variable, amount of power is required to accelerate the rotor during push-off, contributing to saturation of the motor current reference and distorting the relationship between ankle angle and ankle torque during the push-off state in a variable manner. Further, the precision of the shank angle measurement affects the time at which push-off is initiated and thus the ankle angle offset. Note that the variation in peak ankle moment is actually at its lowest on even terrain–where the ankle kinematics and shank angle measurement are less variable–with version C4 of the powered prosthesis controllers. Also take note of difference between the manner in which the push-off phase of gait is analyzed in healthy subject and is initiated in the powered prosthesis. In healthy subjects, the output torque and power were calculated offline to determine the point of push-off initiation (which was very similar to the point of of maximum torque). However push-off is initiated in the powered prosthesis according to a kinematic threshold (shank angle), which only approximates the time at which push-off should be initiated. Perhaps with measurement of output torque/power and/or better measurement of shank angle, the C4 powered prosthesis controller version could be executed more successfully.

While the study was limited in the number of amputee subjects used, the goal of this work was to show improvement with the introduction of control behaviors modelled after healthy subjects, which was accomplished nicely with one subject. Additional insight might be gained by repeating the C1 and C3 or C4 experiments with multiple amputee subjects. Another limitation was the inability to capture force data for all strides performed due to the nature of an overground force plate walkway. Specifically in the case of C1, there were some strides which particularly illustrated the deficiencies of that controller for use on uneven terrain which had to be omitted because of poor foot placement.

4.1.7 Conclusion

The objective of this work was to develop a controller for a powered ankle prosthesis that better accommodates walking on uneven terrain while preserving performance on even terrain. Since little information exists on the biomechanical behavior of the healthy ankle on such terrain, in order to provide guidance regarding the behavior the controller, the authors conducted a study of healthy subject walking on even and uneven terrain. The healthy-subject study suggested the following hypotheses: 1) powered push-off initiation would be more consistent on uneven terrain, and equally as consistent on even terrain, by using shank angle rather than ankle angle for initiation; 2) middle stance behavior would be better modelled on uneven terrain, and equally-well modeled on even terrain, by using external rather than internal stiffness (i.e., by using shank angle rather than ankle angle); and 3) energy transfer would better match that of healthy subjects by incorporating an configuration-based offset into the impedance model during the push-off state. In order to test these hypotheses, these control behaviors were implemented systematically in a powered ankle prosthesis prototype, and evaluated in an assessment on a single amputee subject walking on both even and uneven terrain. Results of the evaluation validated the first two hypotheses (i.e., improved consistency in push-off and better emulation of middle stance behavior), although showed no clear improvement corresponding to the third hypothesis.

The authors believe, however, that limitations in the implementation–namely in the ability to deliver a desired ankle torque and the ability to accurately measure shank angle in real-time–limited the ability of the prosthesis to faithfully reproduce the desired behaviors. Assuming future improvements to powered prosthesis hardware in this regard, the authors believe the proposed controller has the potential to further improve walking on varied terrain. The overarching value in the versatility of this controller is that the prosthesis need not detect uneven terrain; it simply adapts to it, treating it exactly the same as even terrain. Further investigation into the relationship between shank angle and ankle torque on other types of terrain, such as inclines and declines, should be conducted in order to determine exactly how universally this control strategy can be applied.

4.2 Addendum to Manuscript 3

4.2.1 Additional Results and Discussion

For the sake of concision and clarity in the above manuscript, only the most compelling results from the healthy and amputee subject studies were presented. Table 4.2 has been added here to summarize the data from the above manuscript and to include data which was omitted in said manuscript, in order to present here a more complete representation of the results from these studies. Table 4.2 is divided into five sections: range of local slopes, energy transfer, standard deviations taken during the foot flat portion of gait, peak or maximum values, and results pertaining to push-off.

One type of data in Table 4.2 which was not described/defined in the above manuscript was that pertaining to a unified deformable segment (UDS) model used to describe the power output for a prosthesis which does not have an analog for the ankle joint–the passive DER daily use prosthesis in the above manuscript. The UDS model was used to compare power and energy from the daily-use prosthesis to that of the powered prosthesis and healthy subjects. The power for the UDS was calculated for healthy subjects according

[90], where the proximal rigid component is the shank segment, and the distal deformable component is composed of the ankle and foot. The energy was calculated by integrating the power with respect to time.

Another type of data in Table 4.2 which was not described in the above manuscript was ankle variation compliance, which is defined here as the mean of the following: standard deviation in ankle angle divided by the standard deviation of the BMN ankle moment during foot flat. This provides a metric for the increase in ankle angle variation relative to the increase in ankle moment variation; this metric is labelled "Ankle Var Comp" in Table 4.2. Note that the ankle variation compliance for both C3 and C4 was much closer to that of healthy subjects than were those of C1, C2, and the passive DER prosthesis.

4.2.2 Initial Healthy Subject Study and Controller Development

A great deal of controller development and assessment took place prior to the healthy subject data motion capture and force data collection described in the manuscript above, as this equipment/experimental setup only became available for use in January 2017. The development prior to the availability of this equipment was based on a small healthy subject study performed with motion capture only (using the equipment described in Chapters 2 and 3), which was reported in the version of the manuscript presented at the *2015 Annual Conference of the IEEE Engineering in Medicine and Biology Society* (EMBC 2015) [89]. Additionally, a setup for using real-time motion capture data as an input to the controller was established during this initial development. The following establishes the motivation for this real-time motion capture streaming and includes technical information regarding the method; the following also describes why this motion capture streaming method was omitted from the studies described in the above manuscript. Some of the text in subsection 4.2.2 regarding the healthy subject experiment is excerpted from the aforementioned conference proceedings [89].

Table 4.2: Even and Uneven Terrain Results Summary

Metric	Terrain	Healthy Subject	Daily-Use Prosthesis	Powered Prosthesis C1	C2	C3	C4
Local Slope	Even	2.1	1.2	1.6	1.2	1.3	1.4
Range (deg)	Uneven	15.1	15.8	12.0	15.1	15.1	14.7
Energy Transfer							
Ankle	Even	0.20	–	0.019	0.0059	0.039	0.044
Mean (J/kg)	Uneven	0.17	–	0.075	0.094	0.12	0.12
Ankle	Even	0.047	–	0.019	0.017	0.016	0.019
Std Dev (J/kg)	Uneven	0.064	–	0.11	0.061	0.090	0.085
UDS	Even	0.023	-0.078	-0.059	-0.069	-0.012	-0.019
Mean (J/kg)	Uneven	0.0063	-0.072	0.017	0.027	0.059	0.055
UDS	Even	0.042	0.010	0.027	0.023	0.020	0.024
Std Dev (J/kg)	Uneven	0.059	0.020	0.11	0.055	0.082	0.082
Foot Flat (Standard Deviations)							
Ankle	Even	1.02	0.77	1.22	0.88	0.83	0.69
Angle (deg)	Uneven	3.85	2.60	3.00	2.50	4.67	5.21
Ankle	Even	0.077	0.053	0.061	0.051	0.076	0.17
Moment (Nm/kg)	Uneven	0.14	0.16	0.22	0.20	0.15	0.17
Ankle Var	Even	14.6	14.5	21.2	18.7	12.8	12.2
Comp (deg-kg/Nm)	Uneven	27.7	17.4	13.8	12.6	30.8	31.3
Shank	Even	1.18	1.01	1.50	1.09	1.06	0.87
Angle (deg)	Uneven	1.56	3.89	2.33	2.53	2.90	2.54
Knee	Even	2.20	1.58	2.65	1.68	1.65	1.52
Angle (deg)	Uneven	3.61	6.90	4.93	5.48	4.97	4.05
Peak (Standard Deviations)							
Ankle	Even	0.069	0.028	0.042	0.038	0.044	0.034
Moment (Nm/Kg)	Uneven	0.15	0.12	0.25	0.13	0.16	0.16
Ankle	Even	0.32	–	0.098	0.081	0.13	0.13
Power (W/Kg)	Uneven	0.58	–	0.52	0.31	0.54	0.54
UDS	Even	0.24	0.12	0.085	0.092	0.12	0.10
Power (W/Kg)	Uneven	0.58	0.28	0.54	0.31	0.54	0.59
Push-Off							
Initiation Point	Even	2.7	0.69	0.82	0.62	1.0	0.81
Std Dev (%Str)	Uneven	3.1	2.3	7.4	5.2	3.8	2.8
Sagittal GRF	Even	0.063	0.015	0.024	0.023	0.023	0.020
Std Dev (G)	Uneven	0.075	0.15	0.17	0.069	0.070	0.087
Ankle Angle	Even	1.15	–	–	–	–	–
Std Dev (deg)	Uneven	3.69	–	–	–	–	–
Shank Angle	Even	1.32	–	–	–	–	–
Std Dev (deg)	Uneven	1.56	–	–	–	–	–
Ankle Angle	Even	0.19	–	–	–	–	–
Grad (deg/%Str)	Uneven	0.22	–	–	–	–	–
Shank Angle	Even	1.32	–	–	–	–	–
Grad (deg/%Str)	Uneven	1.38	–	–	–	–	–

4.2.2.1 Initial Healthy Subject Experimental Protocol

Recall that in the study conducted by Voloshina, et al., it was discovered that the variability of the ankle angle more than doubled when walking on uneven terrain (compared to even), whereas the knee and hip variability only increased by approximately 30% [8]. Based on these findings, the author hypothesized that shank angle–orientation of the shank with respect to the ground in the sagittal plane–would be relatively consistent regardless of terrain type (even or uneven), especially compared with ankle angle–relative angle between the foot and the shank in the sagittal plane. Since shank angle was not reported by Voloshina et al. [8], the author collected data on healthy subjects using the overground uneven terrain tiles described in the above manuscript. Note that in the following experiment, only one set of uneven terrain tiles was used, and they were all oriented in the same direction, such that the pattern was repeating and not randomized; the walkway was set up to be 20 feet long.

For this experiment, three healthy subjects (ages 23 - 29) were asked to walk at a self-selected cadence across a room 20 times, first over level ground and then over the uneven terrain walkway, while full body kinematics were collected via a motion capture system. Approval to perform these assessments was granted by the Vanderbilt Institutional Review Board, and informed consent was obtained for the subjects prior to the assessments. Motion capture was performed using an OptiTrack S250e infrared twelve-camera system (NaturalPoint, Inc.) to track a full skeletal marker set (similar to the Helen Hayes marker set) consisting of thirty-four reflective markers. Motion capture data were sampled at 120 Hz using ARENA software (NaturalPoint, Inc.) and subsequently processed in MATLAB in order to extract lower limb joint angles and shank angle in the sagittal plane. Initial and terminal strides for each trial (40 strides per subject per terrain) were excluded from analysis. Additionally, the motion capture software was unable to solve the entire skeletal model for some strides (likely due to the small space in which the trials were conducted), eliminating additional strides. Consequently, n strides remained for analysis for each ter-

rain and subject, where n = 29, 29, 33 strides for even terrain and n = 32, 29, 28 for uneven terrain for subjects 1, 2, 3, respectively. The periodic data were parsed using the inflection in ankle angle to determine heel strike in lieu of the precedented minimum vertical position of the heel marker [75].

4.2.2.2 Initial Healthy Subject Experimental Results

The average standard deviations (variability) for each subject during 20% - 50% of stride–a portion of the stride which begins between foot flat push-off, and which ends after push-off–were calculated for shank angle and ankle angle. In general, the variability of the shank and ankle angles were comparable on even terrain, whereas the ankle angle varies more than the shank on uneven terrain, with the exception of Subject 2, for whom the two were comparable. The variability of the ankle angle (averaged for the three healthy subjects) increased by 180%–comparable to that found by Voloshina et al. [8]–whereas the shank angle variability only increased by approximately 30%. It was this result that initially prompted consideration for a controller which relies on a threshold in shank angle rather than ankle angle to initiate push-off.

4.2.2.3 Initial Prosthesis Experimental Protocol

The first prosthesis study compared only two controller versions: C1 and C2 from the above manuscript (See Table 4.1. The same walkway which was used in the healthy subject experiment was used for the controller assessment. Before assessing the controller with an amputee subject, the controller was assessed on a healthy subject fitted with able-bodied adaptors designed to immobilize the ankle; this subject donned the powered prosthesis on the right side and a passive DER prosthesis on the left side to complete the experiment, the results of which are detailed my Shultz et al. in the aforementioned conference proceedings [89].

For this experiment, the amputee subject was asked to walk at a self-selected cadence

across a room several times under four conditions: even and uneven terrain with each version of the controller (C1 and C2). Ankle angle, angular velocity, motor current, and shank angle were recorded by the embedded system on the prosthesis during these trials. The joint torque experienced by the user was calculated using model described in Chapter 3 regarding Eq. 3.2.

4.2.2.4 Initial Prosthesis Experimental Results

Of particular interest in this work was the variability in ankle torque and energy transfer. Voloshina et al. found no significant changes in mean positive or negative work at the ankle with healthy subjects on uneven terrain compared to even terrain, and there appeared to be very little change in ankle work variability, especially for positive work [8]. There did appear to be a small increase in peak power variability at the ankle on uneven terrain, about 50% [8]. Further, with the powered prosthesis, inconsistency in the amount of energy transferred at the ankle during the stride can indicate inconsistency in the timing of push-off initiation (transition from state 0 to state 1) with respect to the user's configuration. Push-off which comes too early often results in higher energy transfer, due to the user being pushed vertically and/or for a longer period of time. Additionally, push-off which occurs too late results in very little energy transferred, since the user is bearing significantly less weight when push-off occurs. The mean and standard deviation of the energy transferred for all strides was analyzed for each of the four testing conditions. The means for the various conditions are relatively close in value–13.16 J (C1, Even), 13.81 J (C2, Even), 14.52 J (C1, Uneven), 15.05 J (C2, Uneven). The standard deviations–2.72 J (C1, Even), 2.44 J (C2, Even), 5.81 J (C1, Uneven), 2.97 J (C2, Uneven)–were very close for all but the C1, Uneven condition, which is approximately double that of the other 3 conditions. While performance did degrade when the uneven terrain was introduced with C1 (as predicted), it essentially returned to baseline with C2, suggesting that C2 was an effective replacement for C1 on uneven terrain. Note that the suitability of the timing of push-off did not diminish

over even terrain when C2 was introduced, indicating that a single controller (C2) was well-suited for ambulation over both types of terrain.

Voloshina et al. found an approximately 50% increase in ankle torque variability on uneven terrain, compared to even [8]. Here, the ankle output torque was analyzed only from 20% to 50% of stride, as this was a portion of the stride which encompassed middle stance (state 0) and the beginning of the push-off state (state 1), which were the parts of the stride which are weight-bearing and which create a torque reference based on ankle position. Variability or variation is defined as the average of the standard deviation of the ankle torque taken along the torque dimension–i.e., there is one value for each percentage of stride. This is done for all trials used for each testing condition. The variabilities in ankle torque are very similar (within 5% of each other) for the even terrain conditions–8.25 Nm and 8.63 Nm for C1 and C2, respectively. The torque variability for the ankle-based controller on uneven terrain is 14.07 Nm, 70% greater than on even terrain. The torque variability for 2 was 11.4 Nm, 32% greater than on even terrain. The percent increase in variability on uneven terrain is similar in these cases to that found by Voloshina et al. [8]; however, C2 shows clear improvement over C1 on uneven terrain by this metric.

4.2.3 Initial Proposed Research Methods and Prosthesis Controller

4.2.3.1 Control: Stance Phase Equilibrium Modification

One goal of this controller was to minimize the user's perception of changes in ankle behavior–i.e. energy transfer and ankle torque–due to terrain changes. While variation in ankle torque with C2 was already similar to that seen in healthy subjects [8], the reason for increased variation in healthy subjects was unclear, and the author believed that it can be reduced in amputee subjects with the powered prosthesis. When the foot is weighted during middle stance, the prosthesis adapts to a local slope and becomes essentially stationary as the ankle and shank progress. (This happens on even terrain as well, only without the

stationary foot angle varying step-to-step.) If the angle of the foot with respect to gravity could be precisely and accurately identified during this time, this angle could be applied as an offset to the ankle equilibrium position during middle and late stance such that the ankle torque profile would be minimally variable step-to-step, which presumably would render this type of terrain easier to traverse. Note that the goal here was to reduce torque variability more than what was seen with C2 alone, as well as more than was observed in healthy subjects [8], seeking to augment ankle behavior beyond that which is seen in the intact ankle. (One example of augmentation which been observed with the powered ankle is increased weight bearing on the powered prosthesis compared to the intact ankle when standing on extreme slopes which might be uncomfortable for the intact joint–Chapter 3, see Fig. 3.8.)

Recall from the ground adaptive standing controller in Chapter 3 that the orientation of the foot in the sagittal plane can be calculated using information from the IMU and ankle motor and output encoders. When the foot is flat on the ground, the foot angle provides an estimate of the ground angle (local slope) for that step. A controller change, termed equilibrium modification, was proposed wherein the estimated local ground slope would be used to offset the nominal equilibrium position for states 0 and 1, as well as the ankle angle threshold for the state 1-2 transition. The goal was to estimate the local slope within 1 degree of the actual slope for any given slope.

4.2.3.2 Assessment: Stance Phase Equilibrium Modification

Recall that while the ground slope estimation performed well during standing and walking initiation(Chapter 3), the foot was moving slowly with much lower acceleration forces associated with ground contact compared to steady-state walking. Therefore, an experiment was conducted to determine the accuracy and precision of ground slope estimation during steady-state walking, wherein the aforementioned amputee subject walked up and down a hallway (even terrain) with the powered prosthesis using C2, estimating ground

slope. The mean value for the estimated slope (n = 20) at each step was -0.5 deg with a standard deviation of 1.32 deg and a range of 5.44 deg.

A motion capture study was conducted with the amputee subject in order to determine whether the lack of precision in foot angle measurement is due to mechanical compliance (in the shoe and/or foot shell) or measurement error. Motion capture was performed in a manner similar to that described previously in this section. The subject walked on even terrain in the motion capture volume with the powered prosthesis using the C2. Motion capture and prosthesis data were recorded and then later resampled and synchronized in MATLAB via a custom GUI. Strides were manually selected according to apparent heel strikes, where n = 20.

First, the standard deviation and range of the foot angle during middle stance (state 0), which roughly corresponds to foot flat, were calculated for each stride. The maximum values for standard deviation for the IMU-based foot angle and the motion capture-based foot angle were 0.71 deg and 0.43 deg, respectively. The maximum values for range were 2.27 deg and 1.38 deg, respectively. These relatively small values for intra-stride variation suggested that the shoe and foot shell compliance do not play a major role in the inconsistency in ground slope estimation.

The ground slope estimate for each stride was taken as the mean of the foot angle during the same foot flat portion of each stride. The standard deviation and range for the IMU-based foot angle were 1.72 deg and 7.48 deg, respectively. For the motion capture-based foot angle, these values were 0.52 deg and 1.92 deg, respectively. The inter-stride variability much greater for the IMU-based estimate than the motion capture-based measurement, and inter-stride variability was greater than intra-stride variability for the IMU-based foot angles, suggesting that the initial foot angle value is highly variable stride-to stride. This could be the result of accelerations at heel strike and foot flat influencing the low frequency content of the shank angle measurement. Recall that the IMU is located on the shank segment and that shank acceleration is nonzero during middle stance. Note that Sup et al. and

Lawson et. al. estimated ground slope with a 3-axis accelerometer attached to a rigid aluminum foot, where heel and toe load sensors confirmed foot flat, with minimal subsequent movement of the accelerometer [58, 54]. Ground slope estimate errors of up to 2 degrees were experienced during walking [58], and up to 1 degree during standing [54]. Further, transmission dynamics which influence the ankle angle measurement inherently affect the foot angle measurement. All of these factors could contribute to the imprecision of the foot angle estimate, precluding the use of the IMU in estimation of ground slope here.

4.2.3.3 Real-Time Motion Capture Streaming for Foot and Shank Angle Measurement

However, with a more precise foot angle calculation/measurement, the local slope could be determined for each step and then used to offset parameters in the level walking controller. For a proof-of-concept study, the motion capture system described previously was implemented to provide real-time information to the powered prosthesis via Controller Area Network (CAN) communication. The method for performing motion capture for use in streaming was largely the same as described previously for recording data. However, instead of defining a skeleton, rigid bodies (RB's) are defined–one each for the shank and foot segments. RB's are defined by sets of 3-5 reflective markers at fixed, distinct distances. For this study, two rigid objects (RO's) were created to which 3-5 reflective markers could be affixed. These were then rigidly attached to the foot and shank segments of the powered prosthesis, respectively, as shown in Fig. 4.10.

The motion of these RB's was tracked in ARENA and streamed from ARENA at 125 frames per second (FPS) (1/4 the speed of the embedded system's control loop) via a NatNet server. A MATLAB script taken from this Optitrack's NatNet SDK was modified for this specific application. MATLAB received information (at 125 Hz) about the RB's from ARENA, including the three dimensional position of each RB as well as a quaternion describing the orientation of each RB. The body-fixed Euler angles were then calculated using

Figure 4.10: Gen 3.2 prosthesis experimental setup and axis convention.

the angle convention shown in Fig. 4.10 and YZX rotation order. The foot and shank X Euler angles (approximately aligned with the sagittal plane) as well as X and Y foot position were then transmitted to the prosthesis embedded system via CAN.

The shank and foot angles were not useful in their raw forms and occasionally produced errant values.On such occasions, additional information (from the IMU) was be supplemented in order to prevent discontinuities in the signal, particularly while estimating ground slope. One way the potential for errant values was identified was to set up a virtual boundary within which it was known that the cameras could capture the motion accurately. Following each motion capture system calibration, the positive and negative X and Y limits of the walkway were manually set. (Note that the world coordinate system was set up with the Z-axis aligned with the walkway. This was done so that boundaries could be set up without the need to interpolate between 4 boundary points at each time step.) While this virtual boundary helped to detect most of the errant foot and shank angle values, bogus values (near $\pm$ 180 degrees) and stagnant values could still occur within the boundary.

A complementary filter was used to fuse the high frequency content of the IMU–i.e., the gyroscope–for the sagittal plane. A very small time constant (16 ms) was used, such

that the output was heavily weighted toward the motion capture signal. In the case where the motion capture angles jumped suddenly to bogus values (detected by a large difference between the new raw value and the old accepted value), the low frequency component of fused signal was replaced by a projected value based on the gyroscope; essentially, the fused signal depended entirely on the gyroscope for this brief time. In the case that the prosthesis was out of bounds or the signal value stagnant (detected by a difference of zero between old and new raw values which persisted for 10 motion capture samples), the IMU-based angles temporarily replaced the motion capture-based angles. A flag was set for the remainder of the stride to indicate which, if any, of these occurred.

Only if the controller was post heel strike in state 3 or 0, the foot was in bounds during those states, and the IMU-based foot angle had not been used during those states would ground slope be estimated. These were safety conditions used to ensure that the subject was in good view of the cameras and that he was walking normally. If the controller passed these checks, then the controller looked for foot flat (detected when the (motion capture-based) foot angular velocity was within 30 deg/s of zero at a time when the foot angle was within 20 degrees of zero). At each consecutive sample for which this was true, a counter/timer incremented by 1, and a type of integral was calculated for the slope–this "slope sum" was incremented by the foot angle at each sample. Once this had been true for 15 consecutive samples, the slope estimate was set to the running average of the foot angle during foot flat (slope sum / timer). The ground slope was then set to this slope estimate and used to modify the aforementioned parameters and thresholds. If the foot flat condition was false, a flag was set and logged for user offline to determine which strides should be processed and analyzed

An experiment was conducted to compare the two ground slope estimates on even ground using the IMU-based foot angle and shank angle and then the motion capture-based foot and shank angle for the walking controller. For each condition, the amputee subject walked back and forth across the motion capture volume along a walkway for 40-50 total

strides. Only strides which did not set any of the previously mentioned flags were used for analysis (n = 19 or n = 20). The range of the (mean) ground slope estimate per stride for the MoCap-based estimate was an order of magnitude smaller, at 0.89 degrees, than that of the IMU-based estimate, suggesting that the local ground slope could be estimated with high precision (and accuracy, provided a well-calibrated zero position) for uneven slope conditions.

4.2.3.4 Implications of Final Healthy Subject Study

Recall that the final healthy subject study described in the manuscript above (incorporating motion capture and force plate data collection) prompted controller modification which traded ankle angle for shank angle as the virtual spring reference in state 0 and/or state 1 (C3 and C4). This approach would in theory yield a similar result to that proposed for the Eq Mod controller but with some practical advantages. First, there would be no need to estimate foot angle, which would eliminate any potential for latency in implementing the appropriate angle offset in state 0. Further, any error introduced into the IMU-based foot signal because of the ankle angle (transmission dynamics) was no longer an issue. Recall that the real-time motion capture streaming was originally implemented in order to improve accuracy and precision in the foot angle measurement for proof of concept of such a controller. Since that measurement was no longer needed, the option to investigate elimination of motion capture as a real-time input to the controller became available. The removal of real-time motion capture would not only eliminate complications due to integration with the Vicon data collection system but would also support use of this controller outside of a laboratory setting.

4.2.3.5 Shank Angle Measurement via the Embedded System

The sagittal plane shank angle was calculated onboard the prosthesis using a complimentary filter which fuses the high frequency content of one axis of the gyroscope with the

low frequency content of two axes of the accelerometer, with a time constant of 900 ms. A pilot study was conducted to compare the shank angle measurement from the prosthesis to that of motion capture (from the Vicon system) for both even and uneven terrain. The difference between the motion capture measurement and the prosthesis measurement for shank angle during foot flat was found for a small number of strides over even terrain and uneven terrain, For even terrain (n = 9), the mean of the standard deviation of this difference was 1.46 degrees, and for uneven terrain it was 2.21 degrees (n = 12). In order to improve the precision of the shank angle measurement from the prosthesis, tangential acceleration was modelled and incorporated into the accelerometer information for the sensor fusion. Another motion capture data collection was performed, where the means of the standard deviation of the difference were 0.49 and 1.44 degrees for even and uneven terrain, respectively, where n = 18 for both conditions. As a comparison to illustrate some error which exists in the motion capture system, this metric was also calculated for the ankle angle on even terrain; note that the ankle angle measured by the embedded system is the most accurate and precise measurement available in the system. The value of this metric for ankle angle on even terrain was 0.82 degrees. Therefore, the measurement calculated from the IMU on the prosthesis was considered sufficient for use in the study described in the manuscript in this chapter.

4.2.4 Embedded System Design

Recall from Chapter 1 that the Generation 3.2 powered ankle prosthesis prototype (used in the work described in this chapter) included a new embedded system layout, which was designed by the author with the help of other members of the CIM, particularly Don Truex and Brian Lawson. The board shape was dictated by the mechanical device design, by Jason Mitchell, and the vast majority of the components and circuits remained the same as that for the powered knee and ankle prosthesis embedded system, except that circuits related to the knee and the load cell were omitted; the bluetooth circuit was also omitted,

but a header was placed on the board to which a separate bluetooth circuit board might be connected at a later time. Figure 4.11 depicts the PCB design software rendering of the board layout with the top later shown on the left and the bottom layer, with dimensions, shown on the right. Figure 4.12 contains photos of the embedded system top side (attached to the prosthesis) on the left and bottom side on the right.

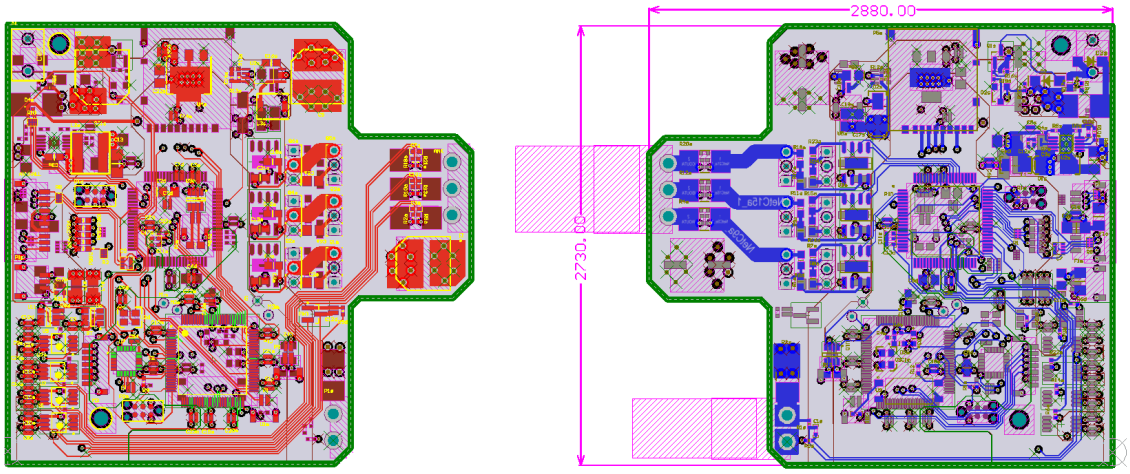

Figure 4.11: PCB design software rendering of board design with the top layer shown on the left and the bottom layer and board dimensions shown on the right.

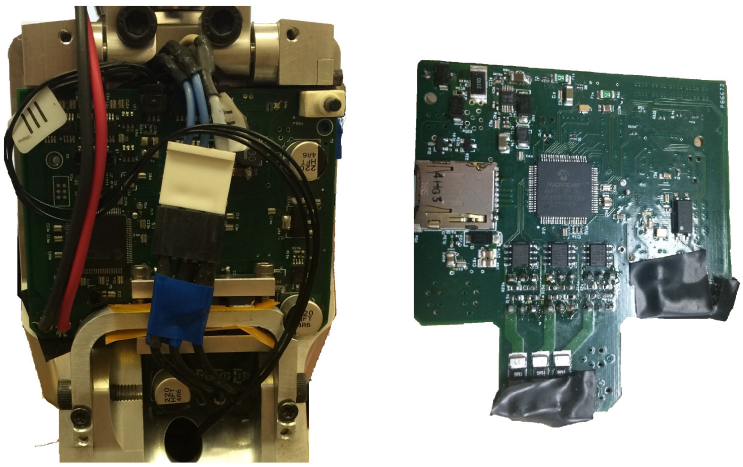

Figure 4.12: Photos of the embedded system top side (attached to the prosthesis) on the left and bottom side on the right.

There are many factors which must be considered when creating a layout for a circuit board. In general, it is important to identify an isolate circuits which generate noise

(digital traces with fast rise and fall times, such as pulse-width modulated signals) and which receive noise (analog circuits with high impedance termination, such a operational amplifiers); to minimize loop inductance (by minimizing loop area), and to use bypass (decoupling) capacitors on all power pins to short high-frequency noise to ground.

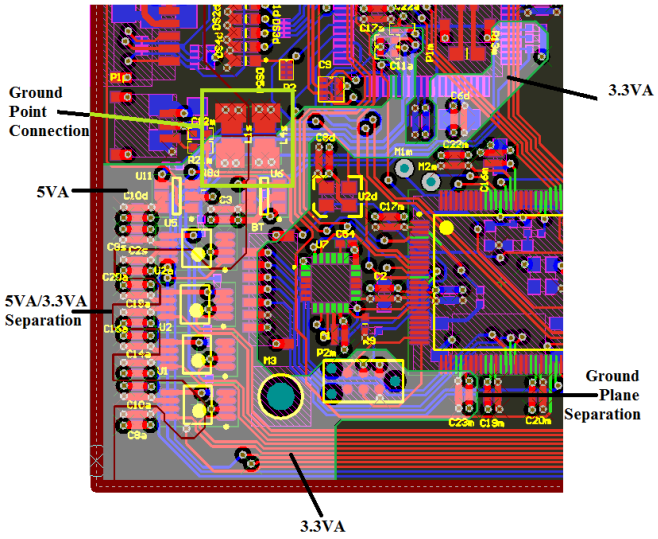

Figure 4.13: Illustration of the analog circuit design requirements.

Figure 4.13 depicts the lower lefthand corner of the board, from the perspective of the top layer, which is where the analog circuits were placed. The 5-Volt and 3.3-Volt analog (5VA and 3.3VA, respectively) power planes are highlighted in light grey; these planes are completely isolated from the other power planes. Notice also the thin dark red line separating the 5VA and 3.3VA power planes. The 5VA plane is connected to the 5V plane by a low Q lossy inductor, the same being true of the 3.3VA and 3.3V planes; this connection is shown inside the bright green box in Fig. 4.13. In addition to power plane separation, the the ground plane for the analog circuit is isolated from the other ground plane except for a single point connection; the green boundary line represents this separation, with the connection point being located inside the bright green box as well. Further, in order to minimize loop area, traces in and out of the analog area should not cross breaks in the plane. While the current sense traces violate this rule, they are routed

as differential pairs such that the loop areas is minimized, and essentially the same noise is coupled to both traces in the pair. The current sense amplifiers are designed to attenuate this common mode noise and to amplify only the difference between the paired signals.

It is also important to keep traces as short as possible and to be careful of routing in order to minimize loop area. Due to the space restrictions of the board, this could not always be prioritized. However, one way in which loop area was minimized was by grouping components according to voltage needs (when possible) and locating the various power planes such that voltage could be sourced using vias to the respective power planes. Finally, note that bypass capacitors were placed as close as possible to their respective power pins in order to minimize parasitic inductance.

CHAPTER 5

CONCLUSION

5.1 Contribution

This document has presented the motivation, design, development, and evaluation of controllers for two types of powered lower limb prostheses. The powered prosthesis prototypes used in this work were created by members of the CIM and were designed to have relatively transparent transmissions in order to serve as testbeds upon which controllers such as these might be developed. These controllers were designed with the aim of improving and/or restoring mobility and stability for persons with lower limb amputation for a number of situations. Specifically, this worked has produced the following:

- A controller for emergency, short term running in the course of daily living for a powered knee and ankle prosthesis, incorporated into an existing suite of activities by a supervisory controller which facilitates natural transitions between walking and running.

- A suite of controllers for a powered ankle prosthesis for below-knee amputees which enables biomechanically healthy walking on level ground at various speeds with walking speed mode selection via cadence estimation, as well as stable, supportive ground adaptive standing on a variety of slopes; further, a supervisory controller enables natural transitions between walking and standing based on biomechanical cues from the user.

- A unified controller for walking on even and uneven terrain, modified from the walking controller for level, even terrain, which automatically adapts to the local slope, enabling biomechanically healthy walking on both types of terrain; the controller was motivated by a healthy subject study from which behavioral models for the healthy

ankle were formulated and implemented in the design.

Essentially, the running controller supplemented a suite of controllers for a powered knee and ankle prosthesis for above-knee amputees which was already functionally versatile, and the remaining work provided a solid foundation for a suite of controllers for a powered ankle prosthesis which might be supplemented in the future by others at the CIM.

5.2 Clinical Significance

As the product of a mechanical engineering laboratory, the primary goal of this work was to develop controllers for a powered prosthesis for persons with lower limb amputation and to verify the effectiveness of their design in order to demonstrate potential to benefit the target population. For each branch of the work described in this document, the controllers were evaluated on a single amputee subject using a powered prosthesis prototype. While full scale clinical evaluation was out of the scope of this work, another team of researchers might conduct such a study in the future should any of these controllers be considered for use in a commercial product.

5.3 Commercial Translation and Competing Interests

One goal of the work presented in this document was to produce controllers which might be translated to the commercial market. This process has involved patent applications filed by the Vanderbilt University Office of Technology Transfer, of which I am co-inventor. Some of this intellectual property has been licensed by Vanderbilt University to Freedom Innovations, LLC, giving me a small financial interest in its successful translation into commercial product(s).

5.4 Future Work

The work presented in Chapters 3 and 4 introduced a suite of controllers which enable walking and standing under various conditions. However, not only were there hardware limitations which adversely affected the performance of the walking controllers, these controllers do not necessarily accommodate the majority of the situations which an amputee might encounter through the course of daily living. Suggested future work first includes hardware revision, particularly with regard to integration of a motor with much lower rotor inertia. Subsequently, re-evaluation of the controllers presented in Chapter 4 should be performed, with additional evaluation on inclines and declines. Further, other controllers which are available in the powered knee and ankle prosthesis should also be translated for use in the powered ankle prosthesis, including stair ascent and descent, as well as emergency running, with a suggested focus of making the walking controller as versatile and adaptable as possible. Finally, a supervisory controller which can discern intent to use each activity-level controller should be implemented.

BIBLIOGRAPHY

[1] K. Ziegler-Graham, E. J. MacKenzie, P. L. Ephraim, T. G. Travison, and R. Brookmeyer. Estimating the prevalence of limb loss in the united states: 2005 to 2050. *Arch Phys Med Rehabil*, 89(3):422–429, 2008.

[2] B. J. Hafner and D. G. Smith. Differences in function and safety between medicare functional classification level-2 and-3 transfemoral amputees and influence of prosthetic knee joint control. *J Rehabil Res Dev*, 46(3):417, 2009.

[3] T. F. Novacheck. The biomechanics of running. *Gait Posture*, 7(1):77–95, 1998.

[4] M. L. Palmer. Sagittal plane characterization of normal human ankle function across a range of walking gait speeds. Master's thesis, Massachusetts Institute of Technology, 2002.

[5] A. H. Hansen, S. C. Miff, D. S. Childress, S. A. Gard, and M. R. Meier. Net external energy of the biologic and prosthetic ankle during gait initiation. *Gait Posture*, 31(1):13 – 17, 2010.

[6] A. H. Hansen, D. S. Childress, S. C. Miff, S. A. Gard, and K. P. Mesplay. The human ankle during walking: implications for design of biomimetic ankle prostheses. *J Biomech*, 37(10):1467 – 1474, 2004.

[7] D. C. Morgenroth, A. D. Segal, K. E. Zelik, J. M. Czerniecki, G. K. Klute, P. G. Adamczyk, M. S. Orendurff, M. E. Hahn, S. H. Collins, and A. D. Kuo. The effect of prosthetic foot push-off on mechanical loading associated with knee osteoarthritis in lower extremity amputees. *Gait Posture*, 34(4):502 – 507, 2011.

[8] A. S. Voloshina, A. D. Kuo, M. A. Daley, and D. A. Ferris. Biomechanics and energetics of walking on uneven terrain. *J Exp Biol*, 216(21):3963–3970, 2013.

[9] https://www.ossur.com/prosthetic-solutions/products/dynamic-solutions/power-knee.

[10] http://www.bionxmed.com/patients/the-empower-advantage/.

[11] J. Hitt, J. Merlo, J. Johnston, M. Holgate, A. Boehler, K. Hollander, and T. Sugar. Bionic running for unilateral transtibial military amputees. Technical report, DTIC Document, 2010.

[12] A. M. Huff, B. E. Lawson, and M. Goldfarb. A running controller for a powered transfemoral prosthesis. *Conf Proc IEEE Eng Med Biol Soc*, 2012:4168–71, 2012.

[13] A. H. Shultz, B. E. Lawson, and M. Goldfarb. Running with a powered knee and ankle prosthesis. *IEEE Trans Neural Syst Rehabil Eng*, 23(3):403–412, May 2015.

[14] J. K. Hitt, T. G. Sugar, M. Holgate, and R. Bellman. An active foot-ankle prosthesis with biomechanical energy regeneration. *J Med Devices*, 4(1), 2010.

[15] R. D. Bellman, M. A. Holgate, and T. G. Sugar. Sparky 3: Design of an active robotic ankle prosthesis with two actuated degrees of freedom using regenerative kinetics. In *Proc IEEE/RAS-EMBS Int Conf Biomed Robot Biomechatron*, pages 511–516, 2008.

[16] B. J. Bergelin and P. A. Voglewede. Design of an active ankle-foot prosthesis utilizing a four-bar mechanism. *J Mech Design*, 134(061004):1–7, 2012.

[17] G. K. Klute, J. Czerniecki, and B. Hannaford. Muscle-like pneumatic actuators for below-knee prostheses. In *Proc Int Conf on New Actuators*, pages 289–292, 2000.

[18] J. Zhu, Q. Wang, and L. Wang. Pantoe 1: Biomechanical design of powered ankle-foot prosthesis with compliant joints and segmented foot. In *Proc IEEE/ASME Int Conf on Advanced Intelligent Mechatronics*, pages 31–36, 2010.

[19] S. K. Au, J. Weber, and H. Herr. Biomechanical design of a powered ankle-foot prosthesis. In *Proc IEEE Int Conf on Rehabilitation Robotics*, pages 298–303, 2007.

[20] P. Cherelle, V. Grosu, A. Matthys, B. Vanderborght, and D. Lefeber. Design and validation of the ankle mimicking prosthetic (amp-) foot 2.0. *IEEE Trans Neural Syst Rehabil Eng*, 22(1):138–148, Jan 2014.

[21] H. Zheng and X. Shen. Design and control of a pneumatically actuated transtibial prosthesis. *J Bionic Eng*, 12(2):217 – 226, 2015.

[22] R. Jimnez-Fabin and O. Verlinden. Review of control algorithms for robotic ankle systems in lower-limb orthoses, prostheses, and exoskeletons. *Med Eng Phys*, 34(4):397 – 408, 2012.

[23] M. A. Holgate, A. W. Bohler, and T. G. Sugar. Control algorithms for ankle robots: A reflection on the state-of-the-art and presentation of two novel algorithms. In *Proc IEEE/RAS-EMBS Int Conf Biomed Robot Biomechatron*, pages 97–102, 2008.

[24] M. A. Holgate, T. G. Sugar, and A. W. Bohler. A novel control algorithm for wearable robotics using phase plane invariants. In *Proc IEEE Int Conf on Robotics and Automation*, pages 3845–3850, May 2009.

[25] https://www.springactive.com/odyssey.php.

[26] https://www.springactive.com/jackspring.php.

[27] T. G. Sugar, K. W. Hollander, and J. K. Hitt. Walking with springs. In *SPIE Smart Structures and Materials + NDE and HM*, pages 797602–797602. SPIE, 2011.

[28] S.K. Au, P. Bonato, and H. Herr. An emg-position controlled system for an active ankle-foot prosthesis: an initial experimental study. In *Proc IEEE Int Conf on Rehabilitation Robotics*, pages 375–379, 2005.

[29] S.K. Au, P. Dilworth, and H. Herr. An ankle-foot emulation system for the study of human walking biomechanics. In *Proc IEEE Int Conf on Robotics and Automation*, pages 2939–2945, 2006.

[30] S. Au, M. Berniker, and H. Herr. Powered ankle-foot prosthesis to assist level-ground and stair-descent gaits. *Neural Net*, 21(4):654 – 666, 2008. Robotics and Neuroscience.

[31] M. F. Eilenberg, H. Geyer, and H. Herr. Control of a powered ankle-foot prosthesis based on a neuromuscular model. *IEEE Trans Neural Syst Rehabil Eng*, 18(2):164–173, 2010.

[32] J. Sun and P. A. Voglewede. Powered transtibial prosthetic device control system design, implementation, and bench testing. *J Med Devices*, 8(1), 2014.

[33] J. Sun, J. M. Fritz, D. R. Del Toro, and P. A. Voglewede. Amputee subject testing protocol, results, and analysis of a powered transtibial prosthetic device. *J Med Devices*, 8(4):041007, 2014.

[34] S. Huang, J. P. Wensman, and D. P. Ferris. An experimental powered lower limb prosthesis using proportional myoelectric control. *J Med Devices*, 8(2), 2014.

[35] S. Huang, J. P. Wensman, and D. P. Ferris. Locomotor adaptation by transtibial amputees walking with an experimental powered prosthesis under continuous myoelectric control. *IEEE Trans Neural Syst Rehabil Eng*, 24(5):573–581, May 2016.

[36] S. H. Collins and A. D. Kuo. Recycling energy to restore impaired ankle function during human walking. *PLoS one*, 5(2):e9307, 2010.

[37] J. M. Caputo and S. H. Collins. A universal ankle–foot prosthesis emulator for human locomotion experiments. *J of Biomech Eng*, 136(3):035002, 2014.

[38] S. H. Collins, M. Kim, T. Chen, and T. Chen. An ankle-foot prosthesis emulator with control of plantarflexion and inversion-eversion torque. In *2015 IEEE International Conference on Robotics and Automation (ICRA)*, pages 1210–1216. IEEE, 2015.

[39] A. D. Segal, K. E. Zelik, G. K. Klute, D. C. Morgenroth, M. E. Hahn, M. S. Orendurff, P. G. Adamczyk, S. H. Collins, A. D. Kuo, and J. M. Czerniecki. The effects of a controlled energy storage and return prototype prosthetic foot on transtibial amputee ambulation. *Hum Mov Sci*, 31(4):918–931, 2012.

[40] K. E. Zelik, S. H. Collins, P. G. Adamczyk, A. D. Segal, G. K. Klute, D. C. Morgenroth, M. E. Hahn, M. S. Orendurff, J. M. Czerniecki, and A. D. Kuo. Systematic variation of prosthetic foot spring affects center-of-mass mechanics and metabolic cost during walking. *IEEE Trans Neural Syst Rehabil Eng*, 19(4):411–419, 2011.

[41] J. M. Caputo, S. H. Collins, and P. G. Adamczyk. Emulating prosthetic feet during the prescription process to improve outcomes and justifications. In *Proc IEEE Int Work on Advanced Robotics and its Social Impacts*, pages 127–128. IEEE, 2014.

[42] J. M. Caputo, P. G. Adamczyk, and S. H. Collins. Informing ankle-foot prosthesis prescription through haptic emulation of candidate devices. In *Proc IEEE Int Conf on Robotics and Automation*, pages 6445–6450. IEEE, 2015.

[43] M. Kim and S. H. Collins. Once-per-step control of ankle-foot prosthesis push-off work reduces effort associated with balance during walking. *J Neuroeng Rehabil*, 12(1):1, 2015.

[44] T. Lenzi, L. Hargrove, and J. Sensinger. Speed-adaptation mechanism: Robotic prostheses can actively regulate joint torque. *Robotics Automation Magazine, IEEE*, 21(4):94–107, Dec 2014.

[45] D. H. Gates, J. M, Aldridge, and J. M. Wilken. Kinematic comparison of walking on uneven ground using powered and unpowered prostheses. *Clin Biomech*, 28(4):467–472, 2013.

[46] J. M. Aldridge, J. T. Sturdy, and J. M. Wilken. Stair ascent kinematics and kinet-

ics with a powered lower leg system following transtibial amputation. *Gait Posture*, 36(2).

[47] A. S. McIntosh, K. T. Beatty, L. N. Dwan, and D. R. Vickers. Gait dynamics on an inclined walkway. *J Biomech*, 39(13):2491 – 2502, 2006.

[48] http://www.endolite.com/products/elan.

[49] A. H. Shultz, B. E. Lawson, and M. Goldfarb. Variable cadence walking and ground adaptive standing with a powered ankle prosthesis. *IEEE Trans Neural Syst Rehabil Eng*, page 1, 2015.

[50] http://www.endolite.com/products/echelon.

[51] http://www.endolite.com/products/echelonvt.

[52] https://www.ossur.com/prosthetic-solutions/products/dynamic-solutions/proprio-foot.

[53] http://www.freedom-innovations.com/kinterra/.

[54] B. E. Lawson, H. A. Varol, and M. Goldfarb. Standing stability enhancement with an intelligent powered transfemoral prosthesis. *IEEE Trans Biomed Eng*, 58(9):2617–2624, 2011.

[55] F. Sup, A. Bohara, and M. Goldfarb. Design and control of a powered transfemoral prosthesis. *Int J Rob Res*, 27(2):263–273, 2008.

[56] F. Sup, H. A. Varol, J. Mitchell, T. J. Withrow, and M. Goldfarb. Preliminary evaluations of a self-contained anthropomorphic transfemoral prosthesis. *IEEE/ASME Trans Mechatronics*, 14(6):667–676, 2009.

[57] H. A. Varol, F. Sup, and M. Goldfarb. Multiclass real-time intent recognition of a powered lower limb prosthesis. *IEEE Trans Biomed Eng*, 57(3):542–551, 2010.

[58] F. Sup, H. A. Varol, and M. Goldfarb. Upslope walking with a powered knee and ankle prosthesis: initial results with an amputee subject. *IEEE Trans Neural Syst Rehabil Eng*, 19(1):71–8, 2011.

[59] H. A. Varol, F. Sup, and M. Goldfarb. Powered sit-to-stand and assistive stand-to-sit framework for a powered transfemoral prosthesis. *Proc IEEE Int Conf on Rehabilitation Robotics*, 5209582:645–651, 2009.

[60] B. E. Lawson, H. A. Varol, F. Sup, and M. Goldfarb. Stumble detection and classification for an intelligent transfemoral prosthesis. In *Engineering in medicine and biology society (EMBC), 2010 annual international conference of the IEEE*, pages 511–514. IEEE, 2010.

[61] B. E. Lawson, H. A. Varol, A. Huff, E. Erdemir, and M. Goldfarb. Control of stair ascent and descent with a powered transfemoral prosthesis. *IEEE Trans Neural Syst Rehabil Eng*, 21(3):466–73, 2013.

[62] K. H. Ha, H. A. Varol, and M. Goldfarb. Volitional control of a prosthetic knee using surface electromyography. *IEEE Transactions on Biomedical Engineering*, 58(1):144–151, 2011.

[63] F. Sup, A. Bohara, and M. Goldfarb. Design and control of a powered knee and ankle prosthesis. In *Proc IEEE Int Conf on Robotics and Automation*, pages 4134–4139.

[64] D. A. Winter. *The Biomechanics and Motor Control of Human Gait: Normal, Elderly and Pathological*. University of Waterloo Press, Waterloo, Ontario, Canada, 2nd edition, 1991.

[65] C. R. Lee and C. T. Farley. Determinants of the center of mass trajectory in human walking and running. *J Exp Biol*, 201(21):2935–2944, 1998.

[66] T. A. McMahon, G. Valiant, and E. C. Frederick. Groucho running. *J Appl Physiol*, 62(6):2326–2337, 1987.

[67] R. M. Alexander. Walking and running: Legs and leg movements are subtly adapted to minimize the energy costs of locomotion. *Am Sci*, 72(4):348–354, 1984.

[68] G. A. Cavagna and M. Kaneko. Mechanical work and efficiency in level walking and running. *J Physiol*, 268(2):467–481, 1977.

[69] G. Mensch and P. E. Ellis. Running patterns of transfemoral amputees: a clinical analysis. *Prosth and Orthot Int*, 10(3):129–134, 1986.

[70] J. G. Buckley. Sprint kinematics of athletes with lower-limb amputations. *Arch Phys Med Rehab*, 80(5):501–508, 1999.

[71] B. Burkett, J. Smeathers, and T. Barker. Walking and running inter-limb asymmetry for paralympic trans-femoral amputees, a biomechanical analysis. *Prosth Orthot Int*, 27(1):36–47, 2003.

[72] D. J. DiAngelo, D. A. Winter, D. N. Ghista, and W. R. Newcombe. Performance assessment of the Terry Fox jogging prosthesis for above-knee amputees. *J Biomech*, 22(6):543–558, 1989.

[73] S. Ounpuu. The biomechanics of walking and running. *Clin Sports Med*, 13(4):843–863, 1994.

[74] V. Segers, M. Lenoir, P. Aerts, and D. De Clercq. Kinematics of the transition between walking and running when gradually changing speed. *Gait Posture*, 26(3):349–361, 2007.

[75] I. P. I. Pappas, M. R. Popovic, T. Keller, V. Dietz, and M. Morari. A reliable gait phase detection system. *IEEE Trans Neural Syst Rehabil Eng*, 9(2):113–125, 2001.

[76] J. K. De Witt. Determination of toe-off event time during treadmill locomotion using kinematic data. *J Biomech*, 43(15):3067 – 3069, 2010.

[77] N. H. Molen. 1973.

[78] L. Torburn, C. M. Powers, R. Guiterrez, and J. Perry. Energy expenditure during ambulation in dysvascular and traumatic below-knee amputees: a comparison of five prosthetic feet. *J Rehabil Res Dev*, 32(2):111–119, 1995.

[79] L. Torburn, J. Perry, E. Ayyappa, and S. L. Shanfield. Below-knee amputee gait with dynamic elastic response prosthetic feet: a pilot study. *J Rehabil Res Dev*, 27(4):369–384, 1990.

[80] R. D. Snyder, C. M. Powers, C. Fountain, and J. Perry. The effect of five prosthetic feet on the gait and loading of the sound limb in dysvascular below-knee amputees. *J Rehabil Res Dev*, 32(4):309–315, 1995.

[81] J. M. Donelan, R. Kram, and A. D. Kuo. Simultaneous positive and negative external mechanical work in human walking. *J Biomech*, 35(1):117 – 124, 2002.

[82] A. D. Kuo. Energetics of actively powered locomotion using the simplest walking model. *J Biomech Eng-T ASME*, 124(1):113 – 120, 2002.

[83] A. H. Shultz, J. E. Mitchell, D. Truex, B. E. Lawson, and M. Goldfarb. Preliminary evaluation of a walking controller for a powered ankle prosthesis. In *Proc IEEE Int Conf on Robotics and Automation*, pages 4838–4843, May 2013.

[84] K. Parker, R. L. Kirby, J. Adderson, and K. Thompson. Ambulation of people with lower-limb amputations: Relationship between capacity and performance measures. *Arch Phys Med Rehabil*, 91(4):543 – 549, 2010.

[85] G. K. Klute, J. S. Berge, M. S. Orendurff, R. M Williams, and J. M. Czerniecki.

Prosthetic intervention effects on activity of lower-extremity amputees. *Arch Phys Med Rehabil*, 87(5):717 – 722, 2006.

[86] R. W. Bohannon. Number of pedometer-assessed steps taken per day by adults: a descriptive meta-analysis. *Physical Therapy*, 2007.

[87] T. T. Sowell. A preliminary clinical evaluation of the mauch hydraulic foot-ankle system. *Prosth Orthot Int*, 5(2):87–91, 1981.

[88] E. Nickel, J. Sensinger, and A. Hansen. Passive prosthetic ankle-foot mechanism for automatic adaptation to sloped surfaces. *J Rehabil Res Dev*, 51(5):803, 2014.

[89] A. H. Shultz, B. E. Lawson, and M. Goldfarb. Walking on uneven terrain with a powered ankle prosthesis: A preliminary assessment. In *Conf Proc IEEE Eng Med Biol Soc*, pages 5299–5302, August 2015.

[90] K. Z. Takahashi, T. M. Kepple, and S. J. Stanhope. A unified deformable (ud) segment model for quantifying total power of anatomical and prosthetic below-knee structures during stance in gait. *J Biomech*, 45(15):2662–2667, 2012.